# Designing an optimized closed electrical distribution system for a multi-carrier energy hub on a mixed-use area in Hilversum

Msc Sustainable Energy Technology

**T.J. Broekman**

**Master Graduation Thesis**
Technical University Delft

DC Systems, Energy Conversion and Storage Group

# Designing an optimized closed electrical distribution system for a multi-carrier energy hub on a mixed-use area in Hilversum

## Msc Sustainable Energy Technology

by

T.J. Broekman

to obtain the degree of Master of Science
at the Delft University of Technology,
to be defended publicly on Friday July 11, 2025 at 9:00 AM.

Student number: 4947924

Project duration: September 19, 2024 – July 11, 2025

Thesis committee:

| | | |
|---|---|---|
| L.M. Ramirez Elizondo | TU Delft, DC Systems, Energy, Conversion & Storage | Associate Professor |
| F.A. Munoz | TU Delft, High Voltage Technology Group | Assistant Professor |
| J.A. Castillo | TU Delft, DC Systems, Energy, Conversion & Storage | Researcher |
| Jeroen Pool | HET Cooperative | Project leader innovative charging and system integration |

An electronic version of this thesis is available at https://repository.tudelft.nl/.

TU Delft

# Abstract

The accelerating Dutch energy transition faces a growing challenge: grid congestion is increasingly limiting the integration of local renewable energy and electrification initiatives. This thesis addresses this challenge by designing and optimizing a Closed Distribution System (CDS) for the Werf area in Hilversum, a mixed-use area that aims to achieve energy autonomy by 2028. In collaboration with the HET cooperative and stakeholders from the Vereniging Duurzame Werf (VDW), this research explores the optimal sizing and configuration of a multi-carrier energy hub integrating a fifth-generation district heating network (5GDHN), aquifer thermal energy storage (ATES), photovoltaic thermal (PVT) modules, battery energy storage systems (BESS), and additional photovoltaic (PV) generation.

A python based energy system model was converted to an MILP-based optimization model to minimize costs under a range of future grid connection scenarios, while meeting projected 2028 electrical and thermal demand profiles at a 15-minute resolution. The results of these scenarios are used to predict infrastructure capacity requirements for the future energy system.

The electrical and thermal demand patterns for 2028 were estimated and confirmed, accumulating to 1,244 MWh and 1,371 MWh respectively. The energy system is optimally sized for two connection categories; the AC5a connection category (535–630 kW) requires a relatively modest investment of €427k, while the SolarPark connection (300–350 kW) entails a significantly higher investment of €4.9M. However, this higher investment enables substantially greater energy autonomy for the area. The proposed load shifting technique does not improve the optimal cost solution for all possible connections, but the direct load control does. While parts of the existing electrical infrastructure can be reused, certain sections will need to be upgraded or replaced with higher-capacity components, depending on the selected grid connection size.

This study contributes a replicable framework for CDS-based energy hub design with an ATES in urban environments and demonstrates how energy hubs can at the same time reduce regional grid stress and contribute to the regional energy autonomy. This thesis enables sustainable urban redevelopment aligned with Dutch climate targets.

# Preface

This thesis marks the final step in completing my Master's degree in Sustainable Energy Technology at TU Delft, with a specialization in Power Engineering. The research presented in this report aims to provide stakeholders with insights into the cost implications of minimizing grid connection capacity when implementing a Closed Distribution System (CDS) in combination with a 5th Generation District Heating Network and an Aquifier Thermal Energy Storage. The thesis is grounded in a real-world case, offering practical relevance to a timely and evolving energy topic.

I would like to express my sincere gratitude to those who supported me throughout this journey. First, I thank my supervisor Laura for her continued guidance. After supervising my Bachelor's project in Electrical Engineering, she once again made it possible for me to undertake this Master's thesis under her supervision. I am grateful to Jeroen and the HET Cooperative for providing access to a concrete case study in Hilversum, which formed the foundation of this work. The same holds for the partners of VDW for generously sharing their real-life energy consumption data.

Special thanks go to Joel for the time and effort he invested in helping me with structured writing and assistance with numerous other aspects. I also want to thank Manfredo for his valuable support with coding and optimization, which greatly contributed to the technical execution of this project.

Last but certainly not least, I thank my family for their unconditional support during what was perhaps the most challenging period of my academic journey.

I will definitely visit the Werf area in 2028 to see what has become of the ambitious plans of the innovative owners and advisors.

*T.J. Broekman*
*Delft, July 2025*

# Nomenclature

**Abbreviations**

| | |
|---|---|
| CDS | Closed (Electrical) Distribution System |
| (5G)DHN | (Fifth Generation) District Heating Network |
| HET | Hilversumse Energie Techniek cooperatie (Hilversum Energy Technology cooperative) |
| VDW | Vereniging Duurzame Werf (Association Sustainable Werf) |
| DSO | Distribution System Operator |
| TSO | Transmission System Operator |
| PVT | PhotoVoltaic Thermal |
| ATES | Aquifier Thermal Energy Storage |
| BESS | Battery Energy Storage System |
| PV | PhotoVoltaic |
| COP | Coefficient Of Performance |
| CHP | Combined Heat and Power |
| EMS | Energy Management System |
| PWL | Piece Wise Linear |
| CAPEX | Capital Expenditures |
| OPEX | Operational Expenditures |

# Contents

# 1

# Introduction

The urgency of the energy transition has never been greater. Driven by the accelerating impacts of climate change [1] and the geopolitical instability highlighted by the war in Ukraine, the Netherlands and the rest of Europe face a dual imperative: reducing greenhouse gas emissions and ensuring energy autonomy. These challenges require not only a swift shift toward renewable energy sources, but also a fundamental transformation of how we produce, distribute, and consume energy.

A central part of this transformation is the electrification of processes that currently rely on fossil fuels, coupled with a significant increase in renewable electricity generation, such as solar and wind power. However, while technological developments and public support for sustainability continue to grow [2], the energy transition is increasingly constrained by a critical bottleneck: grid congestion. The electricity grid, both at transmission and distribution levels, is struggling to accommodate the rising number of new connections and the volatility of renewable energy. Ironically, this infrastructure limitation is slowing down the very transition that must be accelerated.

In response to these constraints, the energy system is becoming increasingly decentralized. Local generation, energy storage, and demand management are emerging as essential components of a more resilient energy infrastructure. One technical solution gaining traction in this context is the Closed Distribution System (CDS), a privately managed local electricity network that can operate more flexibly than the public grid. When combined with a District Heating Network (DHN), a CDS forms the basis for a local energy hub, where heating and electricity demands are met using local, sustainable sources and smart coordination.

By integrating supply and demand within a closed system, and minimizing the size of the external grid connection, CDS-based solutions allow for a more efficient use of existing grid capacity. This not only reduces costs for the stakeholders involved but also helps reducing regional grid congestion, thereby freeing up space for other users and accelerating the broader energy transition.

These benefits are also desired by the stakeholders of the case study of this research, namely the HET cooperative and the VDW association, who will be elaborated on in the next section (1.1). Their goals to achieve a sustainable and autonomic energy system on the case study area is aligning with the proposed solution involving a CDS.

This project will investigate the scaling and sizing of a CDS, as a part of a more elaborate energy hub containing a 5GDHN and ATES, by minimizing the grid power connection to the external grid. It will define the way energy is consumed in an outlook involving future sustainability plans. Furthermore, it will minimize costs for the components in the CDS to the available net connection sizes offered by the DSO, thereby determining the sizing of the system. This minimization will connect investments to the minimization of grid connection power. Next, the influence of load shifting and direct load control will be investigated, determining their efficiency and feasibility on the project area. Lastly, the electrical infrastructure requirements for the proposed solutions and sizing will be determined.

This chapter starts with an explanation about the case study of this project, defining the stakeholders, physical area and the challenges defined for it. Next, the problem is stated, defining the causes which make this research valuable. Lastly the research questions are defined, elaborating on how this problem can be solved by stating questions to be answered through the investigation.

## 1.1. Case study

This thesis is written in collaboration with the HET (Hilversumse Energie Techniek / Hilversum Energy Technology) cooperative. This cooperative has collaborated with the DCE&S group of the TU Delft for multiple projects. HET is a local energy cooperative founded in Hilversum, a city in the Netherlands between Amsterdam and Utrecht. The cooperative assists in local sustainability projects as well as rolling out pioneering initiatives. For instance, the cooperative set up a local car sharing program [3] and it assist residents by making their houses more sustainable.

The project which acts as case for this research, is the Werf area. This now mixed-use area, an old municipality area, is located in Hilversum Oost and it holds industrial and residential buildings, containing restaurants, offices and medium industrial processes (for impressions see Appendix C). The property on the area is owned by four real estate partners, which have unified themselves in an association named VDW (Vereniging Duurzame Werf / Association Sustainable Werf). This association is collaborating with as goal making the Werf area a future proof sustainable area. HET is assisting the VDW with their roadplan to sustainability by conducting research on the possibilities, creating sustainable projects as well as guiding the VDW through those projects.

A large contribution of HET is the investigation they executed on behalf of VDW, mapping the possibilities for a sustainable Werf area [4]. The VDW is exploring opportunities for new buildings, mostly residential, to give the area a more hybrid character. This new construction is paired with the ambition to make the area more sustainable, with as goal to achieve energy autonomy at 2028. In this research HET investigated the current and new buildings, the energy consumption, the existing sustainable plans and the possibilities for further development on sustainable energy and other steps to achieve the energy neutrality.

An already existing sustainable plan is the development of a Solar Car Park on the Mussenstraat, a large street on the Werf. This involves plans to cover a parking lot with solar panels or optionally with PVT panels, making a large step in sustainable energy generation in the area. For this solar car park, a grid connection has been permitted by the DSO. The contracted capacity amounts 300 kW of supply and 350 kW of return injection into the grid. The possibilities of this permitted connection to contribute to a CDS will also be evaluated in this thesis.

HET has previously collaborated with a TU Delft master student on this project area. T. Beijneveld investigated the opportunities of a 5GDHN on the area, assisted by a PVT system and a thermal aquifier storage system [5]. That PVT system is proposed to be located on the solar car parking. In this research he investigated the storage distribution and configuration and the sizing of the components with as goal minimizing total grid interaction and $CO_2$ emissions. He concluded that a single ATES of 380,000 $m^3$ was the optimal size and configuration of the storage, assisted by the maximum possible PVT modules of 800. This configuration led to the highest DHN temperature and with that the highest COP for the heat pumps, leading to the highest efficiency and the lowest $CO_2$ emissions.

This thesis will use the previously noted work as groundwork to start the investigation to a CDS. It will use the heating network and thermal storage (ATES) as the first components of the energy hub, but expands the electrical network with a BESS and additional PV generation. In addition, this electrical network is being isolated from the external grid, with only one main connection. Wind generation will not be considered, as the research by HET concluded that this technology is not applicable on the area due to permitting issues.

Where Beijneveld studied the minimal grid interaction, this thesis will investigate the minimum grid connection power which also takes into account the broader picture of regional and national net congestion. This means that apart from only the energy produced and consumed in total, also the moment in time when that happens will be of importance.

## 1.2. Problem statement

The Netherlands is making significant progress in the field of sustainable electricity. As of recent years, more than half of the national electricity production is derived from renewable energy sources [6]. This marks a commendable shift toward de-carbonization and aligns with the country's climate goals. However, despite this progress, the continued expansion of renewable energy generation and the electrification of processes and infrastructure face a major obstacle: grid congestion [7].

Grid congestion occurs when the existing electricity infrastructure is no longer capable of handling the increasing supply and demand for electricity. As a result, new energy consumers and producers are frequently unable to obtain or expand grid connections. This has created a bottleneck that slows down the national energy transition and prevents the efficient integration of new renewable sources.

This national issue manifests at the local level as well. TSOs and DSOs are forced to invest heavily in grid expansion and reinforcement, which entails long timelines and significant costs [8]. These costs are often passed down through increased transport tariffs, placing a greater financial burden on energy prosumers. At the same time, local stakeholders—such as municipalities, businesses, and residents—are unable to electrify heating, mobility, or industrial processes due to limitations in their connection capacity. New solar or wind projects are frequently stalled, not due to lack of technology or funding, but because of the inability to connect to an already overloaded grid [9].

One of the most effective and immediate solutions to this problem lies in optimizing the use of existing grid connections. By combining connections and spreading out energy demand, peak loads on the grid can be significantly reduced, which in turn frees up capacity for others. This approach becomes even more effective when combined with local renewable energy generation and energy storage, allowing demand and supply to be balanced more efficiently on-site or within closed energy systems.

In this context, minimizing the total grid connection size of a closed distribution system emerges as a cost-effective strategy. It not only reduces grid fees for the stakeholders involved but also alleviates pressure on the public grid. As such, this local-level solution contributes directly to resolving regional and national challenges associated with grid congestion and supports a more resilient and flexible energy system.

## 1.3. Research questions

The objective of this research is to efficiently size the proposed multi-carrier energy hub on the Werf area, in order to minimize the grid connection. This goal will be achieved by formulating a main research question, which is divided into four sub questions. The answers to these sub questions will lead to a final answer to the main research question, thereby concluding this research. This conclusion will lead to an energy hub with a 5GDHN, PVT system, ATES and an optimally sized CDS containing a BESS and additional PV generation.

**Main question:**

**What is the optimal configuration and sizing of a multi-carrier energy hub (closed distribution system) in the Werf area in Hilversum towards the minimization of the grid connection size as a step toward achieving energy autonomy?**

This main question captures the aim off the study, to size an integrated energy system that maximizes local generation and consumption, thereby reducing the dependency on the electricity grid and with that support the broader goal of decentralization and sustainability. Due to the broad definition, it is split up in four more narrow sub questions, defining the methodology to answer the main research question.

**Sub questions:**

- What will be the electrical and heat demand pattern of the Werf area in 2028?

Understanding the future energy demand is crucial for the sizing of the energy system. This questions aims to define the thermal and electrical demand pattern for the year 2028. These patterns will be used

for optimizing the energy hub and minimizing the grid power connection. The heat demand is derived by interpreting the model developed by T. Beijneveld, using actual historic weather data [5]. The electrical power demand is adapted from industrial demand data from the Werf area and generated residential load patterns.

- What is the optimal sizing of the multi-carrier energy hub neglecting internal network limitations?

In the approach for answering this research question it is assumed that the electrical energy in the area has no resistance in transportation. This means there are no internal network limitations. Via an optimization solver the costs of reducing the grid connection power is minimized. This minimization is done per available grid connection size defined by the grid operator.

- How can a combination of load shifting of controllable loads and direct load control influence the sizing of the system, and is its implementation feasible in this area?

This question investigates the potential of some flexibility measures on the area in order to reduce peak grid exchange introduced by high demands or production. With those measures recursive optimizations are executed and their results are compared to the results of the base scenario, which are retrieved by running the optimizations introduced in the methodology from the second research question. Next to this technical impact also the practical feasibility is evaluated.

- Depending on the size of the feasible grid connections defined by Liander, what are the required electricity infrastructure capacities?

Finally, this question explores the power exchange between components in a few optimal scenarios. These power flows will determine the capacity of the cables distributing the energy over the area. With this the possibility of reusing current electrical infrastructure is evaluated.

# 2

# State of the art

The concepts of energy hubs and microgrids are no novelties in the world of sustainable energy. They provide a flexible, decentralized, autonomous and resilient approach to the energy supply of local areas. Because the topology and components across the landscape of energy hubs differs, this chapter introduces the key concepts and components related to the microgrid model created and optimized in this paper.

After the introduction of the key concepts, other research on sizing of energy hubs and closed distribution networks is identified. The methods, its results and limitations are analyzed, clarifying the present research gap which this paper intents to fill. With this gap defined, the contribution of this thesis is identified. Lastly, the mathematical formulations of the models of the key concepts are described.

## 2.1. Key definitions

The components, their working and characteristics are briefly described here. In a later section (2.4) a more detailed description of the components and the underlying mathematics and physics is provided.

### 2.1.1. Closed Distribution System

A Closed Distribution System (CDS) refers to an electrical distribution network that operates independently or in limited interaction with the public electricity grid. It is typically used in localized environments like energy hubs where multiple energy sources, loads, and storage systems are managed within an electrical boundary.

In a CDS, power is generated, distributed, and consumed within a defined area under control of the

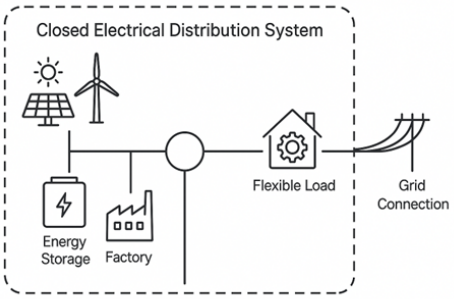


Figure 2.1: Schematic of a possible CDS layout

operator of the CDS. It often includes sustainable distributed energy resources like solar panels, wind turbines, combined heat and power (CHP) units, and battery energy storage systems. These systems can be connected to the public grid, but only through a single or limited point of interconnection, allowing for controlled import and export of electricity.

The “closed” nature refers not only to the physical boundaries of the system, but also to the fact that all operations are managed internally, often through an specifically developed energy management systems (EMS).

A few advantages of a CDS are:

- Grid independency
- Optimal energy consumption
- Optimally sized connection power size
- Simplified renewable integration
- Operation autonomy

On the other hand, disadvantages can be:

- High capital costs
- Complex load management
- Regulatory and compliance challenges

### 2.1.2. Battery energy storage system

A Battery Energy Storage System (BESS) is an electrochemical solution designed to store electricity for later use. It plays a crucial role in modern energy systems by providing flexibility, stability, and reliability across various applications ranging from renewable integration to grid support and behind-the-meter optimization. A BESS typically includes one or depending on is size, more battery banks, power conversion systems (inverters) and a battery management system.

The core function of a BESS is to store energy when it is abundant or inexpensive and release it when demand is high or supply is limited. With these actions the system can also act as a balancing supplier. It serves as a buffer between energy generation and consumption, smoothing fluctuations and improving overall system efficiency. BESS units can operate independently, in combination with renewable energy sources (like solar or wind), or as part of a larger microgrid or energy hub.

### 2.1.3. Heat pump

A heat pump is a thermal energy system that transfers heat from one location to another using electricity, typically moving heat from a cooler source to a warmer one. Unlike conventional heating systems that generate heat by combustion or resistance, heat pumps use a (reverse) refrigeration cycle to extract existing thermal energy from ambient sources such as air, water, or ground.

Heat pumps operate on the principle of reversible thermodynamic cycles, enabling them to both heat and cool spaces depending on the mode of operation. A common setup includes a compressor, expansion valve, condenser, and evaporator, all working together to absorb heat from a low-temperature source and release it into a higher-temperature area.

There are several types of heat pumps, including:

- Air-source heat pumps:
  - draw heat from the outdoor ambient.

- Ground-source (geothermal) heat pumps:
  - extract heat from the earth via heat exchangers buried underground.
- Water-source heat pumps:
  - use lakes, rivers, or wells, or in this case, a thermal network to extract heat.

Heat pumps are known for their high COP and ability to supply both space heating and domestic hot water. The heat pumps are an essential piece of technology enabling a coupling between the electrical and the thermal domain.

### 2.1.4. Photovoltaic modules

Photovoltaic (PV) modules are one of the most widely adopted technologies for generating electricity from solar energy. They operate by converting sunlight directly into electrical energy through the photovoltaic effect, a process in which photons from sunlight excite electrons in a semiconductor material. This creates a flow of electric current that can be used immediately, stored in batteries, or fed into the electrical grid.

The efficiency of PV modules ranges between 15% and 22% for most commercially available systems. Factors influencing performance include cell temperature, orientation, shading, and local weather conditions.

PV modules play a central role in the transition to renewable energy by enabling distributed generation, reducing dependency on fossil fuels, and lowering carbon emissions. They are often integrated into residential, commercial, and utility-scale projects, and increasingly paired with battery energy storage systems (BESS).

### 2.1.5. Photovoltaic thermal modules

Photovoltaic-Thermal (PVT) systems are hybrid energy technologies that simultaneously generate electricity and capture thermal energy from the same surface area. By integrating a photovoltaic (PV) module as described before with a thermal collector, a PVT system enhances the overall energy yield of a solar installation and makes more efficient use of available solar radiation.

A PVT module combines traditional solar cells with a thermal absorber attached to the back of the PV module. As sunlight strikes the module, part of the energy is converted into electricity through the photovoltaic effect, while a significant portion is absorbed as heat. In standard PV systems, this heat raises the cell temperature, which actually reduces electrical efficiency. In a PVT system, however, the thermal absorber captures this waste heat and transfers it, usually via a fluid loop, to be used for heating water or air.

By removing excess heat from the PV cells, the system not only delivers useful thermal energy but also improves the electrical performance of the PV module through passive cooling. The dual output of electricity and heat results in a higher combined energy conversion efficiency compared to standalone PV or solar thermal systems.

### 2.1.6. 5th generation district heating network

A district heating network is an efficient system to deliver energy in the form of water at a certain temperature. This water is mostly transported in an insulated underground piping system from source to consumption.

A 5GDHN is an advanced, sustainable system for heating and cooling buildings. Unlike traditional district heating networks that rely on high-temperature water to warm homes and offices, a fifth generation system operates at much lower temperatures and often integrates renewable energy sources. This makes it far more energy-efficient and environmentally friendly.

In a 5GDHN the circulating flow is low-temperature water, often around 10 to 25 °C. Because the temperature is lower, it allows for the recovery of heat from various sources, such as excess heat from industrial processes, solar thermal collectors, geothermal energy, or even heat from wastewater. Buildings connected to the network can use heat pumps to upgrade this low-temperature heat for space heating and hot water, and in some cases, the system can also provide cooling during warmer months.

The 5GDHN also has challenges which should be noted. Due to the lower temperatures of the circulating water, a higher pumping rate is required to deliver the same amount of energy to the consumers. This pumping rate translates in a higher electricity consumption. Furthermore, the lower temperatures of the network often do not directly meet the temperature required at the end user, so an additional temperature boost is needed. Despite those disadvantages, the 5GDHN offers a large set of benefits including flexibility, efficiency and low costs, which make them a suitable option for modern heating and cooling applications.

Because of the temperate climate in the Netherlands, the Werf has nihil cooling requirements. This leads that in this research only a single warm temperature loop in the DHN is utilized.

### 2.1.7. Aquifier thermal energy storage

The Aquifier Thermal Energy Storage is a form of a Thermal Energy Storage System (TESS). Where a regular TESS has enclosed and insulated volumes for storing thermal energy, the ATES utilizes characteristics of the soil, an underground aquifier. The water is injected and withdrawn through wells, whereby the difference of the incoming water determines if the energy is stored or extracted. The aquifier is a water-bearing geological formation, which makes the system open, in contrary to closed systems where the water is circulated through heat exchangers in the soil.

The aquifier can be used to inject hot water in periods with surplus of energy, for instance with solar PVT generation, or with wastewater from industrial plants. When heat demand is higher, the heat can be extracted from the water which is pumped from the aquifier well. The ATES is a good match with a 5GDHN because of the low temperatures and the seasonal storage capabilities the ATES can supply. The low temperatures ensure the high efficiency of the storage due to lower heat losses to the surrounding soil.

## 2.2. Research gap

The intentions of this research have a twofold nature. On the first hand it is impacting the energy autonomy and the transport costs of the property partners, where on the other hand the regional sustainability is increased due to the creation of extra capacity on the grid. Furthermore, the overall consumption of energy is stemming from more sustainable sources. An energy-hub containing a DHN, an ATES, a PVT system, a BESS and a CDS with as goal minimizing grid connection power is quite unexplored and presents new insights into this field. To establish the novelty of this, a literature review is performed with the direction of the objective of minimizing grid connection power in combination with this type of energy hub. The literature review provides us with the following State of the Art about the described field.

Closely related and fundament of this research is the investigation T. Beijneveld executed on the sizing of a DHN on the Werf area [5]. The paper presented describes the sizing and design of a 5GDHN integrated with an ATES and a contributing PVT system. The study focusses on the configuration, distribution and sizing to minimize the electrical power consumption overall. The goal of this research is the minimization of overall $CO_2$ emissions originating from the energy consumption of the area. His strategy encapsulates a thermal network fed by a PVT system, and supplementary heat pumps per building. The thermal network is coupled to an ATES, providing the seasonal energy storage.

In a paper by Kassab et al., a mixed-integer linear programming (MILP) framework is developed to optimally size and operate a hybrid energy system with solar PV, a BESS, and flexible loads [10]. A key innovation in their approach is the explicit modeling of a maximum grid subscription power. This is a constraint that limits the allowable peak power drawn from the main grid. This aligns closely with the objectives of this paper, sizing the system for a fixed maximum grid power. This is especially relevant

in microgrids or CDS applications where infrastructure costs or contractual limits make peak demand critical, or in this case in an investigation to minimize grid power at the boundaries set by the DSO. Their results demonstrate that imposing such a limit not only smooths the power exchange profile but also increases the local renewable energy utilization. This study provides a valuable methodological precedent for this thesis, which similarly targets the minimization of grid connection power through strategic sizing of distributed energy resources. However, this proposed system lacks a thermal component, which will be introduced in this research in the form of a DHN, an ATES and a complementary PVT system.

Another recent thesis by Gerards presents a comprehensive methodology for the optimization and performance evaluation of in his nomenclature, hybrid energy networks [11]. Using a mixed-integer linear programming (MILP) algorithm in conjunction with partitional clustering for demand profile classification, the study develops an optimization framework capable of minimizing total system costs, $CO_2$ emissions, or a weighted combination of both. While the main optimization objective is not explicitly to minimize grid connection power, the study shows a good blueprint for this thesis. This makes the study relevant to the microgrid and CDS design proposed in this thesis, as it can offer insights into the role of integrated thermal-electrical systems and smart storage sizing in minimizing external grid interaction.

As noted in Chapter 1, the HET research describes the goals and ambitions of the area as aspired by the VDW [4]. In this research, reference areas are described which could be inspiration for the investments on the Werf.
In the research an industrial area in the proximity of Apeldoorn is identified, named “De Ecofactorij”. The Ecofactorij is a medium to large industrial area consisting of approximately 20 companies. The energy consumption of those companies are quite energy extensive with companies in concrete and metal production, but also datacenters are present in the area. The area has a closed distribution network with solar generation, smart control and a battery energy storage system of around 5 MWh [12]. Due to the CDS their transport costs are reduced by 30% and due to the smart control systems they experience a lot of financial benefits.

Where T. Beijneveld studies the overall energy exchange, this research focuses on the grid connection power, so the instantaneous energy exchange with the grid. This broadens the scope of the research beyond just the Werf area and its $CO_2$ emissions. The research also takes into account the impact this area has on the net congestion in the area, which might be preventing other assets of users from electrifying their processes or keep sustainable energy technologies from being connected to the grid. This broadens the qualitative scope of the $CO_2$ footprint this paper investigates, without directly quantifying this.

The Ecofactorij is a good reference point for the feasibility of a CDS. The configuration and the successfulness of this project expresses confidence in the ambitious plans of the VDW. A complementary element of this research is the combination with a thermal network and seasonal storage in the form of an ATES. This combination creates a new interaction between the heating network and the CDS, which has not been investigated before.

## 2.3. Contribution

After the quantitative research in the previous section, the scientific contribution of this thesis can be addressed. This thesis contributes by the construction of a multi-carrier, closed distribution energy system for mixed use areas. This construction with a 5GDHN and ATES in combination with CDS is additionally sized to minimize the grid connection to the DSO, thereby creating space on the grid. This space can then be allocated to other prosumers, preventing net congestion and making room for sustainable energy sources and demands. This contributes to a more sustainable energy generation and consumption, assisting to the climate goals set by the Dutch government, thereby improving the life for current and future generation on our planet.

## 2.4. Mathematical formulations

In this section the mathematical formulations are described which define the model of the energy system on the Werf. The description is divided in components related to heating energy and electrical energy, where the heating components are adopted from the previous work of T. Beijneveld on the heating network on the Werf area [5].

### 2.4.1. Thermal

#### DHN

This subsection describes the physics and mathematics behind the transportation of stored and generated heat from the PVT system and the ATES to the heat loads. In the district heating network, the energy carrier is warm water. This energy is transported through insulated pipes. Depending on the environment, these pipes can either lose or gain energy. This is translated in a temperature difference between the flow at the entrance of the pipe and the exit of the pipe. The pipes lay at a certain depth underground, which is displayed in the following graphic (2.2).

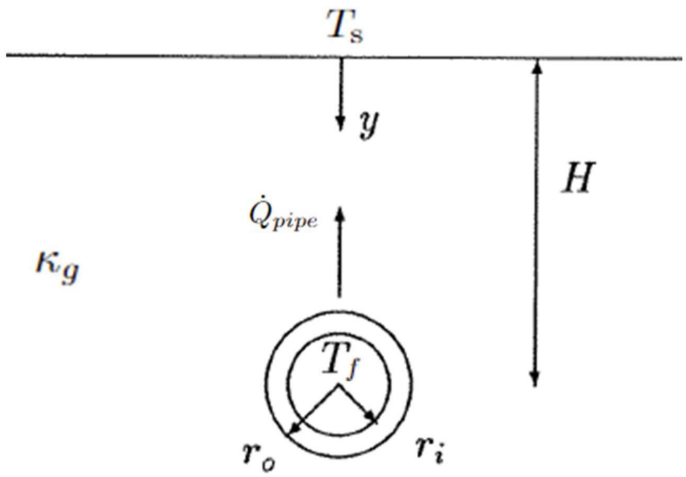


Figure 2.2: Cross section of the DHN transportation pipes [5]

Table 2.1: Parameters related to pipe heat transfer

| Parameter | Description | Unit |
|---|---|---|
| $T_s$ | Surface temperature | [K] |
| $K_g$ / $K_{soil}$ | Soil thermal conductivity | [W/(m·K)] |
| $\dot{Q}_{pipe}$ | Heat losses/gain pipe | [W] |
| $T_f$ | Fluid temperature | [K] |
| $r_0$ | Outer radius | [m] |
| $r_i$ | Inner radius | [m] |
| $H$ | Depth of pipe (surface to center pipe) | [m] |

The temperature of the fluid through a pipe is varying depending on the distance traveled through the pipe. The pipe is modeled with infinitesimal sections of size $dx$ differing in temperature. The heat loss of such a section to the soil, here described with $\dot{Q}_f$, can then be described with equations 2.1 and 2.2. A schematic of the modeling is shown in Figure 2.3.

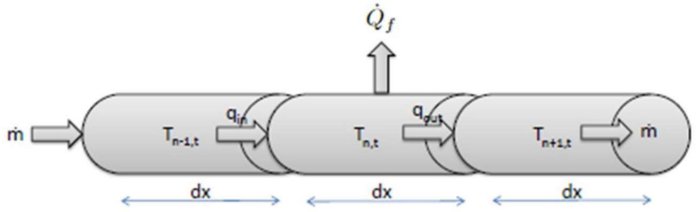


Figure 2.3: Modeling of the DHN pipe with infinitesimal sections [5]

$$\dot{Q}_f(x) = \dot{m}_f c_f \left[T_f(x) - T_f(x+dx)\right] = \dot{m}_f c_f dT_f \tag{2.1}$$

$$\dot{Q}_f(x) = \frac{\left[T_f(x) - T_s(x)\right] dx}{R_t} \tag{2.2}$$

Combining these equations leads to the following expression (2.3), which can be integrated on the fluid differential temperature $dT_f$ and section size $dx$ respectively.

$$\int_{T_{\text{in}}}^{T_{\text{out}}} \frac{1}{T_f(x) - T_s(x)}\, dT_f = \int_0^L \frac{1}{\dot{m}_f c_f R_t}\, dx \tag{2.3}$$

The integration boundaries are the temperatures entering and exiting the pipe over length $L$, which is the integration boundary of the RHS. This integration results in the following expression 2.4, which is rewritten to a different form and shown in equation 2.5.

$$\frac{T_s(x) - T_f^{\text{out}}(x=L)}{T_s(x) - T_f^{\text{in}}(x=0)} = e^{-\frac{L}{\dot{m}_f c_f R_t}} \tag{2.4}$$

$$T_f^{\text{out}}(x=L) = T_s(x) - \left[T_s(x) - T_f^{\text{in}}(x=0)\right] e^{-\frac{L}{\dot{m}_f c_f R_t}} \tag{2.5}$$

The calculation of $T_s$, which is assumed constant everywhere, and the calculation of $R_t$ can be found in the code via Appendix D.
Now that the temperature of the fluid at the end of the pipe is known, the heat loss of a pipe can be calculated (2.6).

$$\dot{Q}_{\text{pipe}}(k) = \dot{m}_f c_f \left[T_f^{\text{out}}(k) - T_f^{\text{in}}(k)\right] \tag{2.6}$$

**Building losses**

The 15 buildings which will be present on the Werf area are categorized in 3 distinctions; small, medium and large. These buildings exchange heat energy with the environment. This transfer is dependent on the difference between indoor and outdoor temperature, and the total heat capacity of the building.

The desired indoor temperature for these buildings is set on a thermostat. This means as the building loses heat to the environment, the temperature decreases below the thermostat setpoint, and heat should be supplied to the building. This heat is supplied by a boiler, and the control process of this boiler is further explained in subsection 3.2.1.

The heat exchange with the environment is determined by losses through walls, windows and the roof. The losses are determined by three components.

First there is the conduction and convection loss (2.4), which are losses through the three previously described components of the building.

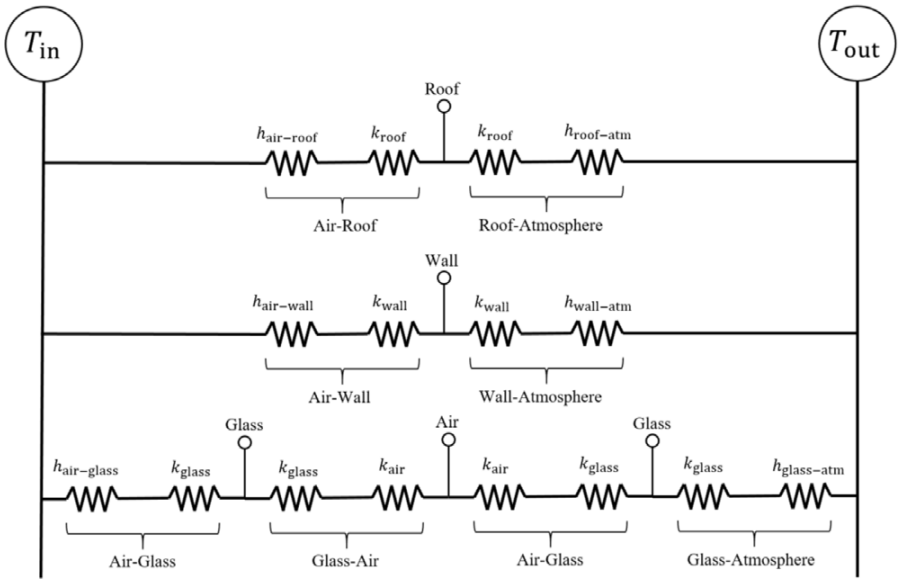


Figure 2.4: Conductive and convective losses of the buildings [5]

The second type is ventilation, which is an intentional mass exchange between interior and exterior, leading to a heat exchange. The third type, infiltration, is a similar type of exchange, but it is unintentional, and is calculated in with a different approach.

These building losses add up to a combined exchange with the following formula (2.7). $Q_D$ is the total building demand per timestep.

$$\dot{Q}_D\,(k) = \dot{Q}_{C\&C}\,(k) + \dot{Q}_V\,(k) + \dot{Q}_I\,(k) \tag{2.7}$$

The buildings indoor temperature changes every timestep depending on their total mass heat capacity, the input heat power from the boiler and the heat loss power.

$$T_{\text{in}}\,(k+1) = T_{\text{in}}\,(k) + \frac{\Delta t\left(\dot{Q}_B + \dot{Q}_D\right)}{\sum_{i=1}^{n} m_i c_i} \tag{2.8}$$

The summation in the denominator of the fraction in the formula above (2.8) describes the buildings and their related capacities per room, summing to the total building mass heat capacity.

**Heat pump**

Heat pumps are an essential part of the energy system on the Werf. They complement the district heating network in fulfilling the heat demand of the area, as well as being able to inject more energy into the DHN at timesteps of surplus sustainable electrical generation.

In contrast to gas boilers or other energy suppliers, heat pumps transfer energy from the source to the demand. In this case the source of the heat pump buildings is the water from the DHN. By compressing refrigerant, heat can be extracted from the colder network flow and this extracted heat is then transferred to the boiler inside the building. The schematic working of the heat pump is displayed in Figure 2.5.

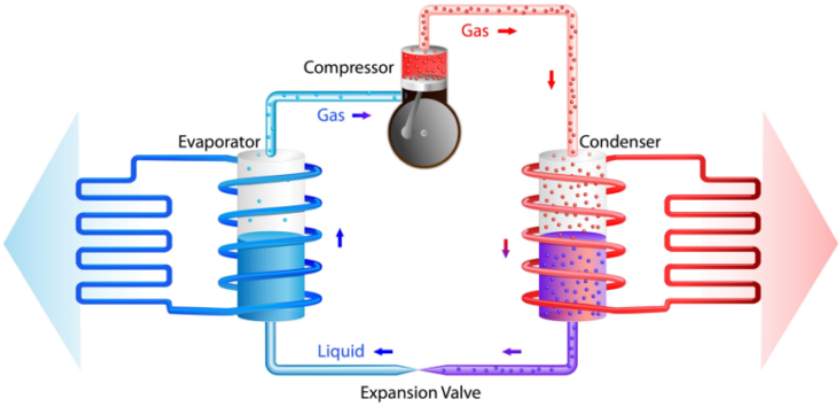


Figure 2.5: Schematic of the working principle of a heat pump *Source:Ventilex.com*

To determine the electrical power required to meet the heating demand, the coefficient of performance is calculated as follows (Equation 2.9).

$$COP\,(k) = 7.90471\; e^{-0.024\Delta T(k)} \tag{2.9}$$

Where $\Delta T$ is the difference in temperature between the flow of the DHN and the temperature of the water returning from the buildings boiler. The electrical power is described by Equation 2.10.

$$P_{\mathrm{HP}}\,(k) = \frac{\dot{Q}_{\mathrm{HP}}\,(k)}{\mathrm{COP}\,(k)} \tag{2.10}$$

The formulation for $Q_{HP}$ differs per control theory, so this is treated in the methodology per research question.
The heat power extracted from the DHN is determined by equation 2.11.

$$\dot{Q}_{\mathrm{DHN}}\,(k) = \dot{Q}_{\mathrm{HP}}\,(k)\left(1 - \frac{1}{\mathrm{COP}\,(k)}\right) \tag{2.11}$$

**ATES**

The thermal energy storage system (TESS) of the projected energy system on the Werf will be a type of aquifer storage. An aquifer is an underground layer of water-bearing material, capable of storing warm water. The thermal storage system will assist in the heating of the buildings, mainly in the winter. In summer, large quantities of energy will be injected into the aquifer generated by the PVT system, storing it for the following winter.

In theory, the temperature of the soil is constant from 6 meters and deeper [13]. Measurements confirm this as the results for Hilversum show a constant temperature between 25 and 126 meters deep, concluding that environmental effects do not affect the soil temperature at those depths [14].

The DHN will inject and extract water at a constant rate and it is assumed that injected water instantaneously mixes with the rest of the aquifers contents. Further it is assumed that the extracted water temperature is at the general mix temperature of the ATES.

The stored water in the ATES loses a part of its energy to the surrounding soil. This loss is described in three parts, loss to the top (overburden), loss to the bottom (underburden) and loss to the sides. The summation of these losses results in the total heat power that the ATES loses to the surrounding soil.

The deviation in temperature of the aquifer stems from the removal of energy from the outlet, the energy loss to the environment and the injection of energy at the inlet. These components relate as displayed

in expression 2.12 and influence the main temperature of the ATES at the next timestep. Here $m_w$ is the mass of the water in the aquifier and $c_f$ is the specific heat of the fluid (water). $m_r$ is the mass of rock and $c_r$ is the specific heat of this rock.

$$T_{\text{ATES}}^{\text{out}}(k+1) = T_{\text{ATES}}^{\text{out}}(k) + \left[\dot{m}_f c_f \left[T_{\text{ATES}}^{\text{in}}(k) - T_{\text{ATES}}^{\text{out}}(k)\right] + \dot{Q}_{\text{soil}}(k)\right] \cdot \left(\frac{dt}{m_w c_f + m_r c_r}\right) \tag{2.12}$$

**PVT**

T. Beijneveld describes a sophisticated method to describe the heat power generated by a PVT panel, depending on global irradiance, ambient temperature and wind speeds [5]. However, this model is computationally too expensive to implement in the optimization model. Next to the fact that it would make the model non-linear and therefore harder to solve, the computation itself must be calculated per second in order to keep stability of the PVT-model.

This is why an approximation has been developed, together with a implementation which makes the PVT characteristics easy for the optimization model to process.
The physical configuration of the PVT system is as follows. It contains of PVT modules, a temporary storage tank and a heat exchanger. The fluid from the temporary storage tank circulates through the modules, which heats up the tank temperature. When the temperature in the tank is higher than that of the passing fluid from the heating network, it is transferred to the network via the heat exchanger.

In order to mitigate this complex behavior, the following is assumed.
In the modeling of the process of heating water in the PVT system, for every 15 minutes it is checked how much energy the PVT system as a whole can contribute to the heating network. This depends on the environment, but also on the current temperature of the heating network. With a lower DHN temperature, it is easier for the PVT system to add energy. This contribution of energy is calculated from the possible temperature increase in that timestep, for a set of possible DHN temperatures with a resolution of 1°C. The temperature of the DHN is assumed to enter the PVT collector. The physical PVT model calculates the temperature of the fluid coming out of the panel considering the environmental data of that timestep. The temperature deviation from the temperature entering the panel is used to calculate the heating power in that timestep.

This power versus DHN temperature curve can easily be linearized. The next step is to filter out the negative values, as the PVT system will not extract energy from the heating network. The remains is a set of possible powers delivered by the PVT system depending on the timestep and the DHN temperature at that timestep, which can be interpreted by the optimizer.

The original expression and its linearization can be found in equations 2.13 and 2.14.

$$\dot{Q}_{\text{PVT}}(k) = N\eta\dot{m}_f c_f \left[T_f^{\text{out}}(k) - T_f^{\text{in}}(k)\right] \tag{2.13}$$

$$\dot{Q}_{\text{PVT}}(k) = \alpha T_f^{in}(k) + \beta \tag{2.14}$$

To make sure that the PVT system does not cool down the DHN, the power output is nonnegative. This means that if the result of the linear expression yields a negative output, $\dot{Q}_{\text{PVT}} = 0$.

The equations used to calculate the fluid temperature out of the modules can be found in the code via Appendix D.

## 2.4.2. Electrical

**PVT**

The electrical energy generated by the PVT system is described by Equation 2.15.

$$P_{\mathrm{PVT}}(k) = \eta_{\mathrm{PV}}(k)\, A_{\mathrm{PV}} G(k) \tag{2.15}$$

The efficiency noted above, is in theory also dependent on the temperature of the PV layer of the panel and varies per timestep. However, for the scope of optimizing this CDS and the sake of linearity this efficiency is roughly estimated by a value of 0.18 for all timesteps, which keeps the model suitable for the goals set for this research. This results in Equation 2.16 where the only time dependent variable is the irradiance, which is not an optimization variable.

$$P_{\mathrm{PVT}}(k) = \eta_{\mathrm{PV}} A_{\mathrm{PV}} G(k) \tag{2.16}$$

**PV**

As the area of the additional PV modules is not important to the sizing, the electrical power of the PV modules is determined is a different way. The panels are sized to their rated power, expressed in $kWp$. This is an optimization variable, and is multiplied by the irradiance, resulting in the power of the PV system (Equation 2.17).

$$P_{\mathrm{PV}}(k) = \mathrm{kWp}_{\mathrm{PV}} G(k) \tag{2.17}$$

**Battery**

The BESS acts as the electrical balancer and it is scaled by the optimizer. The energy change as a result of the battery power in a single timestep is described below (2.18).

$$E_{\mathrm{BESS}}(k+1) = E_{\mathrm{BESS}}(k) - P_{\mathrm{BESS}}(k) \cdot h \tag{2.18}$$

Where $h$ is the amount of hours in a timestep, in this case 0.25. The internal energy of the battery is related to the SOC (state of charge) with Equation 2.19.

$$SOC_{\mathrm{BESS}}(k) = \frac{E_{\mathrm{BESS}}(k)}{E_{\mathrm{BESS}}^{\max}} \cdot 100 \tag{2.19}$$

**ATES hydraulic pump**

The water in the ATES is at a depth, requiring a pump to overcome the potential energy to get the water back to ground level, where it is used by the demands of the DHN.

The electrical power consumed by such a hydraulic pump is described by Equation 2.20.

$$P_{\mathrm{pump}} = \frac{\dot{V}\left(\rho_f g_h + L p_l\right)}{\eta_{\mathrm{pump}}} \tag{2.20}$$

Where $\dot{V}$ is the volume flow of water through the pipe, $\rho_f$ is the fluid density, $h$ is the height that the water has to overcome, $L$ is the length of the vertical pipe, $P_l$ is the pressure loss in the pipe per unit length (Equation 2.21) and $\eta_{\mathrm{pump}}$ is the efficiency at which the pump runs.

$$P_l = f \cdot \left(\frac{1}{D}\right) \cdot \left(\frac{\rho_f\, v^2}{2}\right) \tag{2.21}$$

Where $D$ is the pipe inner diameter, $v$ is the velocity and $f$ is the friction coefficient. This friction coefficient is determined by the Reynolds number, a value related to flow patterns.

If the Reynolds number is larger than 4000, the friction coefficient is determined by Equation 2.22, if the number has another value, expression 2.23 holds.

$$f = 0.3164 \cdot Reynolds^{-0.25} \tag{2.22}$$

$$f = \frac{64}{Reynolds} \tag{2.23}$$

### 2.4.3. Network connections and layout

In this section the network and its interconnections will be explained, by describing their topology and underlying math.

#### Thermal

The thermal network is constructed by nodes, where heating energy is exchanged at a certain power. The nodes have an incoming and outgoing water flow at the same flow rate. The difference in temperature between in and outgoing flow is determined by net heating power delivered to a node.

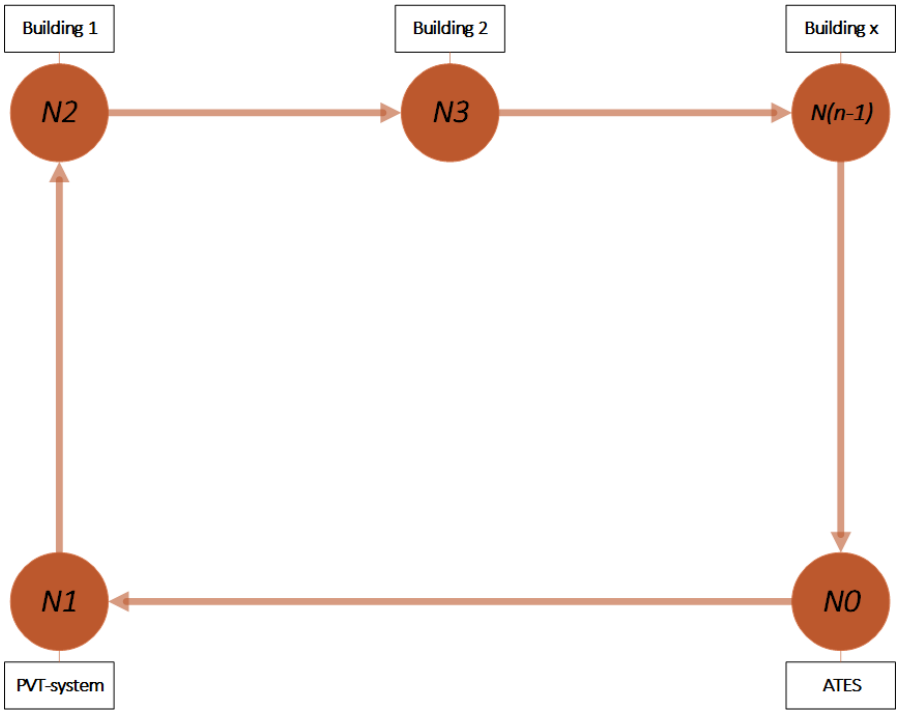


Figure 2.6: Schematic of the thermal network

The nodal power balance is given by equation 2.24.

$$\dot{Q}_n^N(k) = \dot{m}_f c_f \left[T_{\text{out}}^N(k) - T_{\text{in}}^N(k)\right] \tag{2.24}$$

The temperatures are connected via expressions 2.25 and 2.26.
For $i, j \quad \text{if} \quad j = N$:

$$T_{\text{in}}^N(k) = T_{\text{pipe-out}}^{i,j}(k) \tag{2.25}$$

For $i, j \quad \text{if} \quad i = N$:

$$T_{\text{out}}^N(k) = T_{\text{pipe-in}}^{i,j}(k) \tag{2.26}$$

### Electrical

The electrical components are assumed to be coupled via a network with no limitations, leading to a resistance-free flow between all components. The electrical network schematic is shown in Figure 2.7.

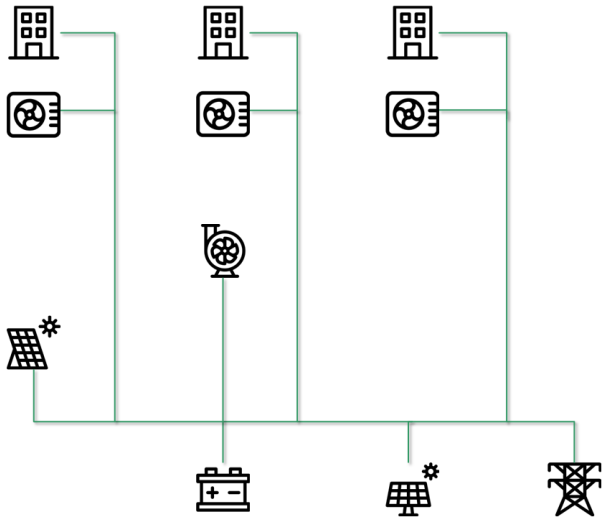

Figure 2.7: Proposed electrical network on the Werf

The power balance must always hold between all those components, hence expression 2.27.

$$P_{\text{grid}}(k) + P_{\text{BESS}}(k) + P_{\text{PVT}}(k) + P_{\text{PV}}(k) - P_{\text{demand}}(k) - P_{\text{pump}} - \sum_{i=2}^{16} P_{\text{hp}}^{i}(k) = 0 \tag{2.27}$$

# 3

# Methods

This chapter describes the methodology used to answer the research questions formulated in the introduction. It will first elaborate on the case study on The Werf area, where it will provide details about the buildings in the area, the previous research done on the area and the current energy infrastructure present on the area. Next, the methods to solve the research questions are described. For the relevant research questions these methods are transformed to an optimization problem, describing the objective functions and the constraints.

## 3.1. Detailed case study

This thesis uses a physical area in Hilversum-East as a basis to conduct research on. The area, the Werf area, is a refurbished municipal yard, now containing industry, hospitality, residential housing and multiple small businesses. As described in the introduction, HET has, on behalf of the VDW, investigated the potential of an increased overall sustainability of the energy consumption of the area [4]. This research sets the scope for this thesis.

The Werf area encompasses an area of about 3.5 hectare, which is shown on a map in Figure 3.1. This map describes the current buildings with a notation of **B***XX* and the planned buildings for 2028 with a notation of **N***XX*.


Figure 3.1: A map of the Werf area [4]

The buildings serve different purposes, varying between working and living. The distribution of these purposes with respect to floor area is displayed in Figure 3.2. With the realization of the new built residential buildings, the area will adapt a more hybrid usage character which will lead to more activities in the evening and weekends, diversifying energy demands. This diversification will lead to a more homogeneous energy demand, making the area more suitable to become an energy hub.


Figure 3.2: Purpose of buildings in 2028 with respect to floor area [4]

In the research HET executed, an energy potential scan was performed [4]. This scan estimates the possibilities of sustainable energy generation, and the predicted energy consumption for the year 2028. The possible renewable generation is found to be 1,416 MWh per year, making full use of all the potential. In this research it is investigated if this full potential is beneficial for the minimization of grid connection power.

The energy consumed by building- and production processes is estimated at 1,244 MWh. This means that in theory more energy can be produced then consumed. This thesis is going to investigate if this

is applicable for this area and if the seasonal gaps can be filled so that the energy potential can be fully used for the demand over a year.

In a previous master thesis dedicated to the Werf area, T. Beijneveld investigated the possible sizing and configuration of a 5th generation heating network [5]. The heating network was constructed of an ATES, pipes distributing the heat over the area, a PVT system responsible for the injection of heat in the network, HP's to step up the temperature required by the buildings and a pump which maintained a constant volume flow through the network. The schematic of this thermal network can be found in Figure 3.3.

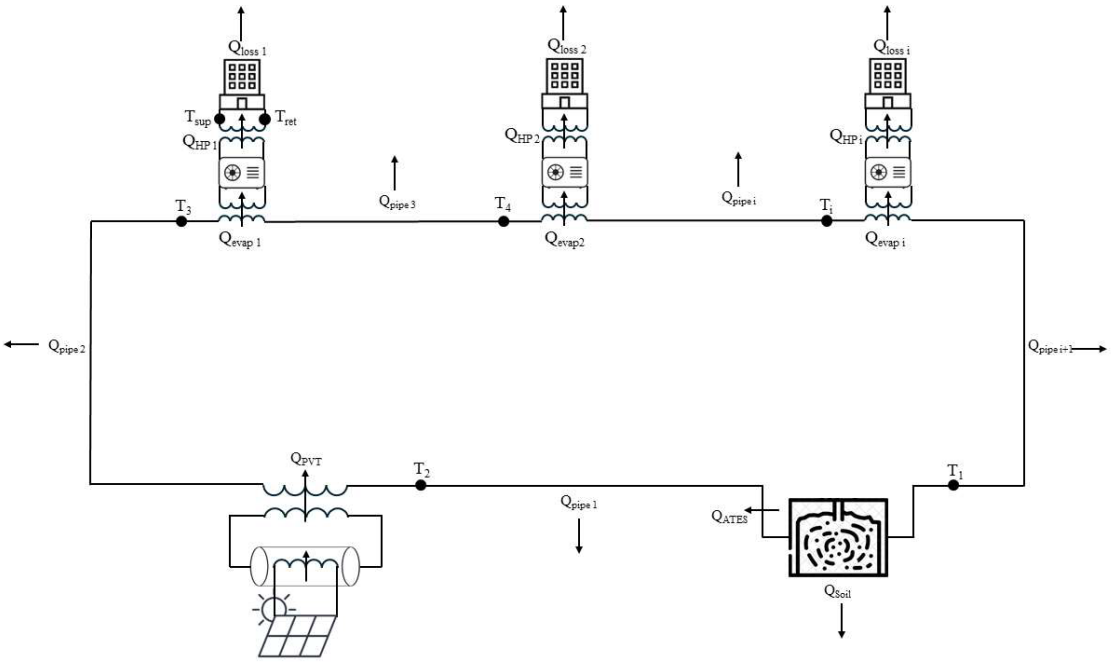


Figure 3.3: Thermal network on the Werf as proposed by T. Beijneveld [5]

The main goal of this research was the minimization of $CO_2$ emissions from the area. The concluded configuration was a single thermal aquifer with the PVT system just after this storage unit, injecting temperature in the network before the loads. This concluded configuration is shown in Figure 3.4.


Figure 3.4: The concluded configuration of the 5GDHN and its additional components on the Werf [5]

It can be seen that the thermal aquifer output is at the orange circle, from which the heat flow first travels to the PVT system. After that, it passes through all the buildings, after which it will enter the aquifer again at the blue circle.

In the proposed energy hub, the energy carriers are heat and electricity. The electricity network Beijneveld used in his model consists of a grid connection, building loads, PVT injection, building heat pumps and a fluid pump (Figure 3.5).

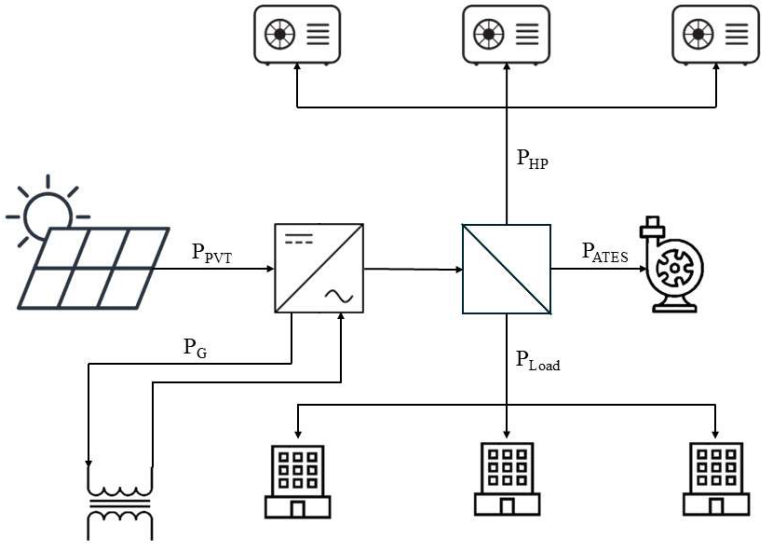


Figure 3.5: Electrical network on the Werf as proposed by T. Beijneveld [5]

As the goal of this thesis is to minimize the maximum grid connection power, the internal production and demand must be matched better at a 15 minute resolution. To reach this goal two new components are introduced, namely a BESS and extra PV capacity. This extra capacity can be placed on the roofs of the buildings, as concluded in [4]. The addition of these elements in combination with the previously defined heating network results in the following complete system diagram (Figure 3.6).

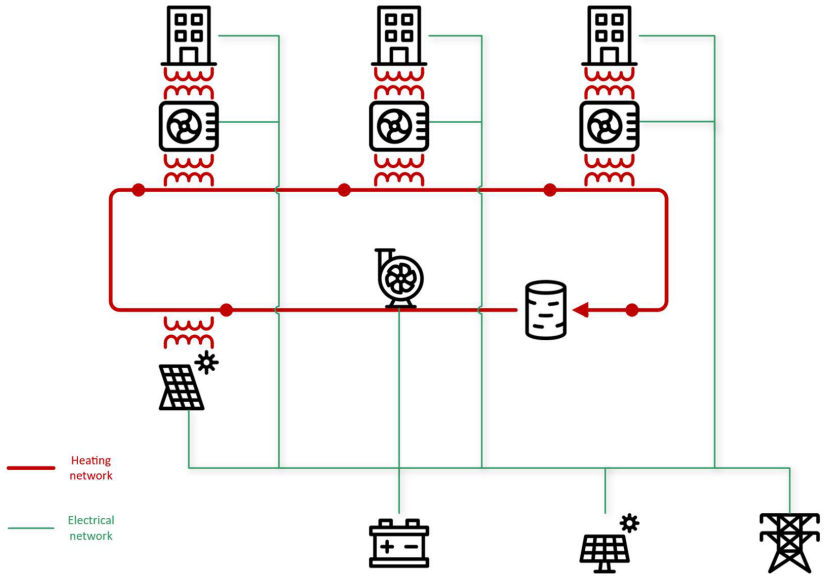


Figure 3.6: Schematic of the desired energy system on the Werf

This hybrid network will offer energy flexibility to the area, as well as functioning as a CDS, as there is only one physical connection to the external utilities.

The last research question of this paper investigates the requirements for the electrical network of the area when the components of the CDS are installed. To make the transition sustainable it is tried to reuse as much of the infrastructure already present on the area. For this purpose, the current infrastructure must be mapped out. Liander (DSO in the Hilversum area) has supplied HET with maps showing the electrical infrastructure (Figure 3.7 and 3.8).

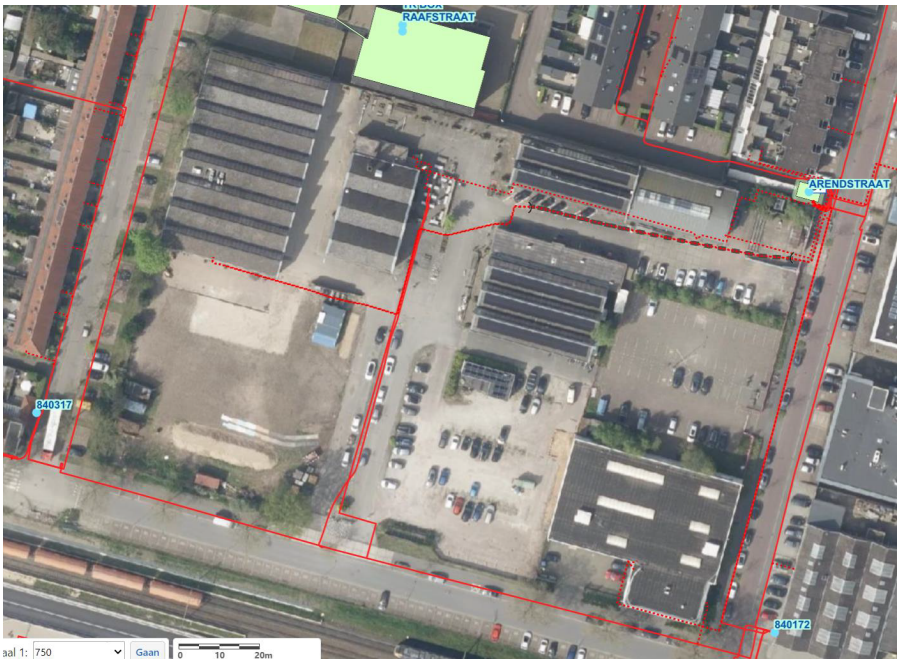


Figure 3.7: The low voltage infrastructure layout on the Werf as supplied by the DSO

On the satellite photo in Figure 3.7, the low voltage distribution cables are drawn. It can be seen that

there are low voltage cables along the edges of the area and that there is one distribution cable in the middle of the area, serving the largest portion of the buildings on the west area of the Werf.

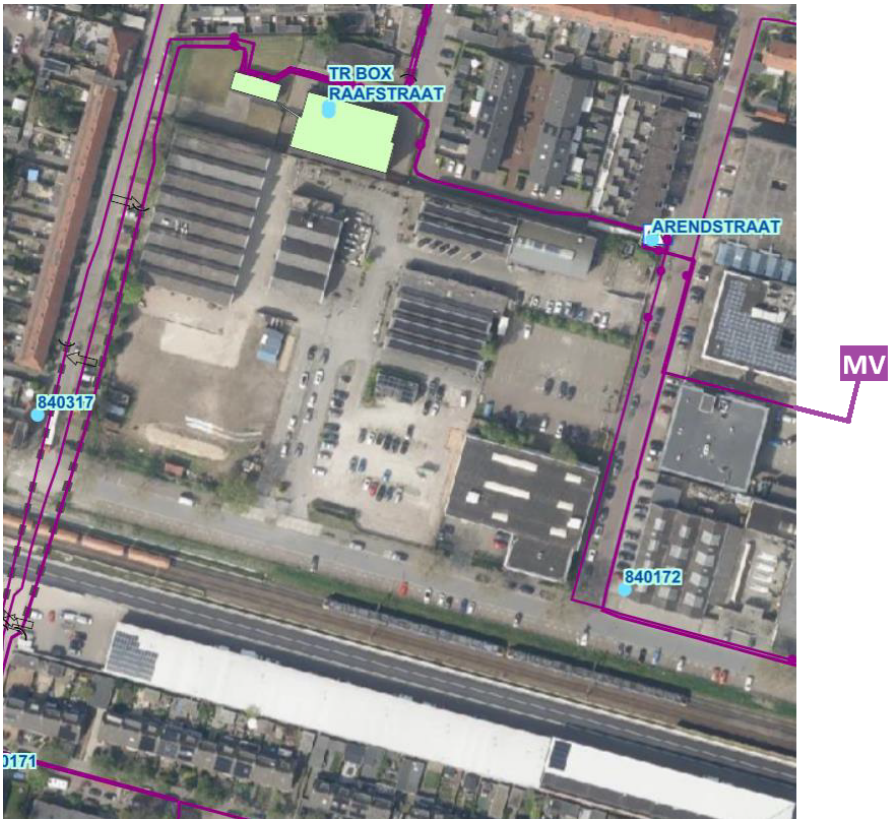


Figure 3.8: The medium voltage infrastructure layout on the Werf as supplied by the DSO

The satellite photo in Figure 3.8 shows the medium voltage network in the area. Across the east area, a medium voltage cable is going southwards and eastwards. This cable splits to a medium voltage transformer in the middle of the Werf east area. This transformer serves the power for the that area.

## 3.2. Research question methodology

### 3.2.1. Electrical and thermal demand pattern forecast

*What will the electrical and heat demand pattern of the Werf area be in 2028?*

The first research question of this thesis aims to find an electrical and heat demand pattern for the Werf area, at a resolution of 15 minutes. This demand patterns will be generated with a combination of data generation, analysis and modulation in order to create a representable load pattern.

On the area are a few bulk energy connections, belonging to industrial buildings. From these bulk connections, the consumption patterns for the years 2022, 2023 and 2024 were retrieved, giving insight into real demand patterns.

#### Heat demand

The heat demand pattern of the buildings on the Werf is adopted from the model T. Beijneveld created [5]. The buildings proposed to be present in 2028 are categorized in three distinct sizes: small, medium and large (Figure 3.9).

As described in section 2.4.1, these buildings lose heat to the environment, depending on the characteristics of the house, the indoor temperature and the ambient temperature.


Figure 3.9: The proposed layout of the district and building distinction

The indoor temperature setpoint is set to 20°C, and every timestep this temperature changes slightly due to losses. This loss in heat is then supplied by the houses internal boiler, trying to reach the setpoint again. The boiler temperature is heated up to 53°C by the buildings heat pump, which extracts the heat from the DHN.

Every timestep $k$ the building is assumed to extract the amount of heat necessary to reach the indoor temperature setpoint. Due to this extraction, the boiler temperature decreases. When the boiler temperature gets below 50°C, the heat pump heats the circulation flow back up to 53°C and the process repeats itself.

Through the equations belonging to the heat pump operation, energy is extracted from the DHN and electrical energy is demanded from the internal grid. This electrical energy is part of the heating demand of the area.

The calculation of the heating demand of the buildings, consisting of a heating demand from the DHN and electrical demand from the heat pumps, can be executed apart from the optimization. The calculations do only depend on factors and data which is already available and do not depend on any optimization variables. The results of this precalculated building model will be described in the results section.

### Electrical demand

Apart from the electrical demand of the individual heat pumps per building, the buildings also demand electricity for additional appliances. First of all for building processes like ventilation, powering of electrical devices and lighting. Secondly the industrial processes in some of the non-residential buildings can also demand large quantities of power.
The scaling of the CDS in 2028 requires a good prediction of the electrical power demands spread over the area. This prediction can determine bottlenecks in infrastructure, but more importantly can deliver constraints for the optimization.

The demand patterns are predicted for industrial and residential buildings separately, after which they are again combined to a total demand pattern which can be used by the solver. The demands are scaled to the electrical energy consumption in the year 2028, predicted by HET cooperation in their research [4]. In a later stage of the research this demand is clustered to buildings sharing the same connection to the CDS in order to determine power flows through the network.

#### Industrial demand prediction

To predict the industrial demand patterns the real consumption data from 4 industrial energy connections is used. The data is delivered in kWh / 15 minutes, so it should be multiplied by 4 to get the power drawn per 15 minutes in kW. These four power demand patterns should be added together, after which they are scaled to the total industrial power demand. This is done according to the building area. The area of the buildings corresponding to the retrieved consumption patterns is compared to

the total industrial area, resulting in a factor of 2.5.

Difficulties lie in the fact that a part of the real electricity consumption of the four buildings is still used for heating. This demand should not be present in the demand pattern in 2028, as the heating demand of buildings will be fulfilled by the DHN and its corresponding heat pumps. This is why this demand was extracted for the buildings that currently use electrical heat appliances. It is assumed that the heating appliance of these buildings are air to air heat pumps, which makes that the COP of the heat pumps can be calculated with the indoor temperature setpoint (20°C) and the ambient temperature dataset beforehand. The electrical power consumed by such a heat pump to oppose the building heat losses can then be calculated at every timestep. The retrieved dataset can then be extracted from the original building demand, resulting in the buildings pure electrical demand.

**Residential demand prediction**
Consumption data of current residential buildings is not available. In combination with the fact that the dominant electrical power consumption stems from the industrial buildings, it is chosen that the residential demand is generated for a residential building of approximately 100 $m^2$ [15].

A daily residential demand pattern is generated with python code, determined by different timeslots with a range of electrical powers that the buildings can possibly demand at that time (Figure 3.10) [16]. This script can be found via Appendix D.

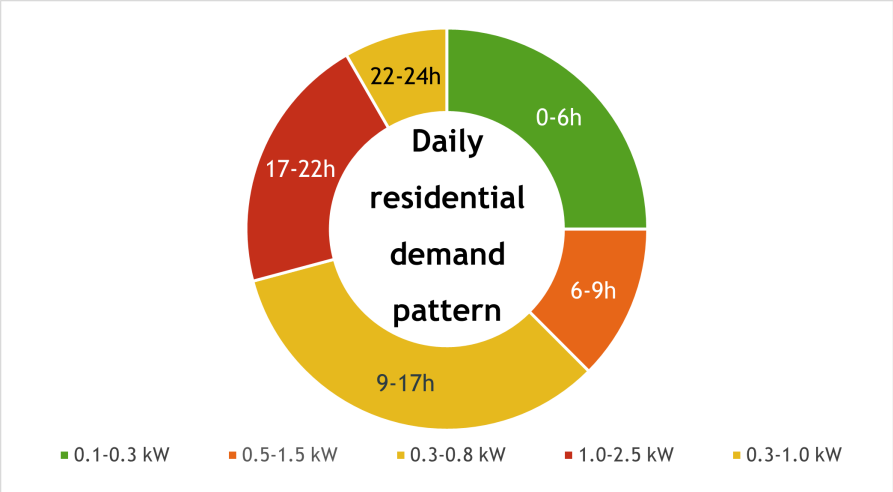


Figure 3.10: Residential demand timeslots and power ranges

From this blueprint, 55 (scaling to approximately 5,500 $m^2$ residential area) daily residential patterns are generated. Due to the random generation they all differ slightly from each other, preventing huge spikes in demand introduced by just multiplying a single demand pattern.

**Total demand prediction**
As previously described, the total electrical energy consumption of buildings (exclusive heat demand) is estimated to be 1,244 MWh. To calculate the total electrical power demand profile of all the buildings, the scaled profile of the residential and industrial buildings is added. After this, the pattern is scaled to sum to 1,244 MWh of energy over a year, resulting in the prediction of the demand pattern for the Werf in the year 2028.

### 3.2.2. Optimal energy hub sizing

*What is the optimal sizing of the multi carrier energy hub neglecting internal network limitations?*

The goal of the optimal sizing of the CDS is minimizing the connection power to the external grid operator. Setting the minimization of grid connection as the only objective is not useful, as the solver will always end with no grid interaction or minimize it at the boundaries of the constraints. This is not the goal of this research, as it is intended to give insights in optimal sizing.

This means there should be a second objective introduced to the optimization, namely economic cost. The cost function will introduce the costs of minimizing grid connection. This cost function will be described by costs related to the PV system and the BESS. The logical hypothesis for this question is the higher the costs, the smaller the grid connection. This is because the PV system will produce extra required energy for the area, whereas the BESS will introduce flexibility to use this generated energy at the timesteps of demand.

The result of an optimization with two objectives (i.e. MultiObjective optimization) is a so called Pareto Front. The Pareto front is the set of optimal solutions where you cannot improve one objective without worsening the other. The computation of such an optimization is very intensive and luckily not necessary for this research. This is because Liander (the grid operator active in the Hilversum area) has fixed sizes for the grid connections they can supply, this is brought back to single objective optimizations (cost function) per available grid connection.

To answer this research question, six optimizations are executed. Five of them stem from the available grid connections supplied by Liander, categories AC4a, AC4b, AC5a, AC5b and AC5. These categories are the sizes in which the DSO offers connections, as shown in Table 3.1. The categories beyond AC5 are ignored, because they will be effectively not different from AC5 as all demand will fall in the connection power range.
The sixth connection is a special connection granted for solar parking lot (PVT). This capacity has already been granted to the area via a permit and has a max production capacity of 350 kW and a max consumption of 300 kW. This connection will from now on be called “SolarPark”.

Table 3.1: Connection categories as offered by the DSO [17]

| Cat | Capacity | Max Consumption | Max Production |
|---|---|---|---|
| AC4a | >3x80A t/m 100kVA | 94kW / 100kVA | 100kW / 100kVA |
| AC4b | >100kVA t/m 160kVA | 147kW / 160kVA | 160kW / 160kVA |
| AC5a | >160kVA t/m 630kVA | 535kW / 630kVA | 630kW / 630kVA |
| AC5b | >630kVA t/m 1MVA | 850kW / 1.000kVA | 1.000kW / 1.000kVA |
| AC5 | >1MVA t/m 2MVA | 1.700kW / 2.000kVA | 2.000kW / 2.000kVA |
| … | … | … | … |

The decision variables are the size of the PV system, expressed in kWp, and the size of the BESS, expressed in MWh. The objective function formulated for cost is the following. Assumed is that the lifetime of solar panels is 25 years and the BESS 12.5 years, meaning that the BESS should be replaced once in the 25 year investment horizon. This leads to the addition of an OPEX cost to the BESS, where the interest rate is $r = 0.045$.

$$C_{\mathrm{PV}}^{\mathrm{CAPEX}} = €1,000/kWp \tag{3.1}$$

$$C_{\mathrm{BESS}}^{\mathrm{CAPEX}} = €600,000/MWh \tag{3.2}$$

$$C_{\mathrm{BESS}}^{\mathrm{OPEX}} = \frac{1}{(1+r)} \tag{3.3}$$

The above formulations are used in the objective function minimizing cost, showed in Formula 3.4.

$$MIN\left[kWp_{\mathrm{PV}} \cdot C_{\mathrm{PV}}^{\mathrm{CAPEX}} + E_{\mathrm{BESS}} \cdot C_{\mathrm{BESS}}^{\mathrm{CAPEX}} + \left(E_{\mathrm{BESS}} \cdot C_{\mathrm{BESS}}^{\mathrm{OPEX}} \cdot C_{\mathrm{BESS}}^{\mathrm{CAPEX}}\right)\right] \tag{3.4}$$

### 3.2.3. Load shifting and direct load control

*How can a combination of load shifting of controllable loads and direct load control influence the sizing of the system, and is its implementation feasible in this area?*

The methodology to answer this research question is many aspects similar to that of the previous one. However, the implementation of load shifting and direct load control introduces some novelties in the optimization. The goal of the implementation of these aspects is to further reduce the grid power connection without an increase in the cost function. The hypothesis is that load shifting will decrease consumption peaks on the grid connection, where a form of direct load control will decrease production peaks on the same connection.

### Direct load control

The most uncomplicated way of removing solar generation peaks is by switching off inverters, thereby curtailing the energy and completely losing the potential generation of sustainable energy. This is why for this issue a direct load control technique is chosen which converts the surplus of electrical energy into heat which can be stored in the ATES. This is done via an air to water heatpump, operating at the same node as the PVT system.

T. Beijneveld researched such a solution and concluded that it was not worth the investment, however this application is different. Where in his research the goal was to minimize $CO_2$ emissions over a year, the goal of this research is to minimize the grid connection, thereby opening new opportunities for an extra heatpump used for direct load control and conversion of electricity to heat.

This direct load control technique is introduced in two equations and constraints of the optimization. First it should be added to the power balance, its power denoted as $P_{hpX}$.

$$P_{\text{grid}}(k) + P_{\text{bess}}(k) + P_{\text{pvt}}(k) + P_{\text{pv}}(k) - P_{\text{demand}}(k) - P_{\text{pump}} - P_{\text{hpX}}(k) - \sum_{i=2}^{16} P_{\text{hp}}^{i}(k) = 0 \quad (3.5)$$

The contribution to the heating network is described at node “N1”, the same node where the PVT heat is injected into the network. Because at moments of surplus solar energy the difference in ambient temperature and DHN temperature is low, the COP of this extra heatpump is assumed to be fixed at 3.8. This simplification is necessary to keep the model linear and thereby keep the computational burden in this scope.

$$\dot{Q}_{n}^{\text{N1}}(k) = n_{\text{PVT}} \cdot \dot{Q}_{\text{PVT}}(k) + P_{\text{hpX}}(k) \cdot 3.8 \quad (3.6)$$

### Load shifting

The main purpose of a battery storage system is to store generated power when there is not enough demand, and feed back that power when there is a deficit in generated power in comparison with the demand. The battery is sized to fulfill this dynamic. A possibility to decrease the mismatch in production and demand is to shift the electric load to the moments when there is sustainable energy generated. Hypothetically, by shifting this load the battery size could be smaller, for the same results in grid connection power.

Due to the complexity, versatility and uncontrollability of the electrical loads in the buildings in the Werf, load shifting is difficult. In this model and also in the case study, the most accessible controllable loads are the heat pumps stepping up the temperature of the DHN to the buildings boilers. That is why the scheduling of these loads are influenced in this methodology of this research question.

The goal of the load shift is to draw power with the heat pumps at moments in time when there is PV/PVT electricity production. This electricity production is correlated with the solar irradiance. The control of the temperature setpoint of the boiler and heat pumps is differentiated in order to match with solar irradiance. With this control, the boilers inside the buildings act as a thermal buffer, storing the generated electricity from solar panels in the form of higher temperature water. This heat is then in later timesteps used to heat up the building and match the heating demands of the building. The solar irradiance is divided in bins ($G_{bins}$), and then connected to a different boiler supply temperature. The arrays are shown in equation 3.7 and 3.8.

$$G_{\text{bins}} = [0, 100, 200, 300, 400, 500, 600, 700, 800, 900, 1000] \tag{3.7}$$

$$T_{\text{sup}}^{\text{setpoints}} = [53 + K, 55 + K, 57 + K, 59 + K, 61 + K, 63 + K, 65 + K, 67 + K, 69 + K, 71 + K, 73 + K] \tag{3.8}$$

In the array above $K = 273$, the temperature conversion from Celcius to Kelvin.

To prevent the large power demands from the heat pumps in a single timestep, the $T_{\text{ret}}$ value is increased with the supply setpoint, with $T_{\text{ret}} = T_{\text{sup}} - 3$.

In addition to this shift from heat pump electrical loads to timesteps with high solar radiation, a second simple load shifting operation is applied. At nights, the indoor temperature setpoint for the buildings is set back to 17°C. This means that the chances are minimized that at night, when there is certainly no solar irradiance and hence solar power generation, the heat pumps must activate and demand power.

#### Optimization methods

The additional implementations are first optimized isolated for all possible connection sizes. After these runs the technologies will be combined and run again for the available connections, after which they can be compared in the results.

### 3.2.4. Infrastructure capacity requirements

*Depending on the size of the available grid connections defined by Liander, what are the electricity infrastructure requirements?*

The implementation of a CDS is advantageous in the scope of sustainability and energy autonomy. However, this implementation makes that a few conditions must be met. One of those conditions is the fact that the electrical power demanded by all appliances on the area must be transported to the location of consumption. Because of the alteration in the way energy is consumed and the fact that the energy flow patterns might be different then there has been on the area for the past years, this electrical infrastructure requirements must be evaluated.

This evaluation is done by first grouping the electricity demands inside the closed area. This grouping leads to locations where the power for these loads must be delivered. After this grouping, the power demand and production of these connections per timesteps are determined. For relevant simulation results the required power flows over the connections can be determined, after which the required electrical infrastructure will be concluded.

#### Building clustering

The total electrical load to be covered by the distribution system is a combination of power demand from building heat pumps, demand from buildings related processes and the possible solar production from the roof of the buildings. The buildings are clustered in a fashion that gives the largest opportunity to reuse the current cabling available on the area. The clustering is shown in Figure 3.11.

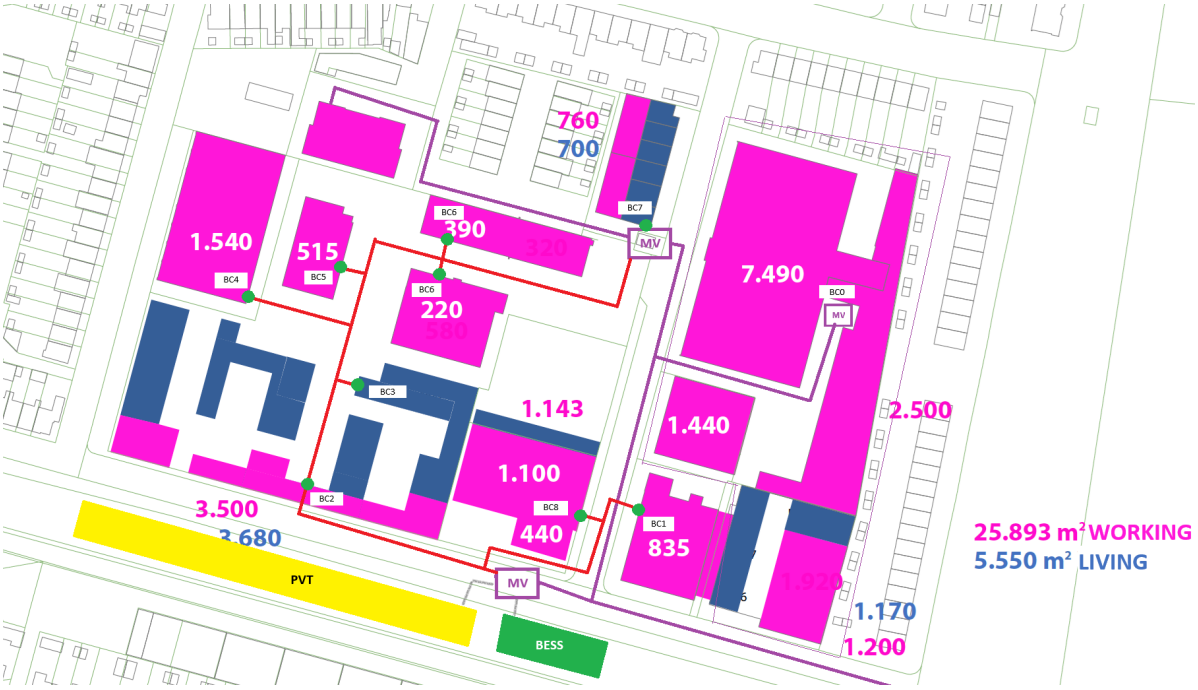


Figure 3.11: Proposed cabling and clustering on the Werf

The medium voltage station closest to the PVT and BESS will act as the gateway connection to the external grid. As there is already a MV station at building cluster 0, this can be reused to transport the power at higher voltage to that cluster.
In order to make the CDS physically closed, a new cable must be placed between the new MV stations and the one present at BC0. However, this might not be required as the already present line from the grid operator can be reused. If so, the result is a CDS on paper, where the consumption from the MV stations will be added and their combined consumptions cannot exceed the agreed boundaries.

The identified clusters can be found in Figure 3.11, and their correspondence to the buildings related to the heating network in Figure 3.12 and Table 3.2, starting with B0 as the Green dot left of L1 and increasing in number along the trajectory of the heating network up to B15. Also the related working and living areas are displayed, which are later used for calculating the electrical demand related to building processes.

Table 3.2: Building clusters and their relations to DHN buildings and their areas

| Building Cluster | Living / Working area ($m^2$) | DHN Buildings |
|---|---|---|
| BC0 | 1170 / 12630 | B8, B9, B10, B11 |
| BC1 | 0 / 835 | B12 |
| BC2 | 0 / 3500 | B0, B14 |
| BC3 | 3600 / 0 | B1, B2 |
| BC4 | 0 / 1540 | B3 |
| BC5 | 0 / 515 | B4 |
| BC6 | 0 / 610 | B5, B6 |
| BC7 | 700 / 760 | B7 |
| BC8 | 0 / 1540 | B13 |

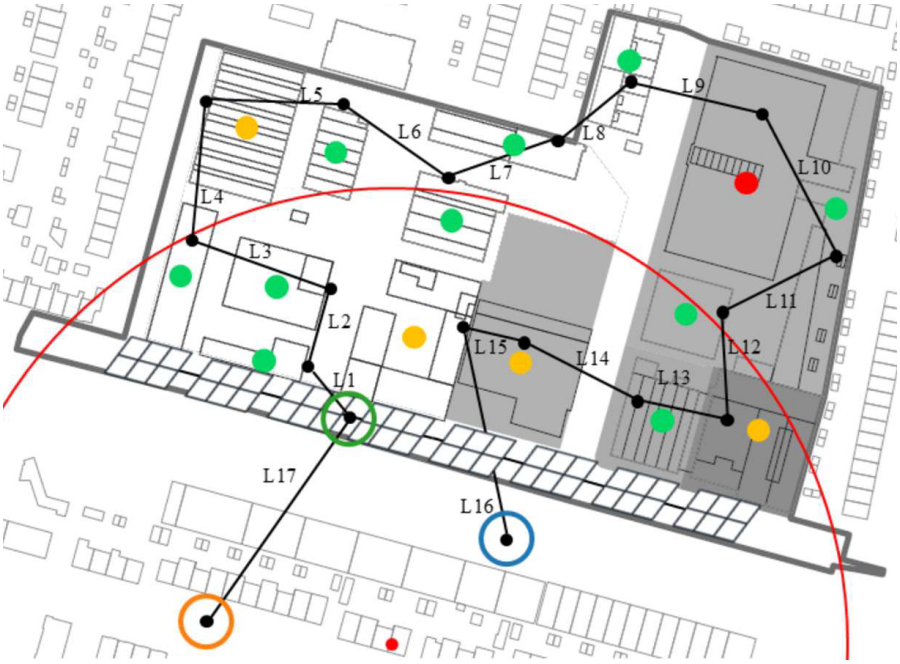


Figure 3.12: The buildings (dots) related to the heating network [5]

With this information all the power demanded and produced can be calculated at the desired locations.

### Locational power demand

The previous clustering can be translated into the total energy interaction with the energy hub per timestep. From the generated demand patterns for residential and industrial buildings in the first research question a scaling can be determined for the energy demand per category per $m^2$. This factor can then be multiplied by the areas defined in the clustering table above, resulting in the demand per cluster per timestep.
The electrical power from the individual heat pumps per building connected to the heating network must also be taken into account. As shown in the table, these buildings and their corresponding heat pumps are also matched to the clustering. The datasets of the relevant optimizations can be added to the energy exchange totals per building clustering.

With the consumption at the clusters defined, the possible solar generation must be subtracted from these values. Per optimization it is known how much additional solar generation will be installed. It is assumed that this total value will be evenly distributed over the roofs of the present buildings on the area. This can then be divided to generate a solar generation power per timestep per square meter of building. Every building clusters area can then be multiplied with this value, resulting in the generation per cluster per timestep.

### Cabling capacities

After defining the locations and values of the energy consumed and produced, the required cable capacities can be determined. There are four bottlenecks investigated for which the required cable capacities will be calculated.

- The low voltage ring on the main area of the Werf
  - Connected clusters: BC1 – BC8
- The medium voltage station at BC0
- The connection from the PVT system to the newly built MV station

- The connection from the BESS system to the newly built MV station

In this investigation we assume that the MV cabling in the area can handle all the powers required, as this cabling is sized for a larger area of operation. The low voltage ring capacity will be calculated by adding all the power profiles of the corresponding clusters and finding the maximum value of power drawn by the clusters. The same holds for the MV station at BC0, but this is only a single cluster so the maximum of this cluster defines the capacity of this station. The maximum electrical PVT generation will determine the cable to the PVT system, where the maximum BESS power will determine that connection to the CDS connection.

These methods are applied to the AC5a and SolarPark optimization of the base scenario and the scenario of direct load control. The direct load control optimization gives the lowest cost for those connection sizes, but also the implementation might not directly be feasible. This is why the base optimization is also translated to infrastructural requirements.

## 3.3. Optimization

To optimize the grid connection of the CDS of the Werf area, a solver is used. This solver, the Gurobi solver, is utilized with the python API. In this way, the solver can be easily integrated with the definition and data of the python model of the energy system. The variables of the constructed model can be found in Appendix B. In this section the constraints of the constructed model will be described.

### 3.3.1. Constraints

The freedom of variables throughout the optimization process is determined by the constraints. For the optimizations executed in this research, the following constraints are constructed for every timestep in the horizon. The constraints are described and a connection is made to the corresponding formulas in the previous Chapter (2) containing the mathematical descriptions. In some constraints there are factors multiplying or dividing by 1000. These transformations are done to match units throughout the model. The solver has difficulties with large numbers, affecting the solve time. This is why all constraints are scaled to units which lead to numbers which are optimal for the solver.

#### Power balance

The power balance describes that all the powers of the components must add up to zero at every timestep $k$ (2.27).

$$P_{\text{grid}}[k] + P_{\text{bess}}[k] \cdot 1000 + P_{\text{pvt}}[k] + P_{\text{pv}}[k] - P_{\text{demand}}[k] - P_{\text{pump}} - P_{\text{hpX}}[k] - \sum_{i=2}^{16} P_{\text{hp}}^{i}[k] = 0 \quad (3.9)$$

#### Grid peak

This constraints is only used for simulation runs where the grid connection is directly minimized. These runs are useful for checking the limitations of the configuration. The knowledge of these limitations prevent wasted time on runs which will turn out infeasible by the solver.

$$P_{\text{grid}}[k] \leq P_{\text{peak}} \quad (3.10)$$

$$P_{\text{grid}}[k] \leq P_{\text{peak}} \quad (3.11)$$

### ATES losses

If there is a temperature difference between soil and the aquifier temperature, the ATES exchanges energy with the surrounding soil. The losses or gains through the interfaces are described by the following three constraints, and the sum of the three is the fourth constraint.

$$\dot{Q}_{\text{top}}[k] = \frac{h_{\text{ATES}} \cdot A_{\text{top}} \cdot \left(T_{\text{soil}} - T_{\text{out}}^{\text{N0}}[k]\right)}{1000} \tag{3.12}$$

$$\dot{Q}_{\text{bottom}}[k] = \frac{h_{\text{ATES}} \cdot A_{\text{bottom}} \cdot \left(T_{\text{soil}} - T_{\text{out}}^{\text{N0}}[k]\right)}{1000} \tag{3.13}$$

$$\dot{Q}_{\text{side}}[k] = \frac{h_{\text{ATES}} \cdot A_{\text{side}} \cdot \left(T_{\text{soil}} - T_{\text{out}}^{\text{N0}}[k]\right)}{1000} \tag{3.14}$$

$$\dot{Q}_{\text{soil}}[k] = \dot{Q}_{\text{top}}[k] + \dot{Q}_{\text{bottom}}[k] + \dot{Q}_{\text{side}}[k] \tag{3.15}$$

### PVT and PV

The constraints corresponding to the electrical power of the PVT and the PV system are described below. For all the optimizations, $n_{\text{pvt}}$ is fixed at 800 panels. The area of a PVT panel is 1.77 m$^2$, and the efficiency of panels is assumed to be 0.18 at all temperatures. (2.17)

$$P_{\text{pvt}}[k] = n_{\text{pvt}} \cdot \frac{G[k] \cdot 1.77 \cdot 0.18}{1000} \tag{3.16}$$

$$P_{\text{pv}}[k] = \frac{kWp_{\text{pv}} \cdot G[k]}{1000} \tag{3.17}$$

### PVT thermal

The constraining of the thermal energy supplied by the PVT system is formulated in two sets of constraints, normal linear constraints and piecewise linear (PWL) constraints. The thermal energy is approximated with as result 10 possible power levels per timestep, depending on the temperature of the DHN at the PVT node (“N1”).

The results of this approximation can be grouped into three possible sets. The first one is where at every DHN temperature input, power can be delivered. This set is sketched in Figure 3.13a and described in expression 3.18. These results can be easily linearized, resulting in coefficients which can be imported as a linear constraint in the solver. Here $Q_{\text{trend},0}$ and $Q_{\text{trend},1}$ are the linearization coefficients.

The second situation occurs when at lower DHN temperatures power can be delivered, but this is not possible at higher temperatures. Because the PVT system cannot draw power from the DHN, at negative PVT power values the constraint must be set to zero. This relation is more difficult to interpret by the solver, which is settled by introducing a piecewise linear constraint (PWL). These constraints make the solving process harder, but it is still doable because there is a limited amount of timesteps where this situation occurs. A linear relationship is determined through the nonzero datapoints, afterwards the DHN temperature value is determined at which the x-axis is crossed. This value is then used in the construction of the PWL constraint. The sketch of the PWL constraint can be found in Figure 3.13b. The description of this constraint is diffult to describe and can be found in the optimizer code through Appendix D.

When the PVT system can deliver no power at every DHN temperature, it is simply set to zero. This results in sketch 3.13c and expression 3.19.


(a) All PVT thermal values positive (b) Positive and negative PVT thermal powers (c) Only negative PVT thermal powers

Figure 3.13: The three possible situations for the $\dot{Q}_{\mathrm{pvt}}$ constraint

$$\dot{Q}_{\mathrm{pvt}}[k] = Q_{\mathrm{trend},0}[k] \cdot T_{\mathrm{in}}^{\mathrm{N1}}[k] + Q_{\mathrm{trend},1}[k] \tag{3.18}$$

$$\dot{Q}_{\mathrm{pvt}}[k] = 0 \tag{3.19}$$

### Heat pumps

The coefficient of performance of the heat pumps is determined by an exponential relationship, which makes optimizing over a year with the set resolution very hard. This is why the COP is also linearized over the operating temperatures of the DHN.

This linearization led to an expression (3.20) the following coefficients, with a coefficient of determination of 0.999.

$$\mathrm{COP}_{\mathrm{hp}}^{n}[k] = -0.082 \cdot \left(T_{\mathrm{ret}}^{n}[k] - T_{\mathrm{in}}^{n}[k]\right) + 6.2917 \tag{3.20}$$

The power extracted from the network by the heat pumps is determined by a formula depending on $\frac{1}{\mathrm{COP}}$. This factor is linearized with the same methods as used with COP, resulting in factors $a = -0.007$, $b = 2.322$ and with a coefficient of determination which is also 0.999.

$$\dot{Q}_{\mathrm{network}}^{n}[k] = \left(\frac{\dot{Q}_{\mathrm{hp}}^{n}[k]}{1000}\right) \cdot \left(1 - \left(-0.007 \cdot T_{\mathrm{in}}^{n}[k] + 2.3222\right)\right) \tag{3.21}$$

The equation for the electrical power consumed by the heat pumps (3.22) also takes the factor $\frac{1}{\mathrm{COP}}$ as input.

$$P_{\mathrm{hp}}^{n}[k] = \left(\frac{\dot{Q}_{\mathrm{hp}}^{n}[k]}{1000}\right) \cdot \left(-0.007 \cdot T_{\mathrm{in}}^{n}[k] + 2.3222\right) \tag{3.22}$$

### Nodal flows and temperatures

The nodal flows and temperatures are described by the following constraints (3.23, 3.24, 3.25, 3.26, 3.27), holding for every timestep $k$.

$$\dot{Q}_{n}^{n}[k] = -\dot{Q}_{\mathrm{network}}^{n}[k] \tag{3.23}$$

$$\dot{Q}_n^{N1}[k] = \frac{n_{\text{pvt}} \cdot \dot{Q}_{\text{pvt}}[k]}{1000} + P_{\text{hpX}}[k] \cdot 3.8 \tag{3.24}$$

$$\dot{Q}_n^n[k] = \frac{\dot{m}_f \cdot c_f \cdot \left(T_{\text{out}}^n[k] - T_{\text{in}}^n[k]\right)}{1000} \tag{3.25}$$

$$T_{\text{in}}^n[k] = T_{\text{pipe\_out}}^{i \to j}[k] \quad \text{where } j = n \tag{3.26}$$

$$T_{\text{out}}^n[k] = T_{\text{pipe\_in}}^{i \to j}[k] \quad \text{where } i = n \tag{3.27}$$

**Pipe flows and temperatures**

The flow through the connection, modeled as pipes, are described by the constraint showed in expression 3.28.

$$\dot{Q}_{ij}^{i \to j}[k] = \frac{T_{\text{out}}^i[k] \cdot \dot{m}_f \cdot c_f}{1000} \tag{3.28}$$

The change in energy and temperature inside a pipe is described by the next constraint (3.29), determining the temperature of the flow exiting the pipe.

$$T_{\text{pipe\_out}}^{i \to j}[k] = T_s[k] - \left(T_s[k] - T_{\text{pipe\_in}}^{i \to j}[k]\right) \cdot \exp\left(-\frac{L^{i \to j}}{\dot{m}_f \cdot c_f \cdot R_{\text{total}}}\right) \tag{3.29}$$

**ATES temperature update**

The temperature of the water entering the ATES influences the total temperature of the aquifier. Although the change is very slight due to the inertia of the tank, the temperature deviations are constraint as shown in equation 3.30.

$$T_{\text{out}}^{\text{N0}}[k+1] \cdot 1000 = \left(T_{\text{out}}^{\text{N0}}[k] + \left(\dot{m}_f \cdot c_f \cdot \left(T_{\text{in}}^{\text{N0}}[k] - T_{\text{out}}^{\text{N0}}[k]\right) + \dot{Q}_{\text{soil}}[k] \cdot 1000\right) \cdot \frac{\Delta t}{m_w \cdot c_f + m_r \cdot c_r}\right) \cdot 1000 \tag{3.30}$$

**BESS**

The battery energy (SOC) in the timestep $k+1$ is constraint in the following way.

$$E_{\text{bess}}[k+1] = E_{\text{bess}}[k] - P_{\text{bess}}[k] \cdot h \tag{3.31}$$

The next two constraints are constructed because the maximum values is used to determine the capacity and scale of the appliance. Whatever value $E_{\text{bess}}$ will take through the run, the maximum value reached will be set equal to $E_{\text{bess\_max}}$. This scaling of the system is then used in the objective function.

$$E_{\text{bess}}[k] \leq E_{\text{bess}}^{\max} \tag{3.32}$$

$$P_{\text{bess}}[k] \leq P_{\text{bess}}^{\max} \tag{3.33}$$

Is is assumed for this BESS that $C = 1$, resulting in constraint 3.34.

$$P_{\text{bess}}^{\max} = E_{\text{bess}}^{\max} \tag{3.34}$$

**Initial and time-invariant constraints**

In order to make the BESS act as a buffer and not as an energy source which can be depleted through a year, boundaries are set that make the BESS have half its capacity available at $k = 0$, as well as at $k = ts{-}1$.

$$E_{\text{bess}}[0] = \frac{E_{\text{bess}}^{\max}}{2} \tag{3.35}$$

$$E_{\text{bess}}[ts-1] = \frac{E_{\text{bess}}^{\max}}{2} \tag{3.36}$$

The initial temperature of the ATES is constrained to be the initial temperature of the complete network.

$$T_{\text{out}}^{\text{N0}}[0] = T_0^{\text{DHN}} \tag{3.37}$$

# 4

# Results and discussions

In this chapter the results of all introduced calculations and optimizations in the previous chapters are described, interpreted and discussed. The relevant graphs, tables and other information are given in the main body of the thesis. Additional graphs and tables for every simulation run, calculation and derivation can be found in Appendices A and B. A hyperlink to the Github repository of this project containing all Python code used in this thesis is given in Appendix D.

## 4.1. Electrical and thermal demand pattern forecast

*What will the electrical and heat demand pattern of the Werf area be in 2028?*

In this section, the results of the energy demand predictions on the Werf for 2028 are described for heating and electricity separately, after which these results are discussed.

### 4.1.1. Results

#### Heating demand

The results of the heating demand prediction is presented for a building of each building type, as the demand prediction for other buildings of the same type is roughly the same. The building at node “N2” is a small building, at “N5” a medium building and at “N10” is a large building. For all three types the energy exchange with the ambient and the heat pump thermal power demand are shown. The electrical power of the heat pump and the demanded heat from the DHN are not yet known. This is because the temperature of the DHN varies per optimization and the COP of the heat pump depends on that temperature. However, these results are a good indication of the overall energy demand by the heat pumps giving insight in the patterns at which the pumps will put burden on the other components of the network.

The heat exchange with the environment and the heat pump thermal power belonging to the small building are given in Figure 4.1 and 4.2. The building loses up to 25 kW of heat power at the coldest periods of the year. The maximum heat pump power is nearly 120 kW at a single timestep.

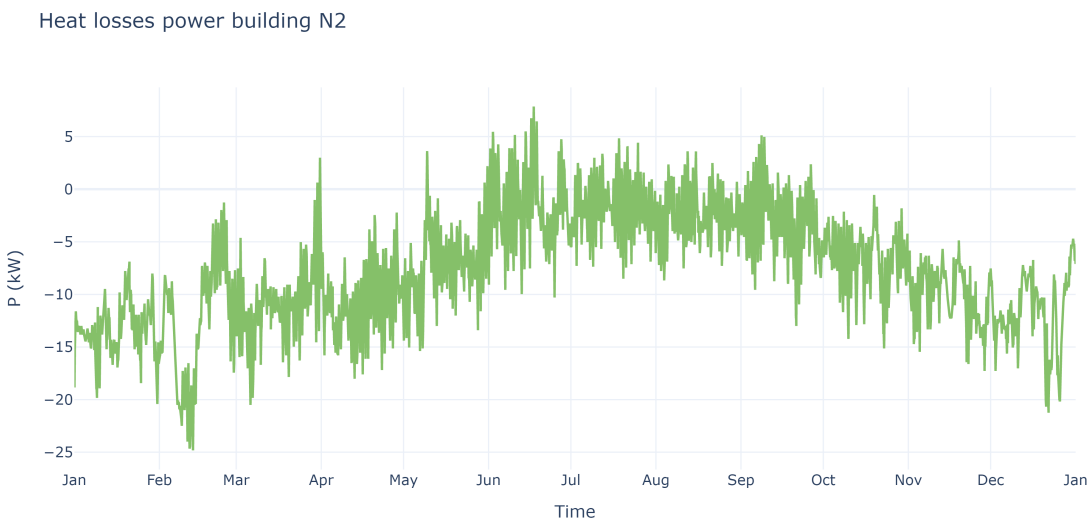


Figure 4.1: Environment losses for a small building type

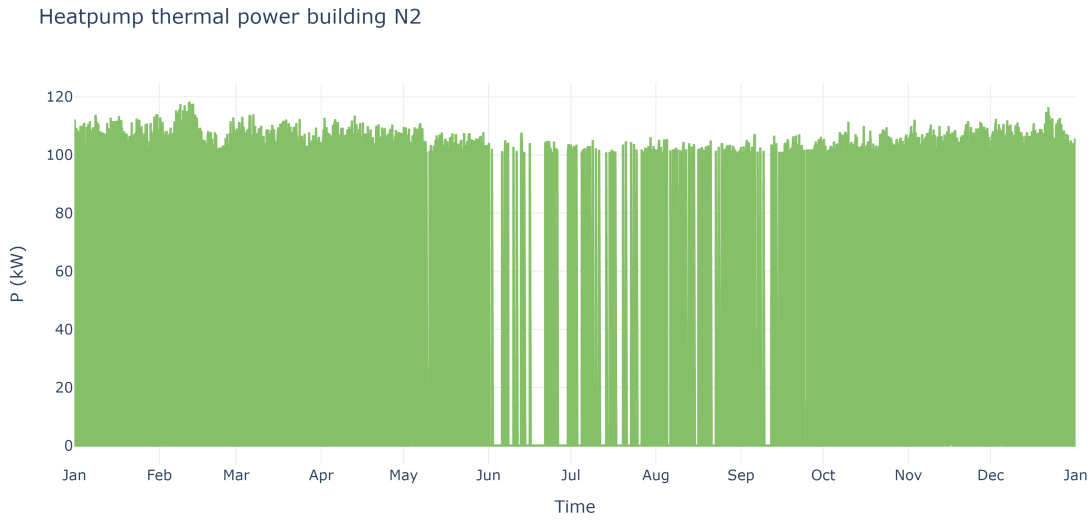


Figure 4.2: Heat pump thermal power for a small building type

The medium size buildings, modeled at 1,500 $m^2$ of floor area, show larger losses to the ambient. This behavior is expected and results in a maximum power loss of over 40 kW in February. This leads to a peak in thermal power delivered by the heat pump of nearly 130 kW in a single timestep. The medium sized building results are showed in Figure 4.3 and 4.4.

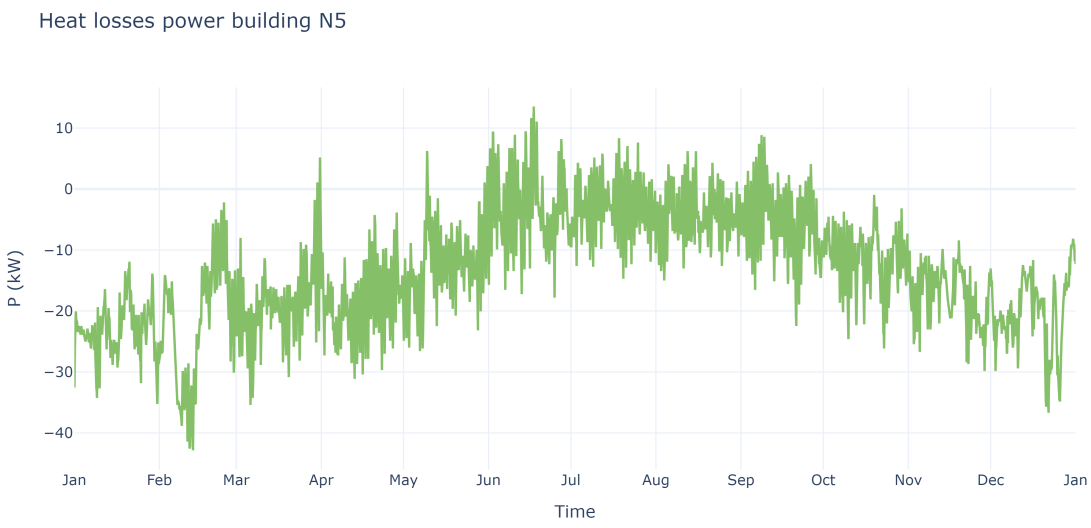


Figure 4.3: Environment losses for a medium building type

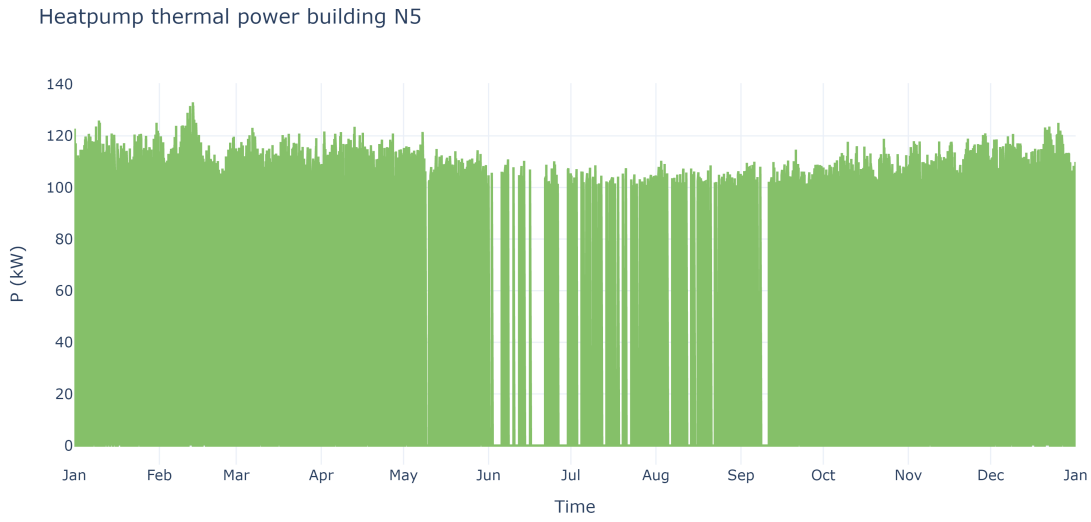


Figure 4.4: Heat pump thermal power for a medium building type

The largest building category only contains a single building, the building at thermal node ”N10”. This large building is losing more than 70 kW of heat at its peak. This is compensated by a peak heat demand from the heat pump of 150 kW, with a high repetition rate of those larger peaks to compensate for all the building losses, keeping the temperature close to the setpoint. (Figure 4.5 and 4.6)

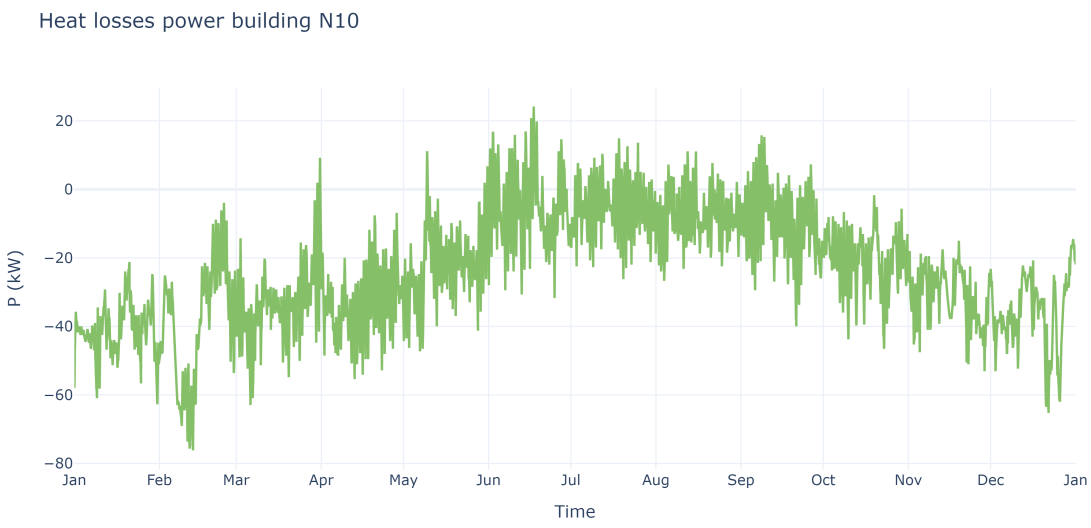


Figure 4.5: Environment losses for a large building type

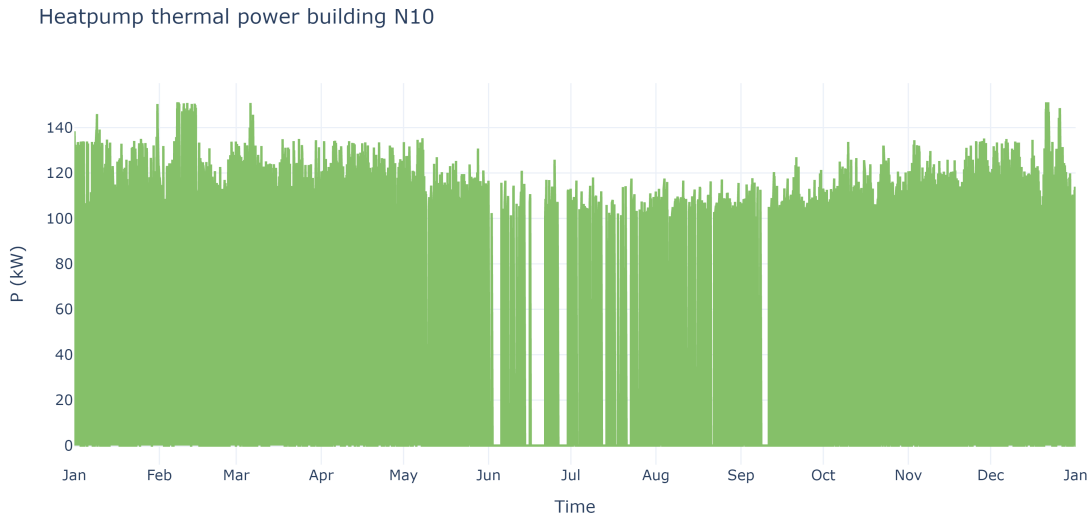


Figure 4.6: Heat pump thermal power for a large building type

For all graph pairs, the correlation in summer is clear where if the heat losses to the environment start to become positive, the heat pump thermal power demands is zero. This indicates that the control theory is working correctly.

### Electrical demand

The electrical demand pattern is derived by a prediction in two building utilization profiles: Residential and industrial. These derivations are described separately, after which the combined demands are shown and discussed.

**Industrial:**
The basis of the industrial demand pattern prediction on the Werf in 2028 are real data patterns from four bulk consumption connections. These patterns were achieved from the real estate partners and are

combined and scaled to result in a combined industrial demand pattern. The yearly demand patterns of the four retrieved data sets are shown below in Figure 4.7, 4.8, 4.9 and 4.10.

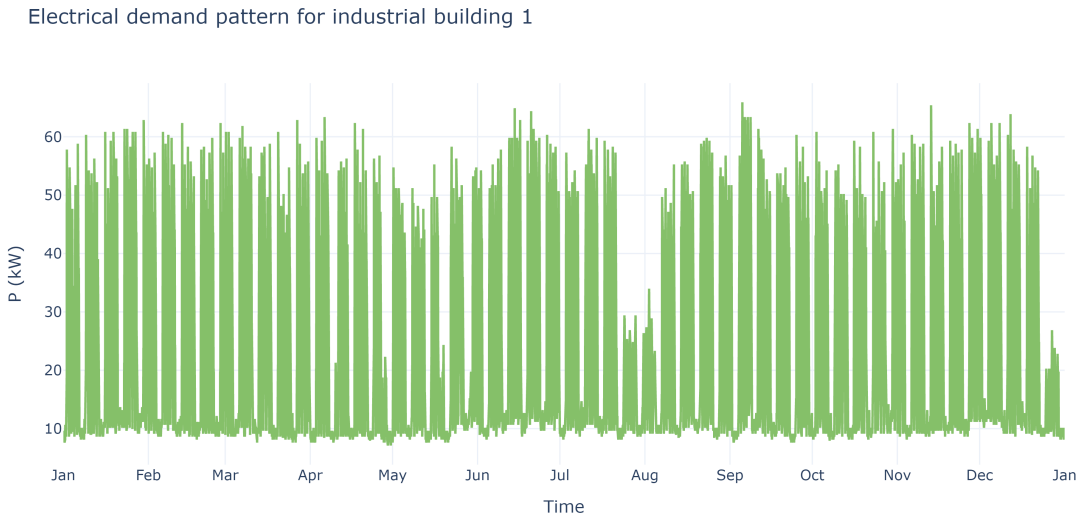


Figure 4.7: Electricity demand pattern industrial building 1

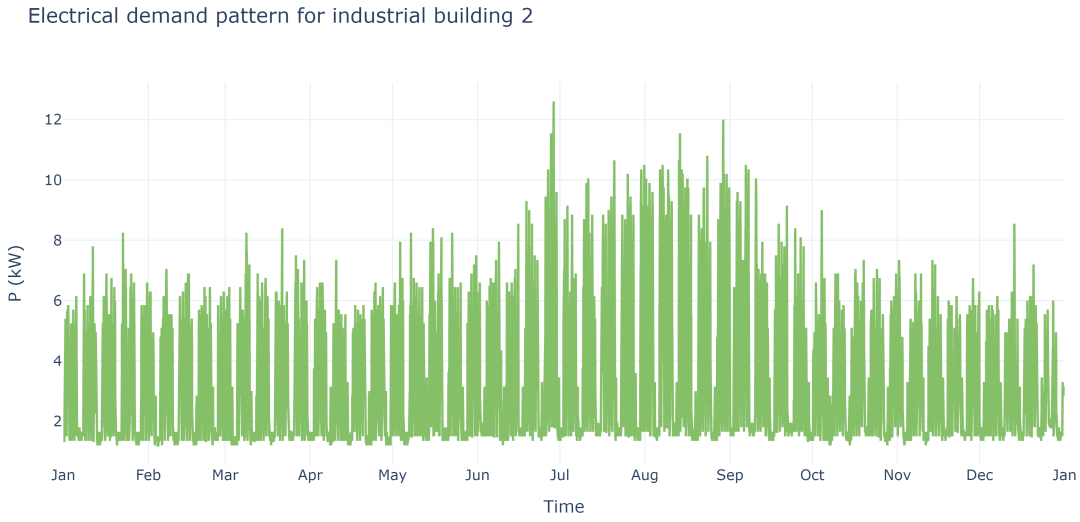


Figure 4.8: Electricity demand pattern industrial building 2

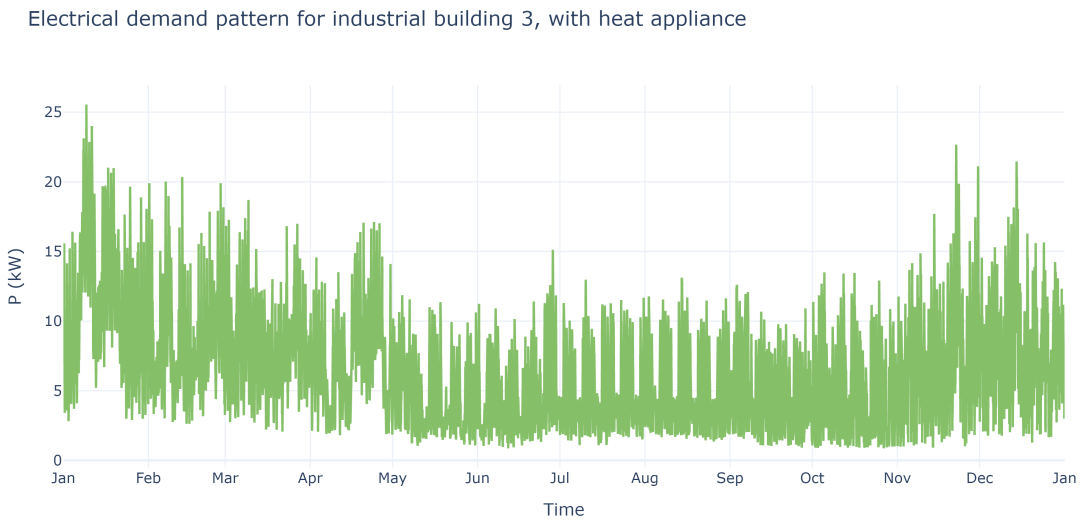


Figure 4.9: Electricity demand pattern industrial building 3

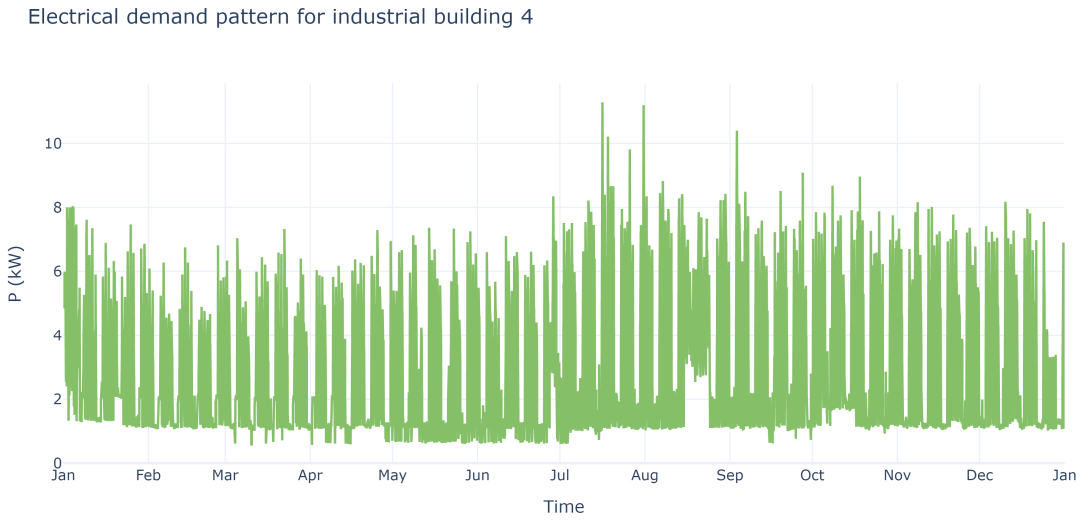


Figure 4.10: Electricity demand pattern industrial building 4

The electrical demand pattern of building 1 (Figure 4.7) shows a clear working week pattern with 52 peaks. In periods of national Dutch holidays (May, August and December/January) dips are present.

This pattern is different in building 2 (Figure 4.8), where in summer the electrical demand is higher. That demand probably belongs to an air-conditioning unit for cooling. The national holidays are less clear which could be due to a larger spread in holidays by employees. Still, the Christmas break is evident, as almost the whole country is on collective leave that period.

Industrial building 3 has an electrical heating appliance present in the data (Figure 4.9). In order to achieve a purely electric demand this pattern is converted with the steps described in the methodology in Chapter 3. After applying this algorithm, the pattern is transformed and the resulting pattern is pictured below in Figure 4.11. The electrical heating demand is mostly vanished, but still some patterns related to ambient temperatures (Figure A.1) are present.

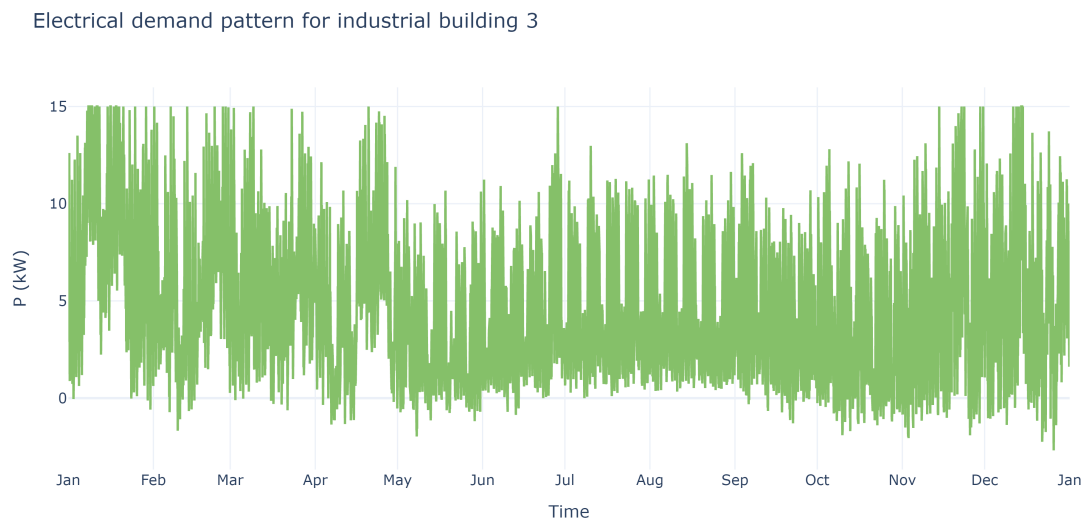


Figure 4.11: Electricity demand pattern industrial building 3 with electrical heat extracted

Industrial building 4 (Figure 4.10) shows a general mixture of the patterns of all other industrial building patterns.

The total electrical demand patterns is shown below 4.12. The quantity of electrical power is not relevant, as this will be scaled in a later stage of the results. This graph purely shows the pattern in which the electricity is consumed relative to other timesteps.

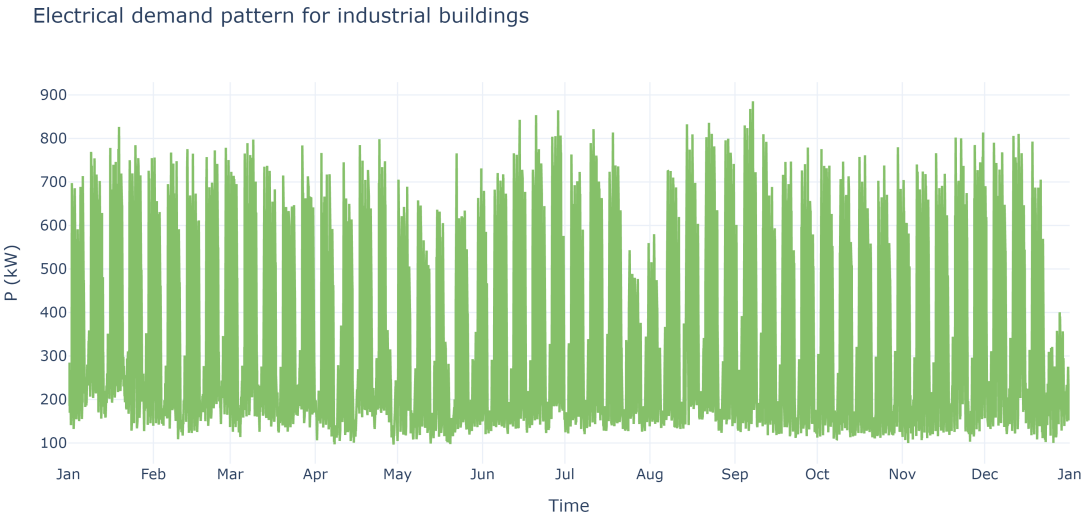


Figure 4.12: Total electricity demand pattern of the industrial building 1 to 4

**Residential:**
The electrical demand pattern of residential buildings is generated for a single household for a day. A single semi-random generated residential pattern for a day looks like the graph in Figure 4.13. In this plot the morning and evening peaks are visible, which matches peaks in residential power demand profiles.

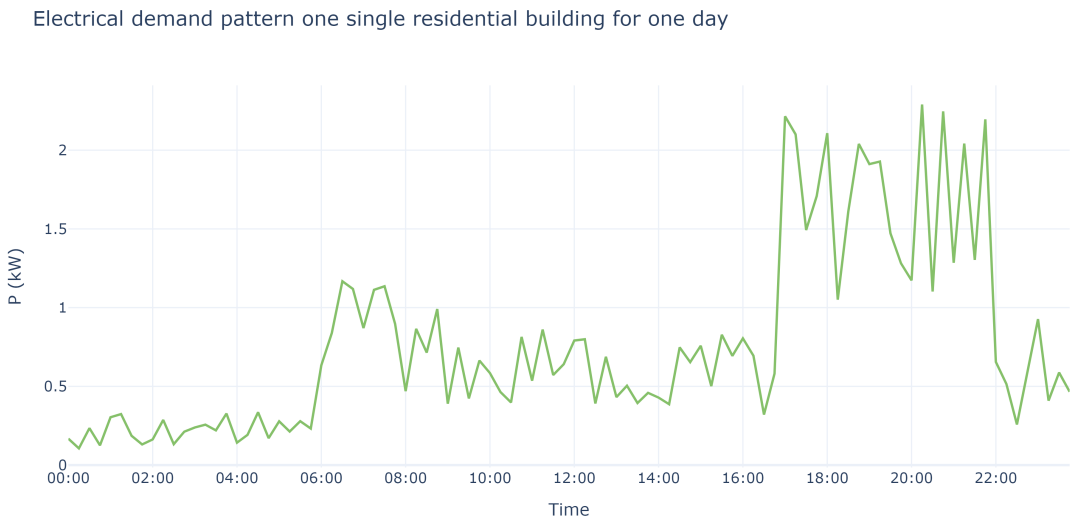


Figure 4.13: Semi-random generated electricity demand profile for a single household

This pattern is generated 365 days for a year and this is generated for 55 different residential homes. After this the powers are summed per timestep, resulting in the total residential electricity demand pattern for a year. Again this dataset is still not scaled correctly, only the patterns are of importance for the next step in the research. A figure of this pattern can be found in Appendix A, Figure A.4.

**Combined:**
The combined demand patterns of the industrial and residential buildings added together and scaled to a total consumption over a year of 1,244 MWh looks like the following graph in Figure 4.14. In this graph the scaling is correct so the values are the real values input for the optimization model.

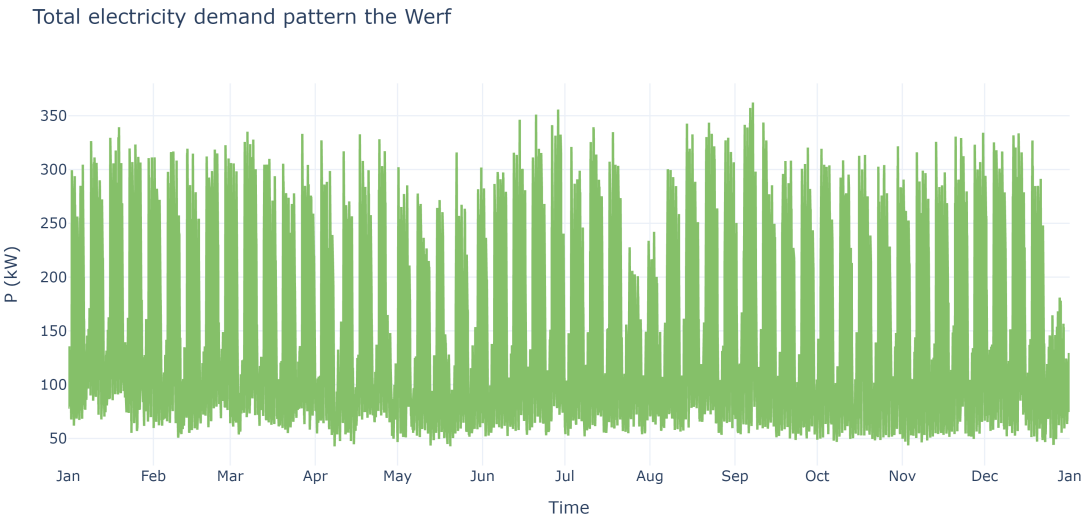


Figure 4.14: The total scaled electricity demand of the Werf in 2028

It can be seen that the industrial pattern dominates. This is to be expected as the largest portion of the building area is industrial, as well as the power intensity of the industrial processes is larger.
The total accumulated energy demand for heat and electricity are shown in table 4.1

Table 4.1: Total accumulated electricy and heat

| Energy carrier | Value | Unit |
|---|---|---|
| Heat | 1,371 | [MWh] |
| Electricity | 1,244 | [MWh] |

### 4.1.2. Discussion

The predictions of the thermal demand of the buildings are generally complete (Figures 4.1, 4.3 and 4.5) and show coherence with the ambient temperature profile. This demand is correctly transformed to the thermal demand of the heat pumps, but the frequency and distribution of heat pump peak demands are not clearly represented visually, which limits intuitive interpretation (Figures 4.2, 4.4, 4.6). While this demand derived from the applied control theory is technically correct, it appears somewhat discontinuous or staccato. The implementation of more refined control strategies could lead to a smoother and more homogeneous heating demand profile. The difference in results across different building sizes is as expected. However, the use of only three distinct size categories as showed in Figure 3.4 may be overly simplistic and could diverge significantly from the actual diversity of buildings found on the Werf area.

The generation of the industrial electricity demand profile was based on the combination of four real datasets (Figures 4.7, 4.8, 4.9 and 4.10), one of which had electricity consumption for heating included (4.9). This embedded electrical heating demand was estimated using a model of an air to air heat pump which delivered the previously calculated building thermal demand. This approach is rather rough, which is confirmed by the fact that the extraction is not perfect and temperature trends are still present in the electrical demand pattern (Figure 4.11).

Residential electricity demand was modeled separately using a script that assigns power ranges to each hour of the day and generates 55 distinct annual profiles (Figure 4.13 and A.4). While this introduces variability and a degree of realism, the approach still relies on static assumptions about daily usage patterns and does not capture the difference between working days and weekend days, seasonal shifts or holidays.

After generating the two profiles, the combined electricity demand was scaled to match the predicted annual energy consumption for the Werf in 2028 (Figure 4.14). Although this ensures consistency at the yearly level and attempts to predict behavior at a 15 minute basis, it may lack peak loads or other temporally relevant features critical for this energy hubs operation. As such, while the methodology provides a structured and scalable approach to electricity demand profile generation, the results should be interpreted with an awareness of these underlying assumptions and limitations.

## 4.2. Optimal energy hub sizing

*What is the optimal sizing of the multi carrier energy hub neglecting internal network limitations?*

The results of this subquestion contain optimization outcomes for every connection category introduced in the methodology introduced in Chapter 3. The tables presenting the numerical solutions are presented below, after which the graphs are shown belonging to the relevant solutions.

### 4.2.1. Results

Table 4.2: Base optimization for connection category AC5

| Parameter | Value | Unit |
|---|---|---|
| Connection Category | AC5 | – |
| Max Consumption – Max Production | 1,700 – 2,000 | [kW] |
| Installed PV power | 0.0 | [kWp] |
| Battery Energy Capacity | 0.0 | [kWh] |
| Total Cost | 0.0 | [€] |
| Maximum Grid Power | 899.0 | [kW] |

Table 4.3: Base optimization for connection category AC5b

| Parameter | Value | Unit |
|---|---|---|
| Connection Category | AC5b | – |
| Max Consumption – Max Production | 850 – 1000 | [kW] |
| Installed PV power | 0.0 | [kWp] |
| Battery Energy Capacity | 48.5 | [kWh] |
| Total Cost | 56,943.0 | [€] |
| Maximum Grid Power | 850.0 | [kW] |

Table 4.4: Base optimization for connection category AC5a

| Parameter | Value | Unit |
|---|---|---|
| Connection Category | AC5a | – |
| Max Consumption – Max Production | 535 – 630 | [kW] |
| Installed PV power | 0.0 | [kWp] |
| Battery Energy Capacity | 363.5 | [kWh] |
| Total Cost | 426,804.3 | [€] |
| Maximum Grid Power | 535.0 | [kW] |

Table 4.5: Base optimization for connection category SolarPark

| Parameter | Value | Unit |
|---|---|---|
| Connection Category | SolarPark | – |
| Max Consumption – Max Production | 300 – 350 | [kW] |
| Installed PV power | 1,045.2 | [kWp] |
| Battery Energy Capacity | 3.26 | [MWh] |
| Total Cost | 4,882,203.6 | [€] |
| Maximum Grid Power | 350.0 | [kW] |

Table 4.6: Base optimization for connection category AC4b

| Parameter | Value | Unit |
|---|---|---|
| Connection Category | AC4b | – |
| Max Consumption – Max Production | 147 – 160 | [kW] |
| Installed PV power | 1,743.5 | [kWp] |
| Battery Energy Capacity | 272.7 | [MWh] |
| Total Cost | 321,971,228.4 | [€] |
| Maximum Grid Power | 160.0 | [kW] |

Table 4.7: Base optimization for connection category AC4a

| Parameter | Value | Unit |
|---|---|---|
| Connection Category | AC4a | – |
| Max Consumption – Max Production | 94 – 100 | [kW] |
| Installed PV power | 1,743.5 | [kWp] |
| Battery Energy Capacity | 468.7 | [MWh] |
| Total Cost | 552,099,761.2 | [€] |
| Maximum Grid Power | 100.0 | [kW] |

Some of the upper results are excluded from further investigation. From Table 4.2 the results from the base optimization of AC5 can be read and it is clear that this connection is not a minimization of its size. The maximum grid power is calculated to be 899.0 kW, where the connection category ranges to 1700 and 2000 kW.
As the required grid power for the base case with no extra PV power and additional BESS is 899.0 kW, the category AC5b with a maximum consumption of 850 kW is also neglected (Table 4.3).
Higher on the connection ladder the investment costs and BESS sizes for the connections AC4b and AC4a (4.6 and 4.7) transcend the reasonable values applicable for this area. The optimized BESS size enters the scale of the total newly installed BESS capacity in the Netherlands in 2023 ([18]).

Eliminating the neglected results leaves two datasets of interest, the AC5a and SolarPark connections (4.4 and 4.5). For these two results the BESS energy profile and the grid power is plotted and interpreted.

### AC5a

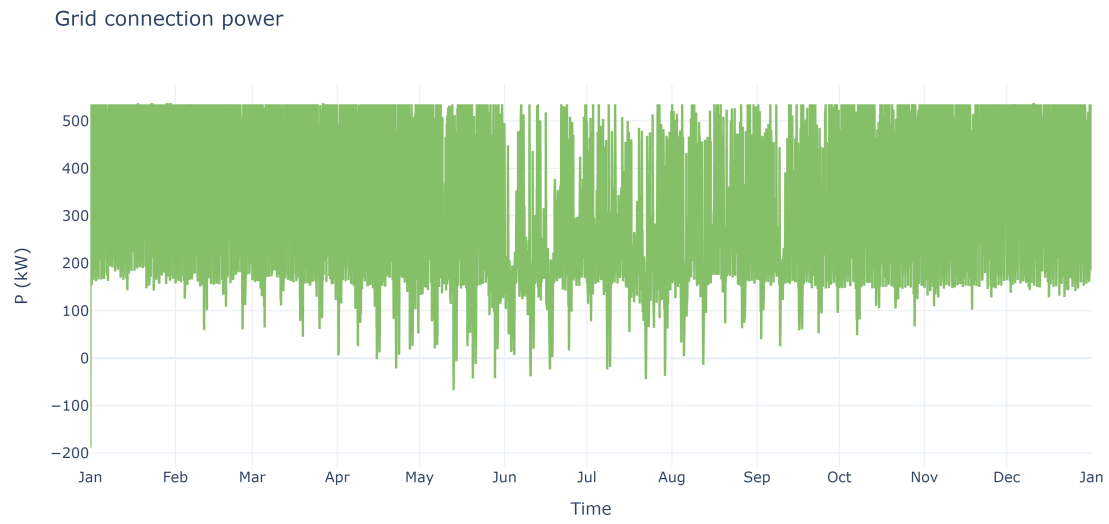


Figure 4.15: Grid power results of base optimization of AC5a connection

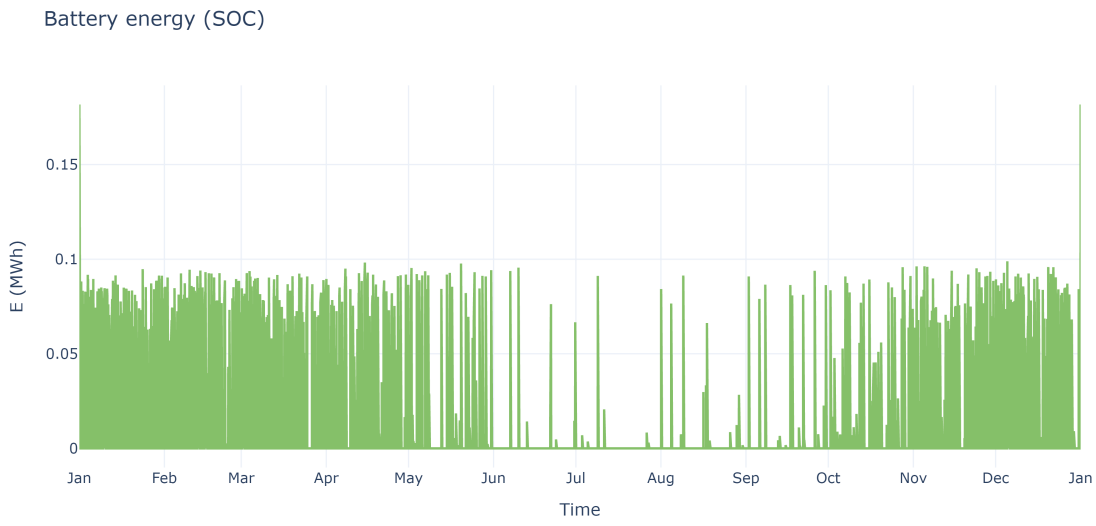


Figure 4.16: BESS energy profile of base optimization of AC5a connection

The grid connection power in the base scenario with AC5a bounds never reaches its lower boundary (630 kW), but the upper boundary is clearly constraining this profile (Figure 4.15). The maximum grid connection capacity is mostly used, except for some periods in summer. However, the grid connection hardly delivers power back to the grid.

The battery energy profile looks quite stable, with a homogeneous peaks over the year except for summer periods (Figure 4.16). There are two peaks present, presumably at the first and last timestep of the simulation, these peaks are around 180 kWh, where most of the battery profile for the rest of the year stays below 100 kWh. Where it might be expected that the battery is very active during summer times to catch solar generation peaks, the contrary seems true, as the battery seems very inactive during summer months.

### SolarPark

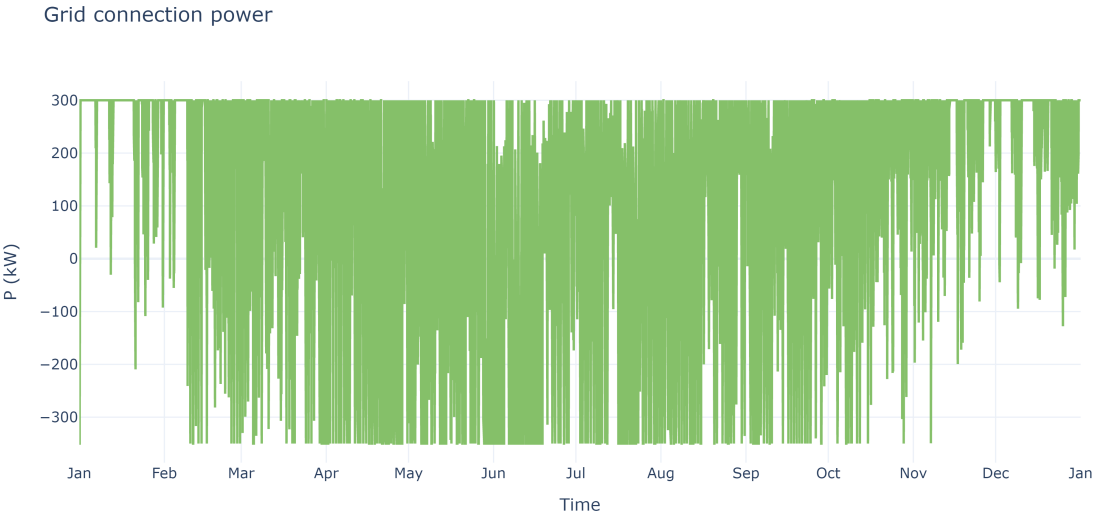


Figure 4.17: Grid power results of base optimization of SolarPark connection

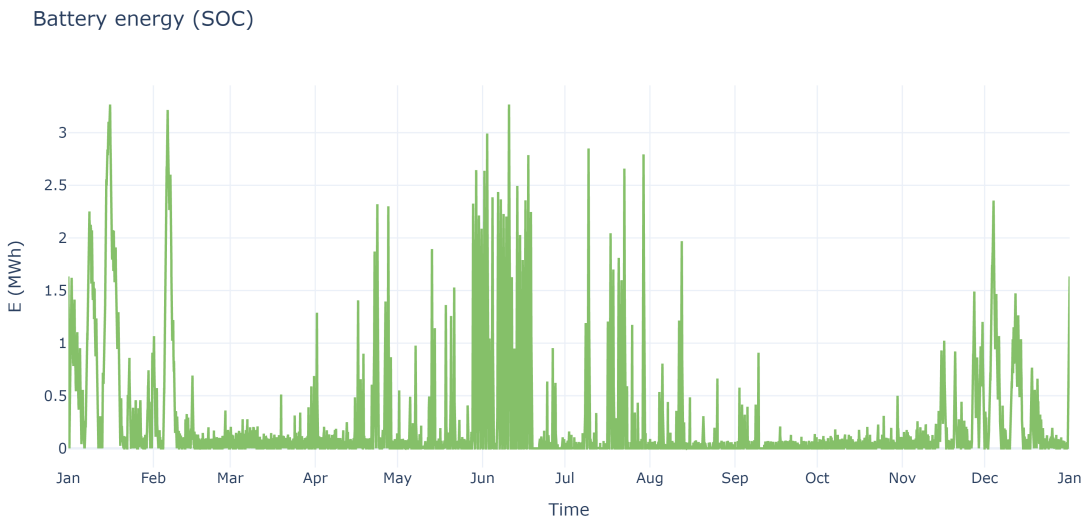


Figure 4.18: BESS energy profile of base optimization of SolarPark connection

Due to the further limitations in grid connection power, the BESS is used more actively for the SolarPark connection (Figure 4.18). Between February and November, the grid interaction indicates frequent shifts between importing and exporting electricity (Figure 4.17). In the winter months electricity is rarely exported and there are even times that the full grid consumption capacity is used for multiple days in a row.
There are high peaks in the battery SOC present in winter and in summer. In spring and autumn, the used battery capacity is about 15% of the total battery capacity.

### 4.2.2. Discussion

The optimization results of the base scenario show that full energy autonomy on this area is impossible for the design of this system as the two most restricted grid connections have proven to be infeasible (Tables 4.7 and 4.6). The ATES provides a large part of the heating demand of the buildings in the coldest months, but still electricity is needed for the heat pumps to step up the temperature. In these periods, the renewable generation from the PV and PVT system can not fulfill the demands of the heat pumps. An appropriately sized BESS can not provide this seasonal gap in energy consumption and generation.

The result of these problems are most clear in the results of the SolarPark connection, where in winter months the grid connection is charging the battery at the maximum grid power for multiple days, saving energy for a cold period later in that month (Figure 4.17). Next to the fact that this cannot be as efficiently predicted as in this optimization model, this also oversizes the BESS greatly.

The battery profile from Figure 4.18 shows the peaks of the battery profile which can be reduced to lessen the total investments costs. In the next section it will be investigated if load shifting and direct load control can improve this profile and thereby reduce the cost function.

The last thing to notice is the discrepancy between the optimized battery size for the AC5a connection and its BESS SOC profile. The optimized BESS capacity is 363.5 kWh (Table 4.4, whereas the battery profile never reaches above a capacity of 180 kWh (Figure 4.16). This is due to the initial value constraint of the BESS, starting that at $k = 0$ the battery SOC should be at half its capacity. As the energy system presumably requests a lot of power from the BESS in the first time step and after this step this power is never demanded again, the battery is calculated to be too large for this setup. This means that as the extra PV capacity is zero, the optimization costs and battery size can be effectively halved, resulting in a total cost of a bit over €200k and a BESS capacity of nearly 200 kWh.

## 4.3. Load shifting and direct load control

*How can a combination of load shifting of controllable loads and direct load control influence the sizing of the system, and is its implementation feasible in this area?*

This section states the results of the optimization runs with additional elements to improve the system sizing and with that the decrease of the cost function. This consists of runs where the load of the building heat pumps are shifted to timesteps with solar irradiation, runs where the surplus of solar generation is used to power a heat pump stepping up the temperature of the DHN and runs with a combination of the previously noted elements.

### 4.3.1. Results

#### Loadshift

The optimizations with the loadshift protocol applied, results in higher costs for all connections. This is why only one connection with results is displayed below, interpreting this as a description for what happens in the results for all the connections independent of size. The remaining result tables can be found in Appendix B.

Table 4.8: Loadshift optimization for connection category SolarPark

| Parameter | Value | Unit |
|---|---|---|
| Connection Category | SolarPark | – |
| Max Consumption – Max Production | 300 – 350 | [kW] |
| Installed PV power | 1,147.1 | [kWp] |
| Battery Energy Capacity | 3.80 | [MWh] |
| Total Cost | 5,611,134.6 | [€] |
| Maximum Grid Power | 350.0 | [kW] |

In comparison with the base scenario the cost is increased from €4,882,203.6 to €5,611,134.6. This increase stems from both an increase in the installed PV power as well as the BESS capacity. The loadshift protocol is interpreted below in Figures 4.19, 4.20, 4.21, 4.22 and 4.23.

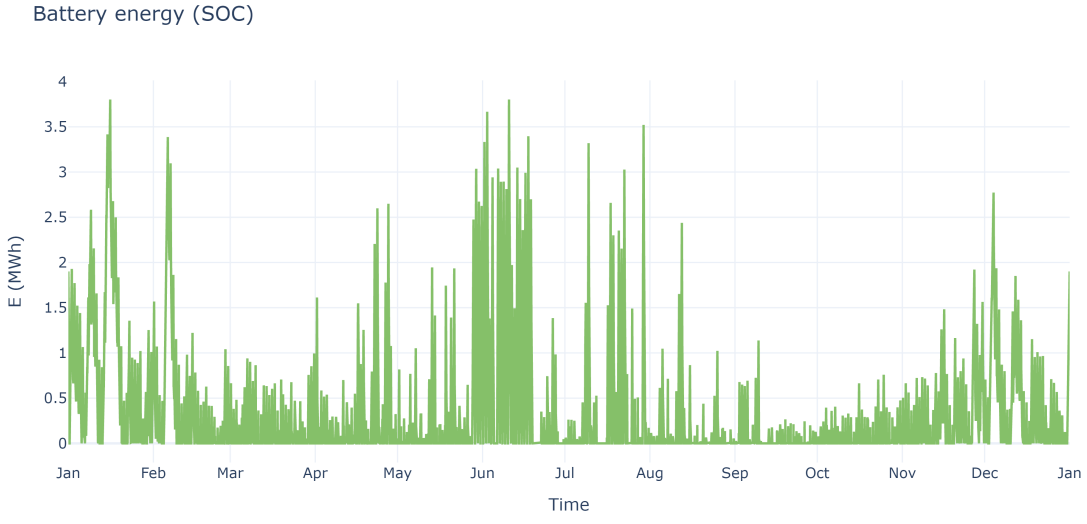


Figure 4.19: Battery energy for loadshift optimization with SolarPark connection

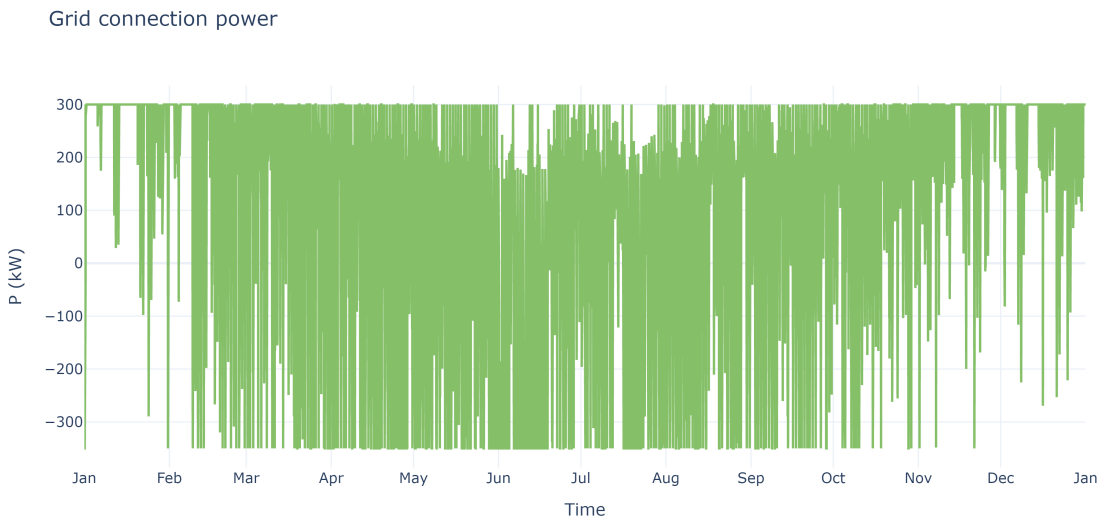


Figure 4.20: Grid power for loadshift optimization with SolarPark connection

The battery energy and grid connection profiles with the loadshifting technique enabled show similarities with the base simulation. However, the size of the energy peaks for the BESS are larger, leading to a larger overall. The grid connection power does not significantly differ from the base scenario.

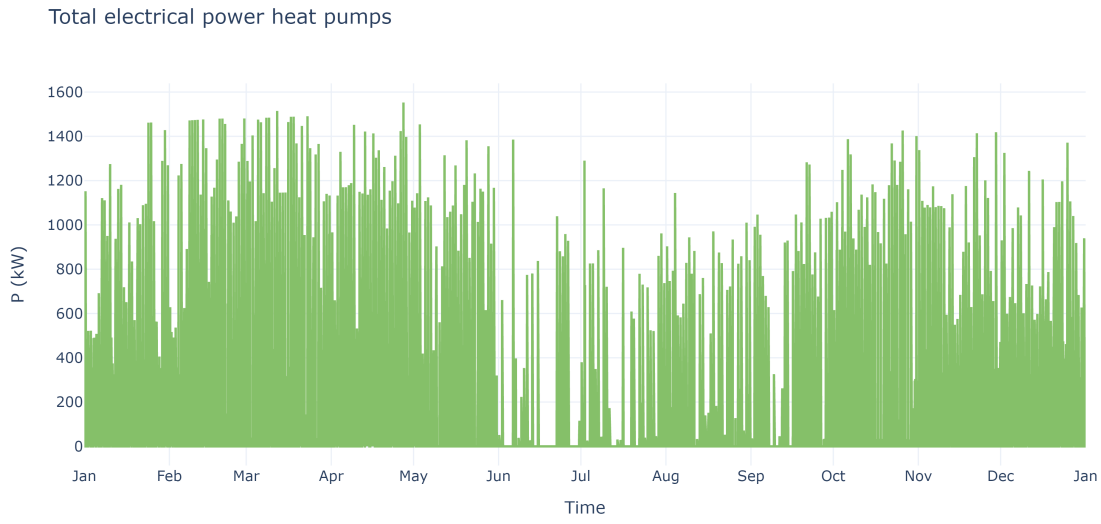


Figure 4.21: Summation of building heat pumps powers for loadshift optimization with SolarPark connection

The total sum of the heat pump powers for all the buildings is significantly larger than in the simulation with no loadshifting enabled. The base scenario optimized these peaks to be 500 to 600 kW maximum, but for this scenario the peak reach above 1,500 kW.

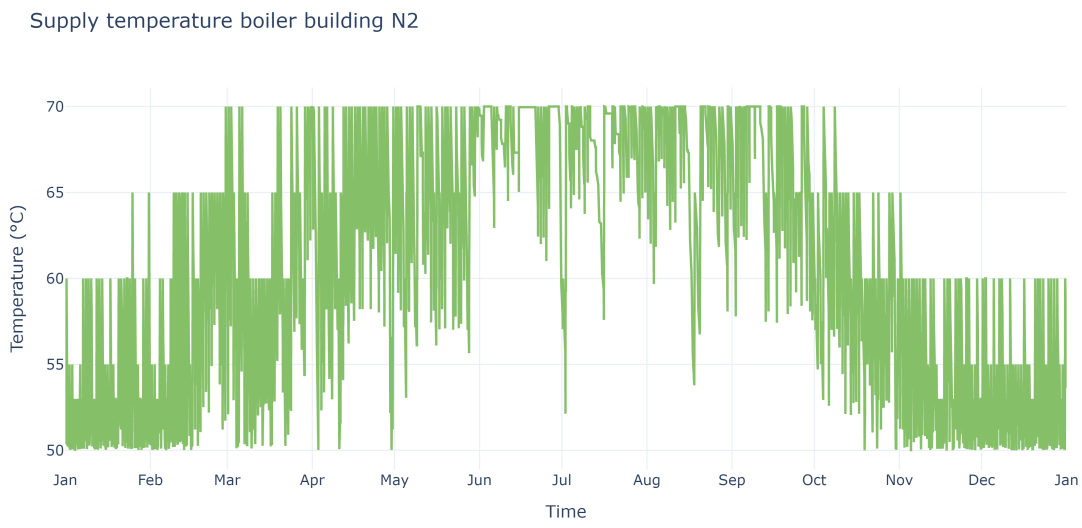


Figure 4.22: Builder supply temperature for a single building for loadshift optimization with SolarPark connection

In the graph showing the boiler supply temperature it is clear that the introduced load shifting protocol works. The boiler temperature rises if there is more irradiance. However, this higher boiler temperature results in a drop in COP of the heat pumps as can be seen in Figure 4.23.

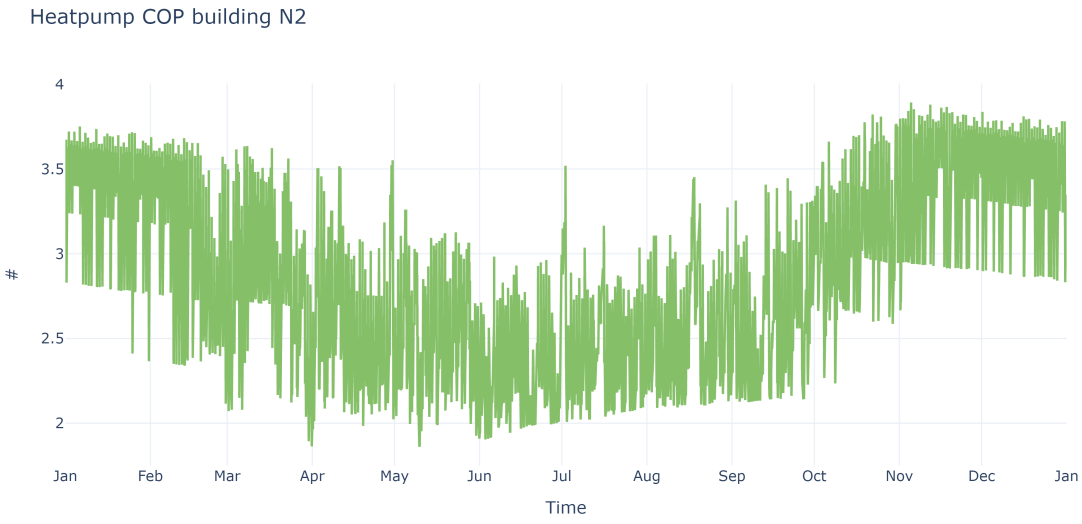


Figure 4.23: Heat pump COP for a single building for loadshift optimization with SolarPark connection

### Direct load control

With the addition of an extra air to water heat pump located at the PVT node of the DHN, surplus generated renewable electricity can be converted to heat and stored in the ATES. The optimization results for all connections gave a lower cost with this extra heat pump. The operation of the system will be evaluated with the two reasonable connection sizes as proposed in the base optimizations. The results for respectively AC5a and SolarPark are shown in Table 4.9 and 4.10.

Table 4.9: Direct load control optimization for connection category AC5a

| Parameter | Value | Unit |
|---|---|---|
| Connection Category | AC5a | – |
| Max Consumption – Max Production | 535 – 630 | [kW] |
| Installed PV power | 0.0 | [kWp] |
| Battery Energy Capacity | 329.5 | [kWh] |
| Total Cost | 386,887.3 | [€] |
| Maximum Grid Power | 535.0 | [kW] |

Table 4.10: Direct load control optimization for connection category SolarPark

| Parameter | Value | Unit |
|---|---|---|
| Connection Category | SolarPark | – |
| Max Consumption – Max Production | 300 – 350 | [kW] |
| Installed PV power | 1,543.2 | [kWp] |
| Battery Energy Capacity | 2.30 | [MWh] |
| Total Cost | 4,247,751.3 | [€] |
| Maximum Grid Power | 350.0 | [kW] |

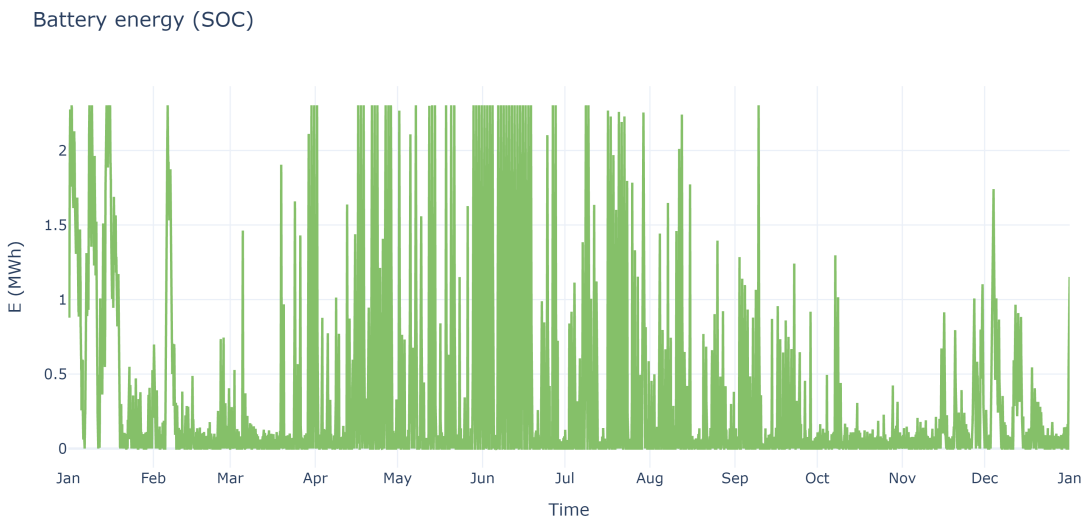


Figure 4.24: Battery energy for direct load control optimization with SolarPark connection

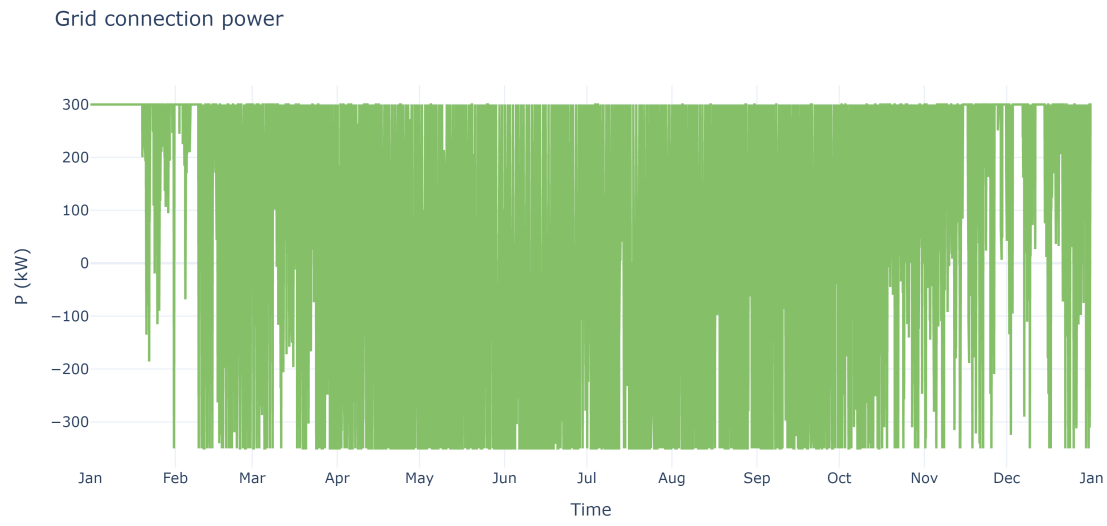


Figure 4.25: Grid connection power for direct load control optimization with SolarPark connection

In the above results (Figure 4.24 and 4.25) it can be seen that the potential of the battery is used better. The grid power is still in the first winter months at its maximum capacity, after which the import and export of electricity are frequently alternated. At the winter months at the end of the year the vast majority is import of electricity, but the burden on the grid is not as large as in the first winter months of the year.

The power draw of the extra placed heat pump can be found in Figure 4.26. The graphs shows large activity in the first wintermonths and some lower activity over a large summer period.
This results in a different ATES temperature over the year than in other scenarios. The normal ATES scenario can be found in Appendix A. The additional heat pump ensures that the minimum temperature in the ATES is lower and that the maximum temperature is higher (Figure 4.27). Where in the normal scenario the ATES temperature at the begin and end of the year is roughly the same, the ending temperature in the direct load control scenario ends above 19°C.
The change in ATES temperature results in a different COP pattern, as shown in Figure 4.28. For reference the normal COP pattern in shown in Appendix A.

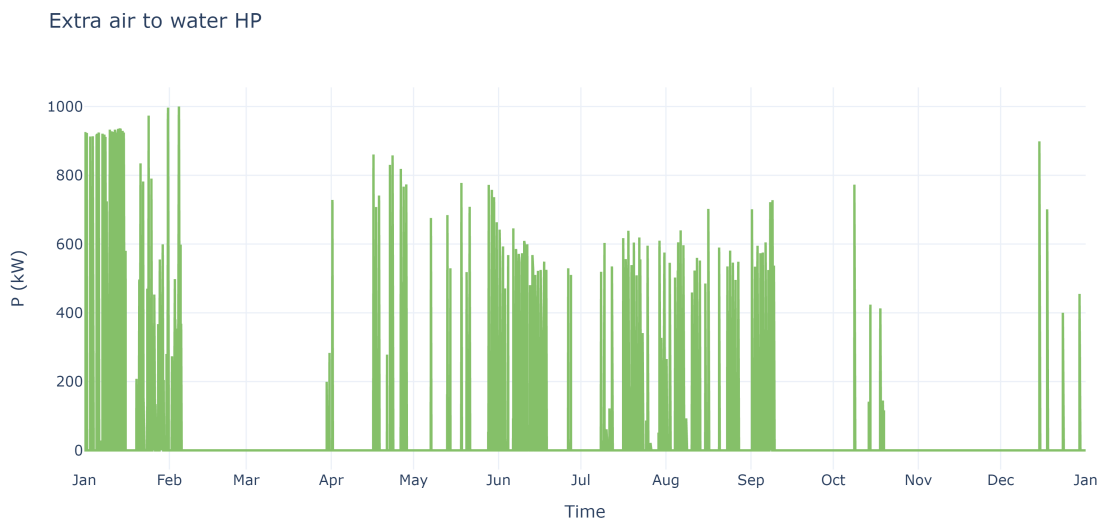


Figure 4.26: Extra heat pump power for direct load control optimization with SolarPark connection

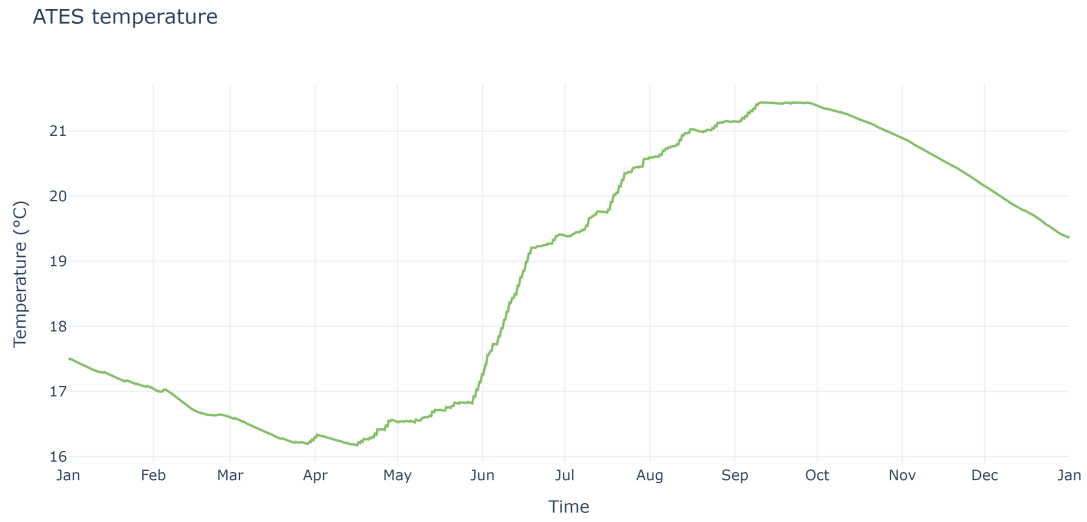


Figure 4.27: ATES temperature for direct load control optimization with SolarPark connection

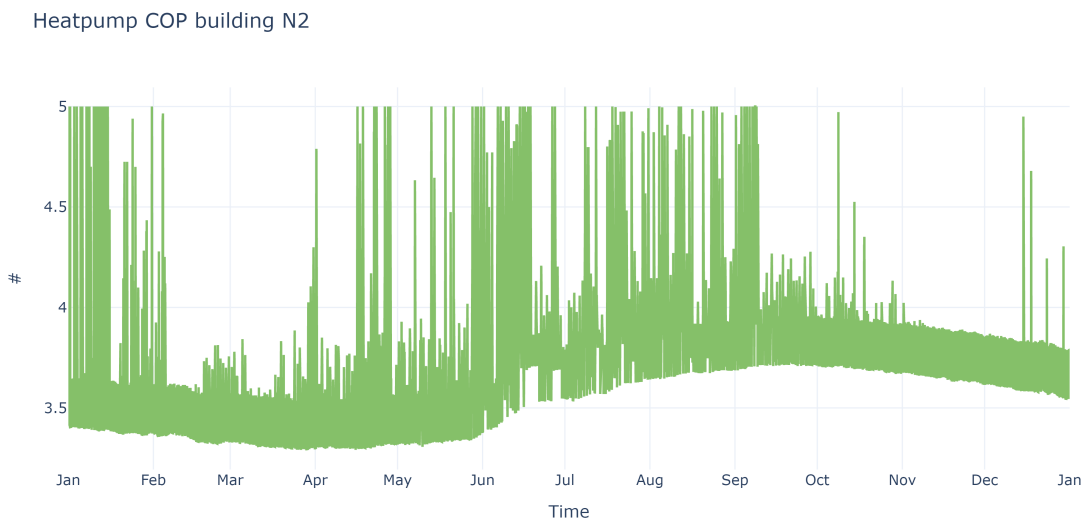


Figure 4.28: COP of a heat pump of a single building for direct load control optimization with SolarPark connection

#### Combination

Where upfront the combination of load shifting and direct load control was expected to show the lowest costs, the results state otherwise. Although the results show lower costs than the base optimization, the direct load control optimization alone gives even lower costs. Because of this, the results are irrelevant for the body of this thesis and the result tables are placed in Appendix B.

### 4.3.2. Discussion

The main goal of this research question was to improve the behavior of the energy system and with that lower the cost of the optimization objective function. The proposed load shifting technique does not contribute to that goal (Table 4.8), as it worsens the COP of the building heat pumps and make them thereby draw more power (Figure 4.23). This higher power draw alone would not directly introduce a problem if the battery can deliver these high powers, but due to the lower efficiency of the heat pumps the total energy consumption in winter is increased. This creates a challenge, given that the energy system is already characterized by electricity shortages in the winter months.

The implementation of an extra direct load control heat pump does improve the result of the cost function of the optimization (Tables 4.9 and 4.10). However, this improvement mainly comes from the operation in winter months where the pump steps up the temperature of the DHN (Figure 4.26), increasing the COP of the heat pumps (Figure 4.28). In summer the heat pump also provides some direct load control from the PV system, which as a result can be larger and deliver more power. Still, the main improvement comes from the operation of the extra heat pump in colds periods, which was not the proposed function of this supplement. With an additional electric generator for the winter months, the heat pump might show an operation closer to the expectations.

As already stated in the results, the hypothesis was that the combination of the two supplements would lead to the lowest cost. Because of the influence of the load shifting protocol, this is not the case (Result tables in Appendix B). However in theory, with a different load shifting protocol the best results could still be achieved with a combination of those implementations.

## 4.4. Infrastructure capacity requirements

*Depending on the size of the available grid connections defined by Liander, what are the electricity infrastructure requirements?*

Following the methodology defined in Chapter 3, the buildings are clustered to a connection within the energy hub. Building demands, heat pump demands and solar generation are assigned to these clusters, giving locational demands and production for every timestep. By assigning the clusters to a part of the electrical infrastructure, the required capacity of the cables is defined. The results of the maximum power through every component for the base and direct load control optimization with the AC5a and SolarPark connections is shown in this section in Tables 4.11 to 4.14. The corresponding graphs can be found in Appendix A.

### 4.4.1. Results

Table 4.11: Base Case – AC5a Configuration

| Component | Max Power | Unit |
|---|---|---|
| LV ring | 531.73 | [kW] |
| MV BC0 | 281.22 | [kW] |
| PVT | 248.5 | [kW] |
| BESS | 392.84 | [kW] |

Table 4.12: Base Case – Solar Park Configuration

| Component | Max Power | Unit |
|---|---|---|
| LV ring | 515.0 | [kW] |
| MV BC0 | 464.14 | [kW] |
| PVT | 248.5 | [kW] |
| BESS | 917.96 | [kW] |

Table 4.13: Direct load control – AC5a Configuration

| Component | Max Power | Unit |
|---|---|---|
| LV ring | 517.2 | [kW] |
| MV BC0 | 276.2 | [kW] |
| PVT | 716.2 | [kW] |
| BESS | 470.4 | [kW] |

Table 4.14: Direct load control – Solar Park Configuration

| Component | Max Power | Unit |
|---|---|---|
| LV ring | 694.9 | [kW] |
| MV BC0 | 705.6 | [kW] |
| PVT | 971.3 | [kW] |
| BESS | 1326.2 | [kW] |

Comparing the base optimization scenarios, it can be seen that the cabling requirements to the PVT system are the same. This is because the PVT system generates the same amount of power for every type of simulation and connection. In the direct load control configuration, the PVT stills generates the same power, but the extra heat pump is connected at the same node as the PVT, introducing different power flows.

Where the extra restrictions on the grid connection power result in a lower maximum power on the LV ring for the base case, the results of the direct load control show that this peak power is increased. Due to the higher solar injection, the BESS and the MV station maximum powers are increased with the decrease in grid connection.

### 4.4.2. Discussion

The main point of discussion in this last research question is the translation from these maximum powers to the requirements of the cabling. Selecting appropriate cables for this energy systems will require more research on not only the peak powers, but also how long those peaks last and other aspects as the length of the proposed cable connection. Due to the introduction of the electric heat pumps assisting the DHN an upgrade in the low voltage cables on the west area of the Werf is unavoidable. However, the rating of those cables could be minimized by a better control theory for the heat pumps. The current control theory introduces spikes in the demand of the clusters. If these spikes are removed by a more sophisticated control the cable investments could be decreased.

The MV transformer (contracted at 326 kW) on the east side of the Werf can currently not handle the powers introduced in the SolarPark configuration optimizations (Tables 4.12 and 4.14). This is mainly due to the introduction of extra PV generation on the roofs in those optimization configurations (Tables 4.5 and 4.10). This generated solar power introduces more return power flows to the battery or the grid, putting extra strain on the transformer. However, the maximum power level of the transformer could be a contractual limit and its physical ratings could be different.

# 5

# Conclusions and recommendations

This thesis identified a problem, formulated corresponding research questions to address it, and applied the proposed methodology to generate results that answer those questions. This final chapter will answer those initial research questions, using the results stated in this thesis.

After the conclusions, this chapter will state recommendations for future research, identifying the shortcomings of this thesis and with that the opportunities that other investigations might have.

## 5.1. Conclusions

The conclusions of thesis thesis will be drawn by answering the four sub questions and finalizing with the answer to the main research question.

- What will be the electrical and heat demand pattern of the Werf area in 2028?

The demand in terms of industrial electricity was estimated by scaling four retrieved demand patterns to the total area of industrial buildings. The residential electricity demand patterns were estimated by generating 55 demand profiles for a residential building, each differing from each other with a randomness. The industrial and residential patterns are then combined and scaled to the total predicted demand by HET of 1,244 MWh. The heat demand is calculated from a model where the buildings are categorized in three distinctions and their losses through conduction, convection and infiltration are determined. This determination is stemming from the interaction of the building with the environment, which is determined from weather patterns.

The calculated and scaled electricity patterns show a good representation of the electrical and heat demand of the area. There are clear industrial and residential patterns, which together make the electrical demand of the Werf more homogeneous. The demand is correctly scaled to a total energy consumption in a year of 1,244 MWh, thereby excluding the electrical energy consumption of the building heat pumps.

The predicted heat demand results in a heat power profile for each time step, representing the thermal energy lost to the environment. Summing these results over all the buildings on the area over a year, the heat demand is accumulated to 1,371 MWh.

- What is the optimal sizing of the multi-carrier energy hub neglecting internal network limitations?

To determine the optimal sizing of the energy hub the python model of the energy system is implemented in a solver. This solver minimizes a cost function, with a different constraint on the grid power connection per optimization. The conclusions from this research questions are generated from optimizations where

the CAPEX of a PV system is assumed to be €1,000 per kWp. The BESS CAPEX is assumed to be €600 per kWh and the interest rate is set to 4.5%.

The optimal sizing is a twofold conclusion, depending on the desires of the stakeholders. The connection category AC5a (535 – 630 kW) requires an investment of €427k. Using the SolarPark connection as the gateway to the main grid, the investments will come to €4.9M. This is investment is substantially higher but delivers a larger contribution to the energy autonomy of the area due to higher renewable generation.

- How can a combination of load shifting of controllable loads and direct load control influence the sizing of the system, and is its implementation feasible in this area?

To find out if a load shifting technique or a form of direct load control would contribute to this system, these options are implemented and compared to the base optimizations. The load shifting technique was based on moving the buildings heat pump demand to moments in time with solar irradiation and thus solar power generation. Direct load control is implemented with an air to water heat pump converting electricity to heat which can be stored in the ATES.

The introduced load shifting technique impairs the cost function compared to the base scenario. Increasing the boiler temperature setpoint shifts the load more towards solar irradiation, but also leads to a lower COP for the heat pumps.

The use of an additional heat pump to convert surplus electrical energy into heat, which is then injected into the DHN, was shown to be an effective control strategy as these optimizations resulted in lower costs. However, the behavior of this heat pump was not as expected. The heat pump utilizes some excess solar power during the summer, allowing the system to accommodate a larger PV installation. However, its primary operation occurs in the winter months, when it uses non-surplus electricity to raise the temperature of the DHN. This temperature increase improves the COP of the other heat pumps, thereby reducing their overall power consumption.

Beforehand, the combination of the two additions to the power system seemed to have the highest chance of success, but the contrary was proven. This is mainly due to the bad load shifting outcomes. A better load shifting technique might prove the previously stated hypothesis about the potential of the combination of assets right.

- Depending on the size of the feasible grid connections defined by Liander, what are the required electricity infrastructure capacities?

The locational electrical power demand per timestep is determined and calculated by grouping the building into clusters and assigning the buildings from the proposed heating network to these clusters.

The results showed that to adopt the proposed energy system on the Werf, the electrical infrastructure must be partially upgraded, independent of the grid connection size. The LV ring on the west side of the area must be upgraded to handle higher capacities, mainly introduced by the heat pumps of the buildings and the solar injection from the PV system.

The PVT system and the BESS will both need a high capacity cable connection to the main MV station. The specific capacity of these connections depends on the selected grid connection size and the implemented control strategies. Fortunately, the distance between these assets is relatively short compared to the other infrastructure in the area.

The substation at building cluster 0 (BC0) is contracted at 326 kW. This rating makes the transformer not suitable for the SolarPark configuration. The return power flows introduced by the PV injection from the roofs exceed the maximum power ratings of the substation. Further investigations must conclude if the transformer might have higher physical capabilities than is contracted, and if replacement is required.

**What is the optimal configuration and sizing of a multi-carrier energy hub (closed distribution system) in the Werf area in Hilversum towards the minimization of the grid connection size as a step toward achieving energy autonomy?**

The energy hub on the Werf can fulfill the electricity demands when the electricity system is assisted by a BESS and additional PV generation. The heating demands are provided by the 5GDHN, a PVT system, an ATES and building heat pumps. The ATES is sized at 380,000 $m^3$ in combination with 800 PVT modules of 1.77 $m^2$.

For the CDS, the optimizations led to two feasible options, minimizing the grid to connection AC5a (535-630 kW) and to connection SolarPark (300-350 kW). These options can be realized with costs of respectively €427,000 and €4,880,000. The AC5a connection is feasible with only a BESS and no additional PV generation. However, the investment is modest, resulting in only a limited step toward energy autonomy. A larger step to autonomy is made with the SolarPark connection, where extra PV power is utilized. However, this investment is quite high, although this might become smaller if an extra electrical generator is placed for electricity scarce winter months. The load shifting theory is not an improvement to the system, but the direct load control slightly improves the cost function to respectively €387,000 and €4,250,000 for the AC5a and SolarPark connections. The combination of the two protocols is also worse than the base scenario. Regardless of the construction of the CDS, with the 5GDHN implemented, the electricity infrastructure must be upgraded. The low voltage ring on the west side must be expanded to a higher capacity low voltage cable and the cables between PVT and BESS must be scaled to the results of the different scenarios. For the SolarPark connections the MV station at BC0 must be evaluated to see if it can physically withstand the increase in peak power.

## 5.2. Recommendations

The results and methodology presented in this thesis are based on several simplifications and linearizations, which should be addressed in future work to improve accuracy and applicability.

Firstly, battery efficiency was not included in the optimization due to the nonlinearity it introduces. For more representative and realistic outcomes, future models should incorporate round-trip efficiency and other losses associated with battery use. Additionally, penalties for battery charging and discharging should be implemented to account for degradation effects, improving the economic and operational realism of BESS modeling.

The cost function used in the optimization is currently incomplete. It does not include electricity prices, production costs, or investment costs for critical infrastructure components such as the electrical cabling, the district heating network (DHN), and associated equipment. Incorporating these costs would provide a more comprehensive total cost picture and enable more informed decision-making regarding investments. Moreover, grid energy usage could be penalized based on real-time electricity prices (15-minute resolution), which would better reflect the cost of consuming or producing electricity at different times. This would also support optimization strategies based on market-based operation, where batteries could be used not only for internal load balancing but also for energy trading or providing ancillary services.

The temporal resolution of 15-minute time steps introduces the risk of underestimating short-term peak loads. Higher frequency data could reveal sharper peaks and lead to different battery sizing or control decisions. Similarly, simplistic building models currently used to estimate heating demand should be refined to better reflect actual thermal behavior, especially when integrated into a thermal network.

Regarding the thermal system, the assumed DHN architecture may not be feasible in all locations due to infrastructural, spatial or financial constraints. Therefore, alternative thermal network configurations and seasonal thermal storage options should be explored in follow-up studies.

It is also recommended to assess combined heat and power (CHP) units, particularly those compatible with future hydrogen use as they could provide a future-proof addition to the energy autonomy of the area. These could serve as a valuable complement to variable renewable electricity during winter months, possibly reducing the need for an oversized BESS.

Lastly, the model could be expanded to evaluate the actual transportation cost benefits. By determining the transportation costs of all the connections currently available on the Werf, the improvements in these costs can be determined by comparing them with the results concluded by this thesis.

# Bibliography


[1] F. Otto, J. Giguere, B. Clarke, *et al.*, "When risks become reality: Extreme weather in 2024," Dec. 27, 2024. DOI: 10.25561/116443. [Online]. Available: http://hdl.handle.net/10044/1/116443.

[2] C. B. v. d. Statistiek. "Groot deel van de bedrijven bezig met verduurzamen," Centraal Bureau voor de Statistiek. Last Modified: 2023-10-18T00:00:00+02:00. (Oct. 17, 2023), [Online]. Available: https://www.cbs.nl/nl-nl/nieuws/2023/42/groot-deel-van-de-bedrijven-bezig-met-verduurzamen.

[3] "Deelauto Hilversum - Elektrisch, betaalbaar en gemakkelijk autodelen in Hilversum," Deelauto Hilversum. (), [Online]. Available: https://deelautohilversum.nl/.

[4] J. Pool, T. Bal, R. Spuijenbroek, E. Schouten, and O. van Rieven, "Naar een energiepositieve werf: Het kan als je het wil!" HET Cooperation, Hilversum, Apr. 12, 2023.

[5] T. O. Beijneveld, "Photovoltaic thermal system design including aquifer thermal energy storage in a fifth generation district heating network in hilversum," 2024. [Online]. Available: https://repository.tudelft.nl/record/uuid:5b7db8b5-fbca-4eb5-89f1-ddf53f7487a8.

[6] C. B. v. d. Statistiek. "Nearly half the electricity produced in the netherlands is now renewable," Statistics Netherlands. Last Modified: 2024-03-07T15:00:00+01:00. (Mar. 7, 2024), [Online]. Available: https://www.cbs.nl/en-gb/news/2024/10/nearly-half-the-electricity-produced-in-the-netherlands-is-now-renewable.

[7] Z. Pato, "Gridlock in the netherlands,"

[8] "TenneT doubles investments while securing long-term suppliers for large-scale expansion of onshore and offshore electricity infrastructure," TenneT. (), [Online]. Available: https://www.tennet.eu/news/tennet-doubles-investments-while-securing-long-term-suppliers-large-scale-expansion-onshore.

[9] "Grid congestion in the netherlands - we must heed the warning," Smart Energy International. (Apr. 27, 2025), [Online]. Available: https://www.smart-energy.com/industry-sectors/energy-grid-management/grid-congestion-in-the-netherlands-and-why-we-must-heed-the-warning/.

[10] F. A. Kassab, B. Celik, F. Locment, M. Sechilariu, S. Liaquat, and T. M. Hansen, "Optimal sizing and energy management of a microgrid: A joint MILP approach for minimization of energy cost and carbon emission," *Renewable Energy*, vol. 224, p. 120 186, Apr. 1, 2024, ISSN: 0960-1481. DOI: 10.1016/j.renene.2024.120186. [Online]. Available: https://www.sciencedirect.com/science/article/pii/S0960148124002519.

[11] M. Geraedts, "Modelling hybrid energy networks: A numerical approach to sustainable energy network design,"

[12] "Energy Control Businesspark – Ecofactorij." (), [Online]. Available: https://projecten.topsectorenergie.nl/projecten/new-energy-garden-xl-businesspark-37466.

[13] W. Van Dalfsen, "The shallow subsurface temperature field in the netherlands," in *Advances in European Geothermal Research*, A. S. Strub and P. Ungemach, Eds., Dordrecht: Springer Netherlands, 1980, pp. 496–505, ISBN: 978-94-009-9059-3. DOI: 10.1007/978-94-009-9059-3_44.

[14] M. Boers and H. van Hateren, "Gebiedsstudie bodemenergie," VHGM B.V., Hilversum, Technical, 2024.

[15] C. B. v. d. Statistiek. "Gemiddeld woning oppervlak," Centraal Bureau voor de Statistiek. Last Modified: 2025-03-28T02:00:00+01:00. (Mar. 28, 2025), [Online]. Available: https://www.cbs.nl/nl-nl/cijfers/detail/82550NED.

[16] M. Pipattanasomporn, M. Kuzlu, S. Rahman, and Y. Teklu, “Load profiles of selected major household appliances and their demand response opportunities,” *IEEE Transactions on Smart Grid*, vol. 5, no. 2, pp. 742–750, Mar. 2014, ISSN: 1949-3061. DOI: 10.1109/TSG.2013.2268664. [Online]. Available: https://ieeexplore.ieee.org/document/6576261.

[17] “Soorten grootverbruik elektriciteitsaansluitingen | Liander.” (), [Online]. Available: https://www.liander.nl/grootzakelijk/aansluiting/soorten-elektriciteitsaansluitingen.

[18] J. de Wit, “Nationaal smart storage trendrapport,” DNE Research, Heerhugowaard, 3050-6395, 2024.

[19] “KNMI - uurgegevens van het weer in nederland.” (), [Online]. Available: https://www.knmi.nl/nederland-nu/klimatologie/uurgegevens.

# A

# Graphs

## A.1. Weatherdata

### A.1.1. Ambient temperature

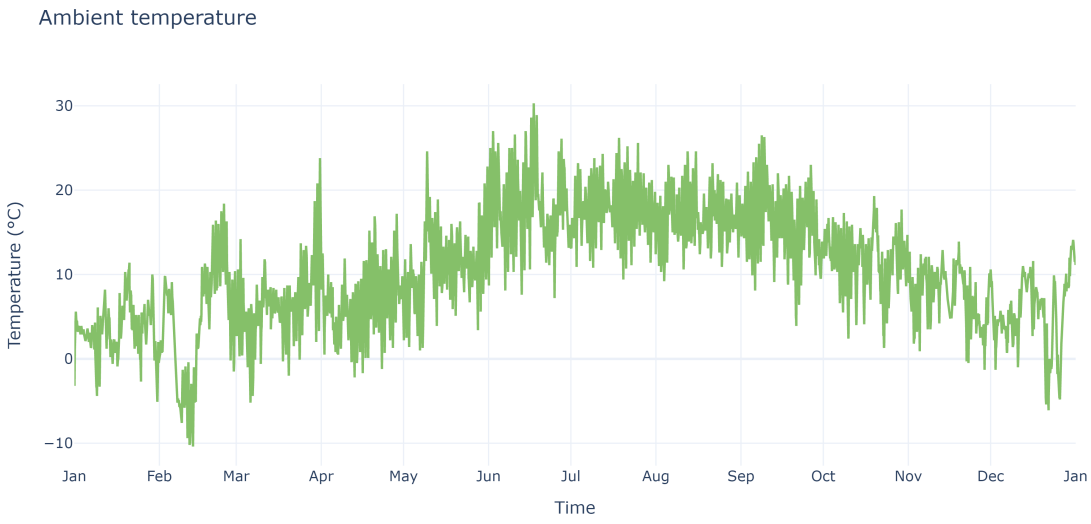


Figure A.1: Ambient temperature in De Bilt [19]

### A.1.2. Global solar irradiance

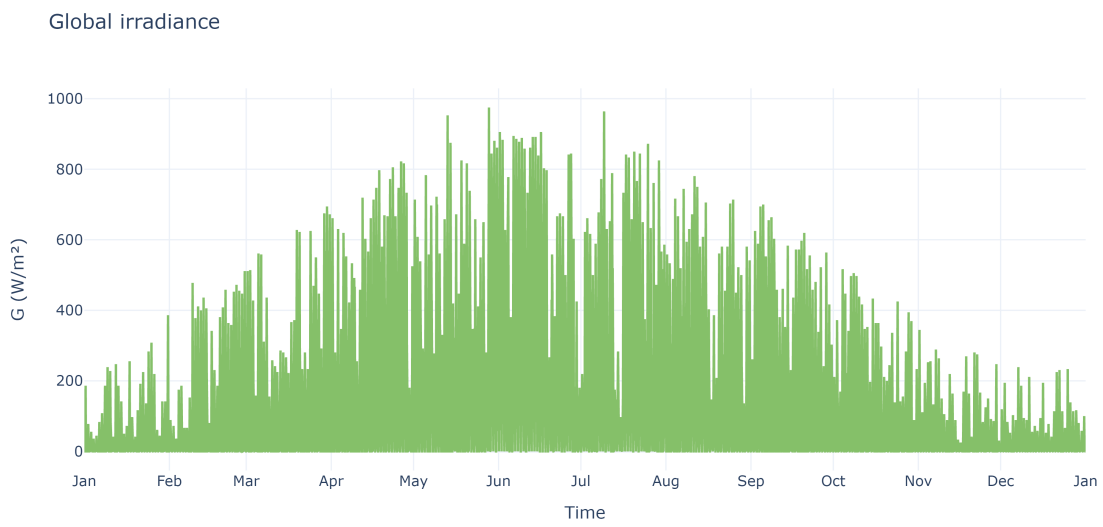


Figure A.2: Global irradiance in De Bilt [19]

## A.2. Electrical PVT generation

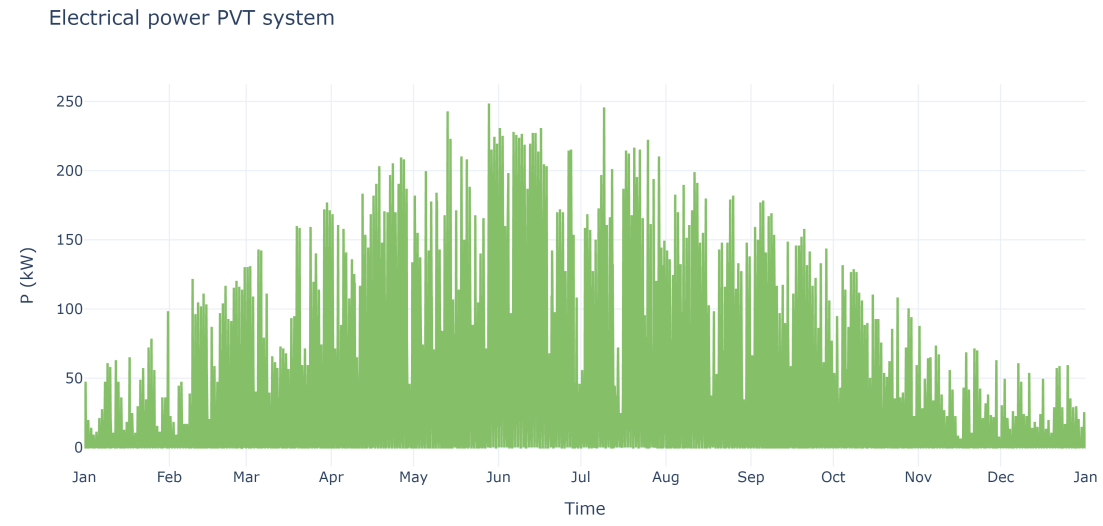


Figure A.3: Electrical power generated by PVT system

## A.3. Total residential electricity demand pattern

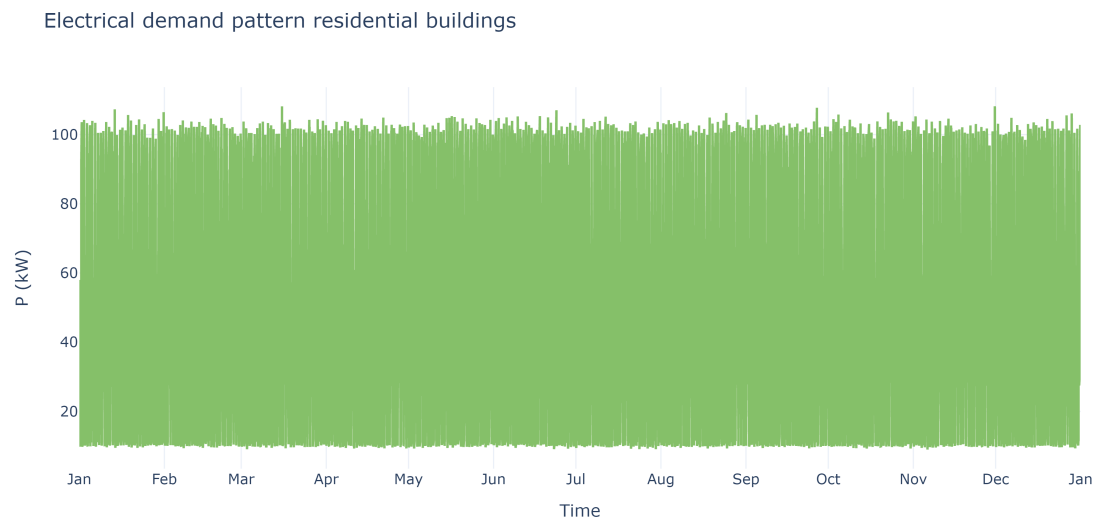


Figure A.4: Semi-random generated electricity demand profile for 55 residential homes for a year

## A.4. Normal operation ATES temperature

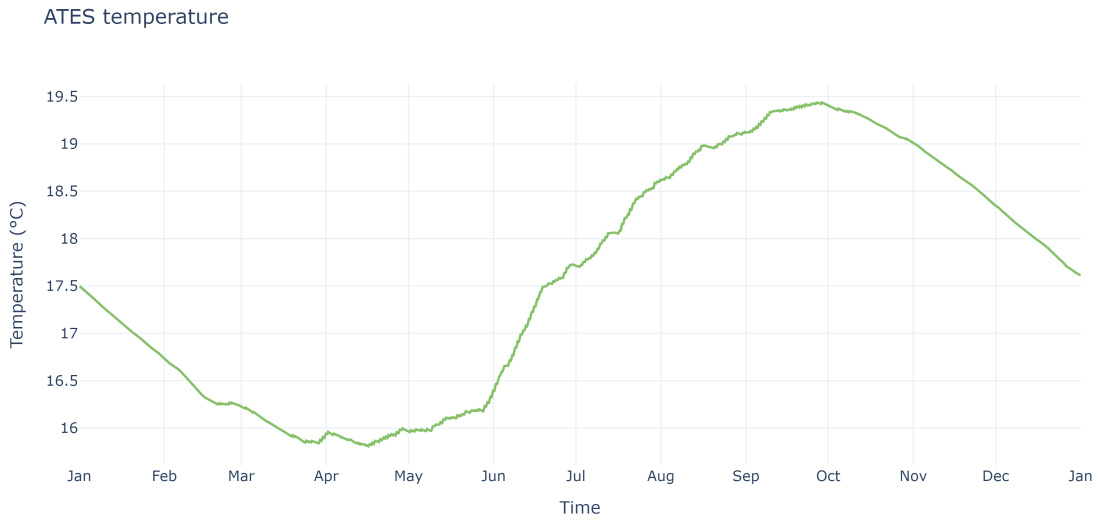


Figure A.5: ATES temperature over a year with normal operation

# A.5. Normal COP pattern

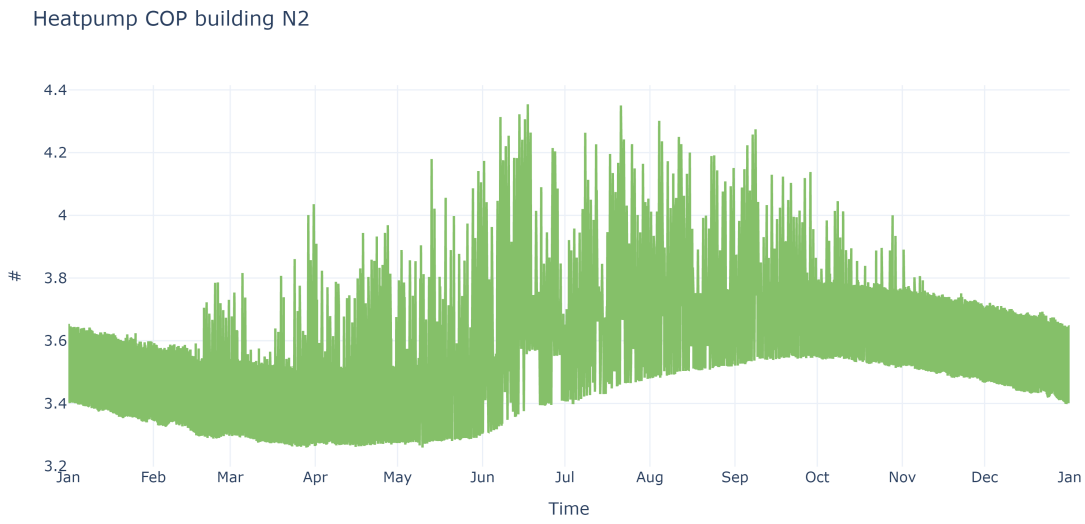


Figure A.6: The normal COP pattern of a heat pump of a single building

# A.6. Graphs RQ4

## A.6.1. Base

### AC5a

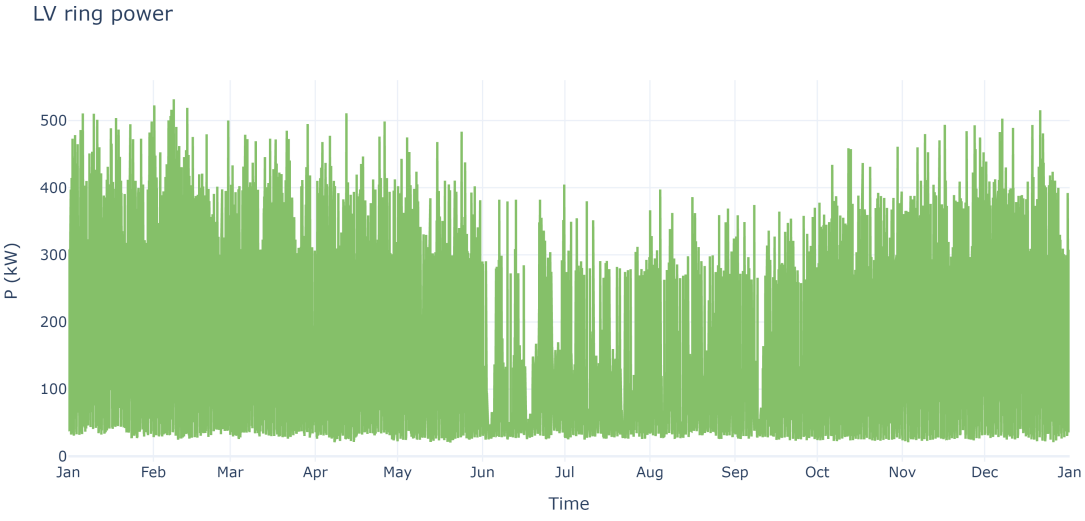


Figure A.7: LV ring power Base / AC5a

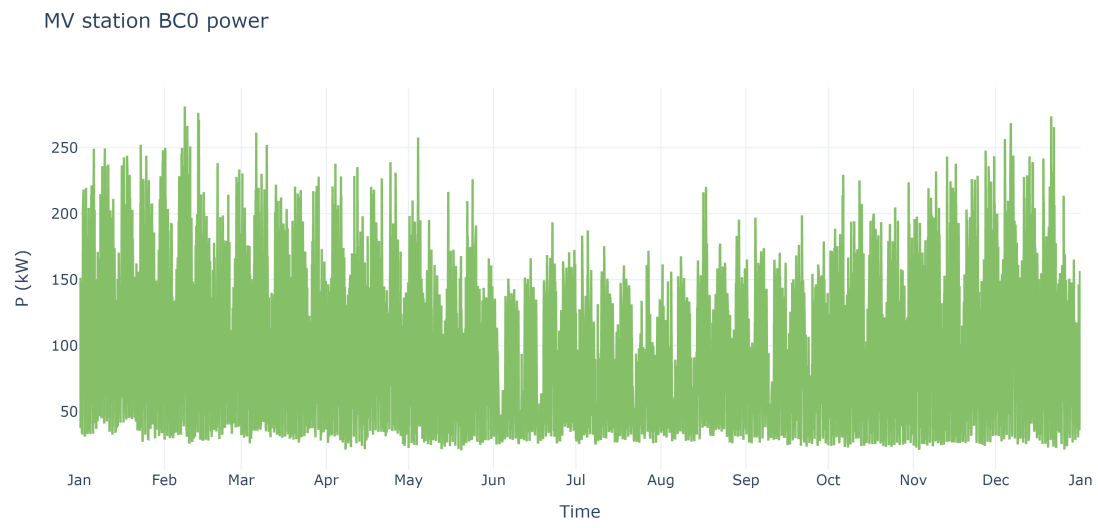


Figure A.8: MV station BC0 power Base / AC5a

### SolarPark

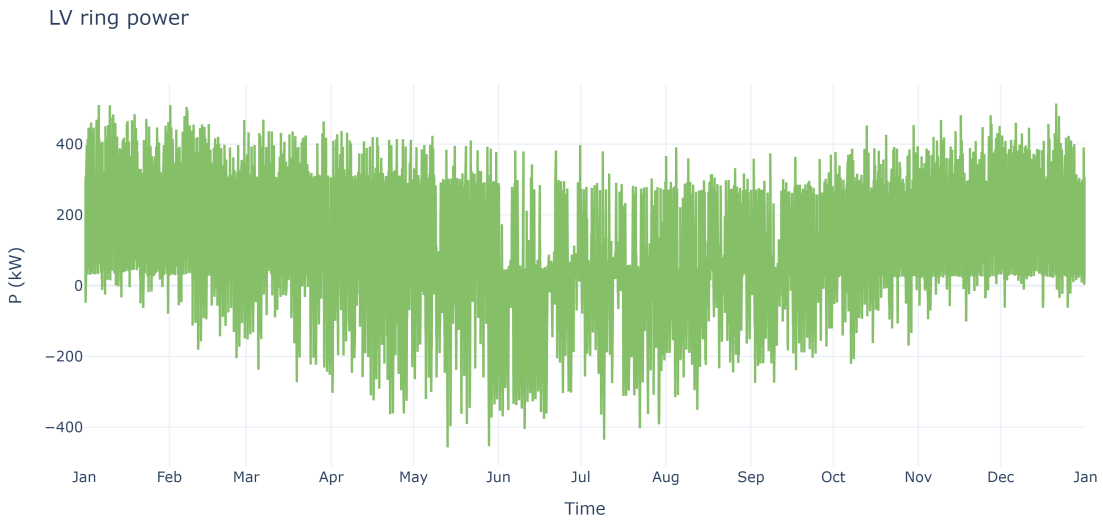


Figure A.9: LV ring power Base / SolarPark

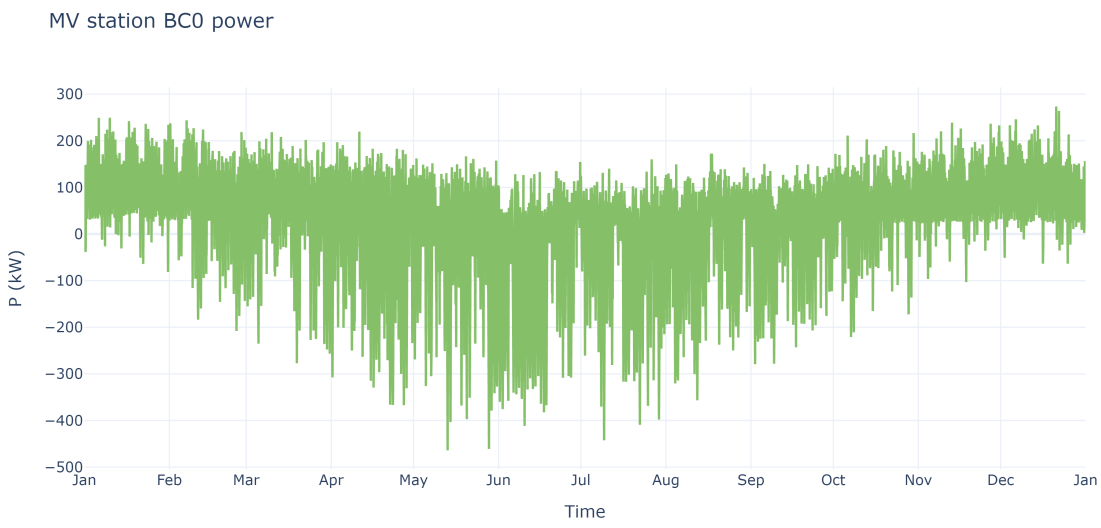


Figure A.10: MV station BC0 power Base / SolarPark

## A.6.2. Direct load control

### AC5a

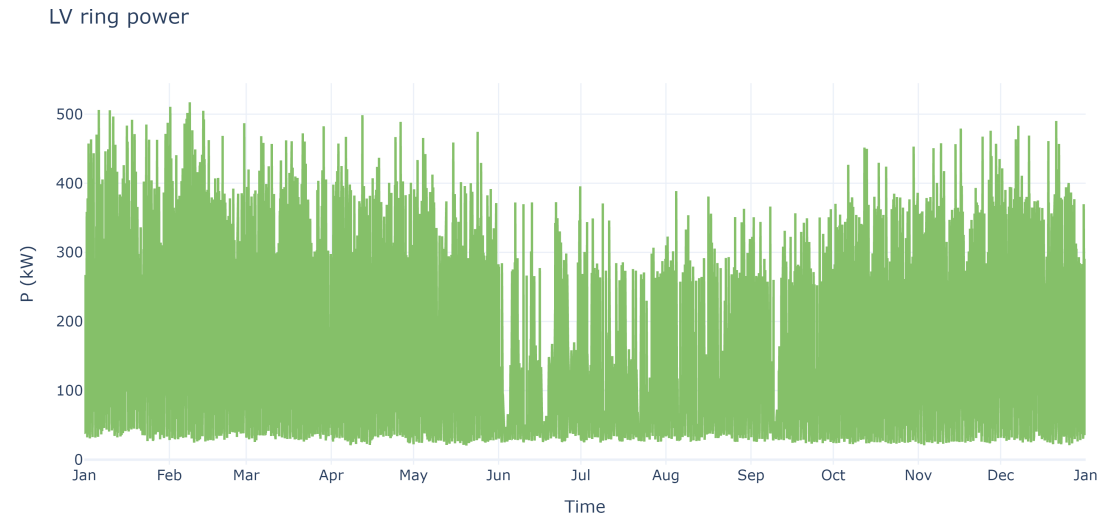


Figure A.11: LV ring power direct load control / AC5a

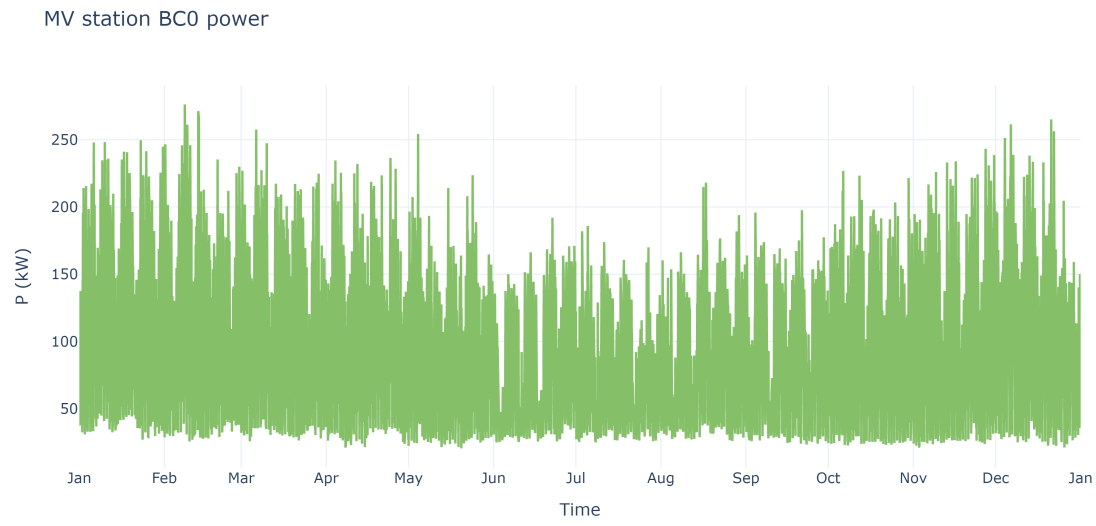


Figure A.12: MV station BC0 power direct load control / AC5a

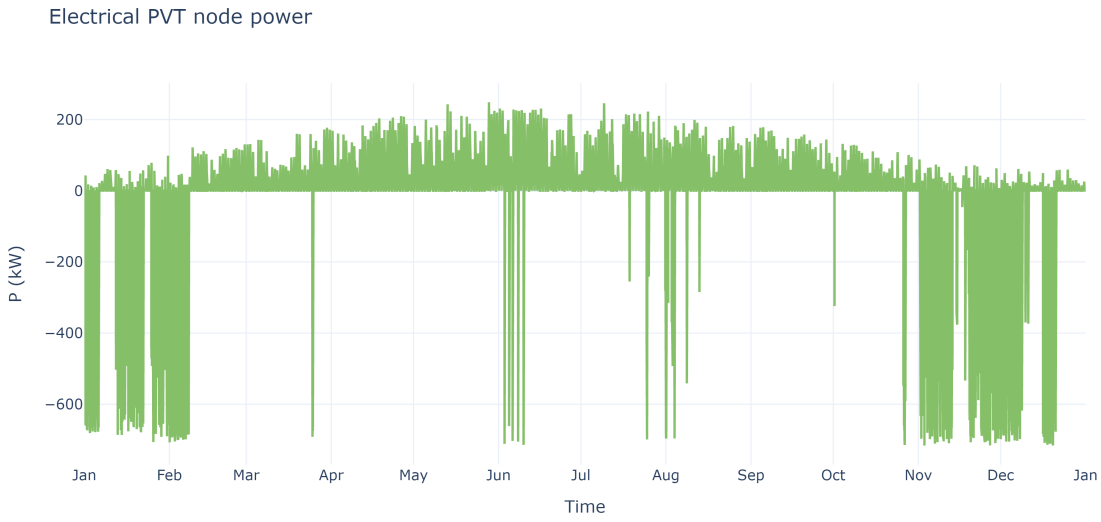


Figure A.13: PVT node power direct load control / AC5a

### SolarPark

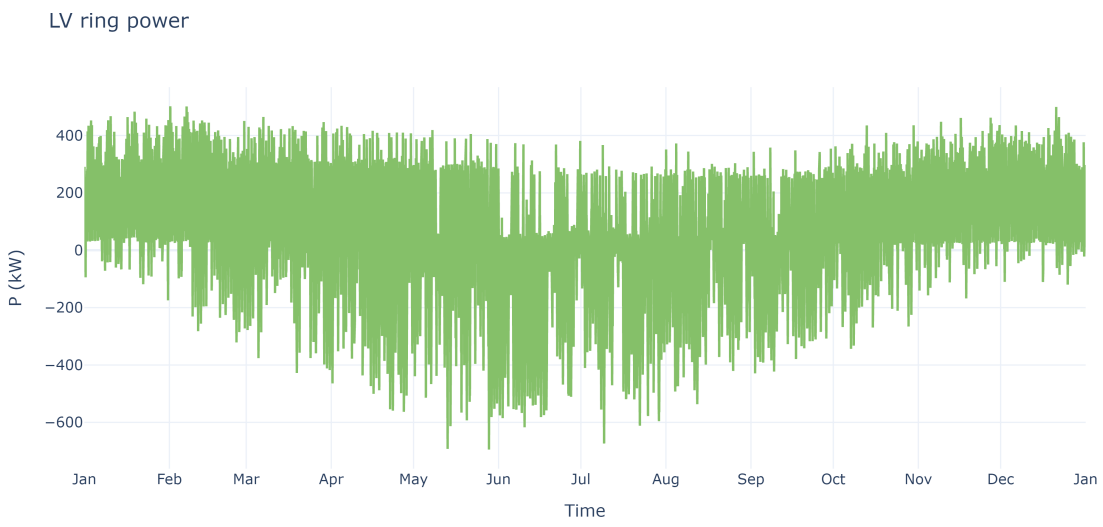


Figure A.14: LV ring power direct load control / SolarPark

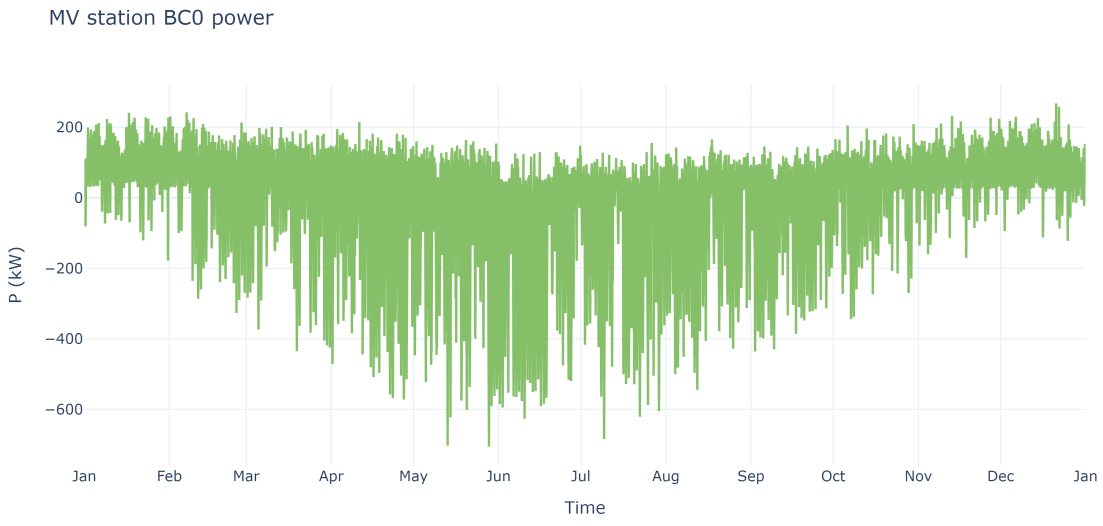


Figure A.15: MV station BC0 power direct load control / SolarPark

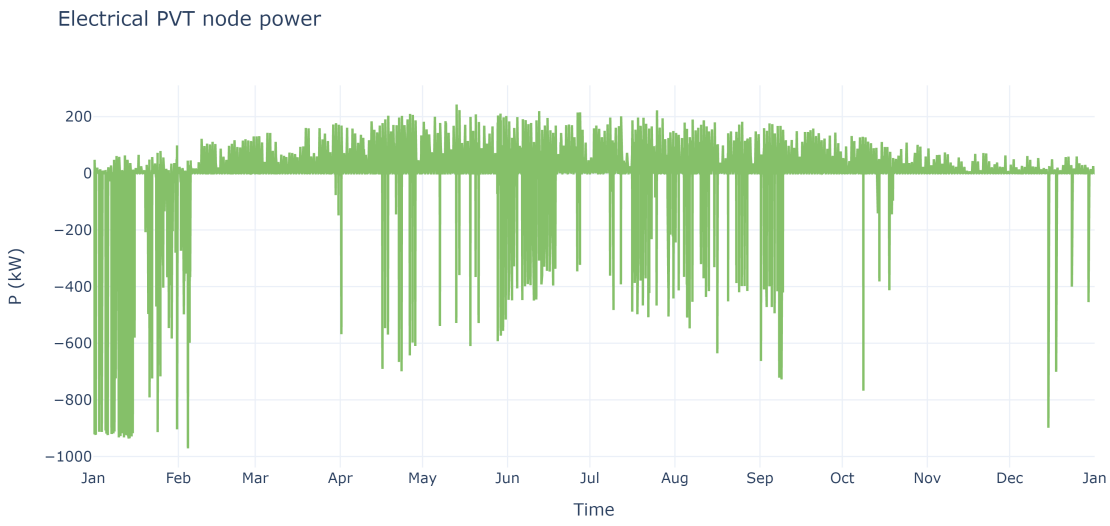


Figure A.16: PVT node power direct load control / SolarPark

# B

# Tables

## B.1. Loadshifting results

Table B.1: Loadshift optimization for connection category AC5

| Parameter | Value | Unit |
|---|---|---|
| Connection Category | AC5b | – |
| Max Consumption – Max Production | 1,700 – 2,000 | [kW] |
| Installed PV power | 0.0 | [kWp] |
| Battery Energy Capacity | 161.5 | [kWh] |
| Total Cost | 189,670.6 | [€] |
| Maximum Grid Power | 1700.0 | [kW] |

Table B.2: Loadshift optimization for connection category AC5b

| Parameter | Value | Unit |
|---|---|---|
| Connection Category | AC5b | – |
| Max Consumption – Max Production | 850 – 1000 | [kW] |
| Installed PV power | 0.0 | [kWp] |
| Battery Energy Capacity | 1.01 | [MWh] |
| Total Cost | 1,187,708.8 | [€] |
| Maximum Grid Power | 850.0 | [kW] |

Table B.3: Loadshift optimization for connection category AC5a

| Parameter | Value | Unit |
|---|---|---|
| Connection Category | AC5a | – |
| Max Consumption – Max Production | 535 – 630 | [kW] |
| Installed PV power | 0.0 | [kWp] |
| Battery Energy Capacity | 1.32 | [MWh] |
| Total Cost | 1,557,570.1 | [€] |
| Maximum Grid Power | 630.0 | [kW] |

Table B.4: Loadshift optimization for connection category SolarPark

| Parameter | Value | Unit |
|---|---|---|
| Connection Category | SolarPark | – |
| Max Consumption – Max Production | 300 – 350 | [kW] |
| Installed PV power | 1,147.1 | [kWp] |
| Battery Energy Capacity | 3.80 | [MWh] |
| Total Cost | 5,611,134.6 | [€] |
| Maximum Grid Power | 350.0 | [kW] |

Table B.5: Loadshift optimization for connection category AC4b

| Parameter | Value | Unit |
|---|---|---|
| Connection Category | AC4b | – |
| Max Consumption – Max Production | 147 – 160 | [kW] |
| Installed PV power | 1,743.5 | [kWp] |
| Battery Energy Capacity | 273.5 | [MWh] |
| Total Cost | 322,871,347. | [€] |
| Maximum Grid Power | 160.0 | [kW] |

Table B.6: Loadshift optimization for connection category AC4a

| Parameter | Value | Unit |
|---|---|---|
| Connection Category | AC4a | – |
| Max Consumption – Max Production | 94 – 100 | [kW] |
| Installed PV power | 1,743.5 | [kWp] |
| Battery Energy Capacity | 470.8 | [MWh] |
| Total Cost | 554,567,868.9 | [€] |
| Maximum Grid Power | 100.0 | [kW] |

## B.2. Direct load control results

Table B.7: Direct load control optimization for connection category AC5

| Parameter | Value | Unit |
|---|---|---|
| Connection Category | AC5b | – |
| Max Consumption – Max Production | 1,700 – 2,000 | [kW] |
| Installed PV power | 0.0 | [kWp] |
| Battery Energy Capacity | 0.0 | [kWh] |
| Total Cost | 0.0 | [€] |
| Maximum Grid Power | 899.0 | [kW] |

Table B.8: Direct load control optimization for connection category AC5b

| Parameter | Value | Unit |
|---|---|---|
| Connection Category | AC5b | – |
| Max Consumption – Max Production | 850 – 1000 | [kW] |
| Installed PV power | 0.0 | [kWp] |
| Battery Energy Capacity | 6.85 | [kWh] |
| Total Cost | 8,039.6 | [€] |
| Maximum Grid Power | 850.0 | [kW] |

Table B.9: Direct load control optimization for connection category AC5a

| Parameter | Value | Unit |
|---|---|---|
| Connection Category | AC5a | – |
| Max Consumption – Max Production | 535 – 630 | [kW] |
| Installed PV power | 0.0 | [kWp] |
| Battery Energy Capacity | 329.5 | [kWh] |
| Total Cost | 386,887.3 | [€] |
| Maximum Grid Power | 535.0 | [kW] |

Table B.10: Direct load control optimization for connection category SolarPark

| Parameter | Value | Unit |
|---|---|---|
| Connection Category | SolarPark | – |
| Max Consumption – Max Production | 300 – 350 | [kW] |
| Installed PV power | 1,543.2 | [kWp] |
| Battery Energy Capacity | 2.30 | [MWh] |
| Total Cost | 4,247,751.3 | [€] |
| Maximum Grid Power | 350.0 | [kW] |

Table B.11: Direct load control optimization for connection category AC4b

| Parameter | Value | Unit |
|---|---|---|
| Connection Category | AC4b | – |
| Max Consumption – Max Production | 147 – 160 | [kW] |
| Installed PV power | 1,743.5 | [kWp] |
| Battery Energy Capacity | 256.4 | [MWh] |
| Total Cost | 302,791,296.4 | [€] |
| Maximum Grid Power | 160.0 | [kW] |

Table B.12: Direct load control optimization for connection category AC4a

| Parameter | Value | Unit |
|---|---|---|
| Connection Category | AC4a | – |
| Max Consumption – Max Production | 94 – 100 | [kW] |
| Installed PV power | 1,743.5 | [kWp] |
| Battery Energy Capacity | 450.4 | [MWh] |
| Total Cost | 530,676,442.3 | [€] |
| Maximum Grid Power | 100.0 | [kW] |

## B.3. Combination results

Table B.13: Combination optimization for connection category AC5

| Parameter | Value | Unit |
|---|---|---|
| Connection Category | AC5b | – |
| Max Consumption – Max Production | 1,700 – 2,000 | [kW] |
| Installed PV power | 0.0 | [kWp] |
| Battery Energy Capacity | 0.0 | [kWh] |
| Total Cost | 0.0 | [€] |
| Maximum Grid Power | 1700.0 | [kW] |

Table B.14: Combination optimization for connection category AC5b

| Parameter | Value | Unit |
|---|---|---|
| Connection Category | AC5b | – |
| Max Consumption – Max Production | 850 – 1000 | [kW] |
| Installed PV power | 0.0 | [kWp] |
| Battery Energy Capacity | 782.2 | [kWh] |
| Total Cost | 918,509.1 | [€] |
| Maximum Grid Power | 850.0 | [kW] |

Table B.15: Combination optimization for connection category AC5a

| Parameter | Value | Unit |
|---|---|---|
| Connection Category | AC5a | – |
| Max Consumption – Max Production | 535 – 630 | [kW] |
| Installed PV power | 0.0 | [kWp] |
| Battery Energy Capacity | 1.20 | [MWh] |
| Total Cost | 1,408,076.7 | [€] |
| Maximum Grid Power | 630.0 | [kW] |

Table B.16: Combination optimization for connection category SolarPark

| Parameter | Value | Unit |
|---|---|---|
| Connection Category | SolarPark | – |
| Max Consumption – Max Production | 300 – 350 | [kW] |
| Installed PV power | 1,743.5 | [kWp] |
| Battery Energy Capacity | 2.57 | [MWh] |
| Total Cost | 4,755,500.0 | [€] |
| Maximum Grid Power | 350.0 | [kW] |

Table B.17: Combination optimization for connection category AC4b

| Parameter | Value | Unit |
|---|---|---|
| Connection Category | AC4b | – |
| Max Consumption – Max Production | 147 – 160 | [kW] |
| Installed PV power | 1,743.5 | [kWp] |
| Battery Energy Capacity | 257.8 | [MWh] |
| Total Cost | 304,422,879.8 | [€] |
| Maximum Grid Power | 160.0 | [kW] |

Table B.18: Combination optimization for connection category AC4a

| Parameter | Value | Unit |
|---|---|---|
| Connection Category | AC4a | – |
| Max Consumption – Max Production | 94 – 100 | [kW] |
| Installed PV power | 1,743.5 | [kWp] |
| Battery Energy Capacity | 453.2 | [MWh] |
| Total Cost | 533,929,399.4 | [€] |
| Maximum Grid Power | 100.0 | [kW] |

## B.4. Gurobi variables

| Name | Description | Unit | Multiplicity | Lower Bound | Upper Bound |
|---|---|---|---|---|---|
| Tin | Temperature coming into a node | [K] | k, node | 273 | 323 |
| Tout | Temperature flowing out of a node | [K] | k, node | 273 | 323 |
| Qdot_ij | Heat flow between nodes i and j | [kW] | k, connection | 0 | - |
| Qdot_n | Net heat flow per node | [kW] | k, node | -10000 | 10000 |
| Qdot_top | Heat losses through the top of the ATES | [kW] | k | -1000 | 1000 |
| Qdot_bottom | Heat losses through the bottom of the ATES | [kW] | k | -1000 | 1000 |
| Qdot_side | Heat losses through the side of the ATES | [kW] | k | -1000 | 1000 |
| Qdot_soil | Total heat losses of the ATES to the soil | [kW] | k | -1000 | 1000 |
| Qdot_pvt | Heat flow from a single PVT panel | [W] | k | 0 | 3000 |
| P_pvt | Electrical power from the total PVT system | [kW] | k | 0 | 1000 |
| kWp_pv | Installed solar power (PV panels only) | [kWp] | - | 0 | - |
| P_pv | Electrical power (PV panels only) | [kW] | k | 0 | 1000 |
| P_hp | Heat Pump power | [kW] | k, building | -1000 | 1000 |
| COP_hp | Heat Pump coefficient of performance | [] | k, building | 1 | 5 |
| Qdot_network | Heat extracted from the network by the Heat Pump | [kW] | k, building | -1000 | 1000 |
| P_hp_x | Direct load control Heat Pump power | [kW] | k | 0 | var |
| Tpipe_in | Temperature flowing in to a pipe | [K] | k, connections | 273 | 323 |
| Tpipe_out | Temperature flowing out of a pipe | [K] | k, connections | 273 | 323 |
| P_grid | Electrical power grid connection | [kW] | k | var | var |
| P_grid_peak | Peak electrical power grid connection | [kW] | - | 0 | - |
| E_bess | Battery energy level (SOC) | [MWh] | k | 0 | 1000 |
| P_bess | Battery power | [MW] | k | -1000 | 1000 |
| E_bess_max | Battery maximum energy level (capacity) | [MWh] | k | 0 | 1000 |
| P_bess_max | Battery maximum power level | [MW] | k | 0 | 1000 |

## B.5. Parameters thermal appliances

For the parameters used in the python model related to thermal appliances, see the Appendix of the master thesis of T. Beijneveld [5].

# C

# Images

## C.1. Impressions of the Werf

(a) Central Werf area and NEP building

(b) Central Werf area view from Arendstraat

(c) Mussenstraat West

(d) ”Ketelhuis aan de Werf”

(a) Arendstraat

(b) Rotor building (East area)

(c) Southeast buildings

(d) Arendstraat view from south

# D

# Code

The main backbone of this thesis is the python code used for calculations and optimizations. This code is uploaded to a Github repository. This repository can be publicly accessed via the following link: `https://github.com/tjbroekman/CDS_optimization`